December 2012

Analysis of Multi-Directional Recycled Jute Fiber Composite Behavior Using Experimental, Numerical, and Analytical Methods

Patrick Severson
University of Wisconsin-Milwaukee

ANALYSIS OF MULTI-DIRECTIONAL RECYCLED JUTE FIBER COMPOSITE BEHAVIOR USING EXPERIMENTAL, NUMERICAL, AND ANALYTICAL METHODS

by

Patrick M. Severson

A Thesis Submitted in

Partial Fulfillment of the

Requirements for the Degree of

Master of Science

in Engineering

at

The University of Wisconsin-Milwaukee

December, 2012

ABSTRACT
ANALYSIS OF MULTI-DIRECTIONAL RECYCLED JUTE FIBER COMPOSITE BEHAVIOR USING EXPERIMENTAL, NUMERICAL, AND ANALYTICAL METHODS

by

Patrick M. Severson

The University of Wisconsin-Milwaukee, 2012
Under the Supervision of Professor Dr. Rani El-Hajjar

Composite materials are increasing in popularity as a material of choice in many engineering applications. Major industries using composites include automotive, construction, and sports equipment. Most of the knowledge, research, and technology that will help decrease the cost of composite materials have been aimed at developing synthetic fibers as the reinforcing constituent.

This thesis characterizes jute fibers obtained as a byproduct from the coffee industry to determine if they can be viable in composite manufacturing. Experimental analysis, finite element analysis, and analytical modeling are used to characterize jute fiber based composites. Experimental analysis consists of jute fiber bundle tensile testing as well as tensile testing of multiple laminates.

Finite element and analytical models were developed to simulate different composite characteristics and their influence on jute composites. Finite element models investigated the influences of fiber undulation, fiber damage, and matrix porosity. Results show that certain manufacturing precautions should be taken to minimize imperfections which have negative influences on the composite. Fiber damage has the largest influence when introduced near the top of the fiber wave and can cause normal stresses to increase 56%. Fiber undulation and matrix porosity also have noticeable influences on the composite.

TABLE OF CONTENTS

LIST OF FIGURES

LIST OF TABLES

ACKNOWLEDGMENTS

This thesis would not have been possible without the guidance of many individuals who have contributed valuable assistance and support through the duration of this study.

First and foremost, I offer my sincerest gratitude to my advisor Dr. Rani El-Hajjar, who has supported me throughout the entire process of preparing this thesis. He has shared valuable insight every step of the way. I attribute the level of my Masters degree and this thesis to his encouragement. Without his support, this simply would not have been possible. I could not have wished for a more knowledgeable and friendlier advisor.

I have been aided in other various academic facilities through my years at UW-Milwaukee. Dr. Adeeb Rahman has shared his wisdom and has also showed support in other numerous ways. I want to thank Rahim Reshadi for his support and knowledge in the mechanics of materials lab and with giving me access for different studies. Also, my friends and colleagues who have shared their knowledge through the years and shaped me into the engineer that I am today.

My gratitude also goes out to the folks at K2 Sports. Without their work and willingness to help, a prototype snowboard would not have been created. I am specifically grateful for the kindness of Paul McGinty. He helped me every step of the way and without him, a large portion of my thesis would not have been possible.

I would like to thank my parents and my brother for encouraging me to finish my Masters degree and offering their support throughout the entire process. Finally, I thank my wife, who has been one of my biggest supporters of all. She has supported me in many ways and I am very lucky to have someone so encouraging in my life.

1. Introduction

1.1 Research Objectives

Composite materials are becoming very significant in many engineering applications. In many instances they are replacing isotropic materials (aluminum, steel, etc.) because of their low specific weight and strength. In the past, researchers have focused more on synthetic fibers in composite materials over natural fibers.

A variety of industries currently use either natural or synthetic fibers in their products. Many natural fibers have sufficient strength and stiffness but are difficult to deal with because of their fibrous structure and variable properties while most polymers do not have sufficient strength or stiffness but serve as a good adhesive to hold fibers together [1]. In composite structures, the fibers serve as the constituent that give the composite strength and stiffness, while the polymer matrix holds everything together and effectively transfers stresses to the fibers. These concepts are true for both synthetic based composites and natural based composites.

One sector currently using natural fiber composites is the automotive industry. Mechanical properties, low weight, low cost, ecological sustainability, low energy requirements, biodegradability, and carbon dioxide neutrality are all driving factors in the push for natural composites [1]. Many of the cosmetic components in automobiles are currently taking advantage of composite materials. Private and commercial construction supplies are also taking advantage of the properties natural composites have to offer. These are only a few examples of natural fibers currently being used in society.

This thesis focuses on characterizing jute fiber composites. Jute belongs to either of two species; *C. capsularis* (white jute) and *C. olitorius* (including tossa and daisee

varieties) which belong to the hibiscus or mallow family, and their fiber [2]. The latter is a bast fiber which is obtained from the inner bast tissue of the bark of the plant's stem [1]. These fibers are readily available and are typically used in the transportation of bulk goods and commonly referred to as burlap. The potential to use recycled jute fibers is made possible by the rapid expansion of the coffee industry which is currently the fastest growing part of the restaurant industry with a 7% annual growth rate [3]. In addition, world coffee production is estimated to be 110-120 million bags per year with Americans consuming 400 million cups of coffee per day making America the largest consumer of coffee in the world [3].

One of the biggest advantages from using recycled jute fabric for engineering applications is the accessibility. On the other hand, one of the consequences is the lack of manufacturing control. These two statements lead to intriguing questions about the possibility of using recycled jute fabric in natural composites. This thesis will answer the following questions:

- Can recycled jute fibers be integrated in natural composites?
- Can the information gathered from numerical analysis and analytical modeling be used to help optimize the manufacturing of natural composites using recycled jute fibers?
- What physical characteristics of a natural composite are detrimental to its performance as a load bearing member?

1.2 Research Program Overview

This thesis uses a combination of experimental testing, numerical analysis, and analytical analysis to characterize jute fiber based composites obtained from recycled

materials. Instead of requiring a manufacturing process to meet certain specifications, the fibers will be categorized based on their physical properties as a way of determining the type of material that is being investigated.

Tensile tests were conducted on single jute fiber bundles and on multiple laminates. The results obtained from tensile tests of single jute fiber bundles were also used to set up the finite element analysis and the analytical analysis models. Single fiber bundle tensile testing characterized individual yarns whereas tensile testing on laminates allowed for global characterization which depends on the orientation of the yarns being used. A modified version of the Classical Lamination Plate Theory and laminate testing can help optimize how to orient jute fabric to cater to the needs of the engineer.

The numerical method analysis took advantage of finite element analysis software to determine the effects of fiber undulation, fiber damage, and matrix porosity. These characteristics were determined using a CAD model (*SolidWorks 2012*) which was then brought into a finite element analysis environment for pre and post processing. The software used for this was *SolidWorks Simulation Premium*. The results from this analysis can help an engineer alleviate foreseeable problems due to poor manufacturing.

The jute fiber composites were also characterized using a combined Classical Lamination Plate Theory and a fiber undulation model. This type of analysis was done to help correlate the results from experimental and numerical analysis to a closed-form solution. The physical and mechanical properties observed during experimental analysis were used as values in the analytical models. The analytical models were broken down into different sections before obtaining global mechanical properties. The first section included all the parameter inputs; modulus of elasticity, Poisson's ratio, lamina thickness,

angle of ply, volume fraction, fiber amplitude, and wave length. The second section calculated the mechanical properties of each layer while the last section calculated the global modulus of elasticity (longitudinal and transverse) and Poisson's ratio of the entire composite. After initial parameter inputs were set from experimental analysis, a calibration factor, K, was used to match the global properties from the analytical model to values obtained from physical laminate testing. The calibration factor accounted for material variability. Once these values were set, the analytical tool was used to measure trends by changing specific variables. The models in this project measured the trend between fiber aspect ratio and fiber volume ratio vs. the modulus of elasticity. These trends were related back to experimental testing and numerical analysis to observe a positive correlation.

Finally, for illustrating the application of these materials, a preliminary design of a snowboard made from recycled jute fibers was manufactured using a press and a mold. The snowboard was then put through testing to determine some of its endurance and strength properties.

2. Literature Review

2.1 Natural Fiber Composite

Natural fibers include bast, leaf, and seed/fruit fibers [1]. Bast consists of a wood core surrounded by a stem which contains a number of fiber bundles consisting of individual fiber cells or filaments [1]. An example of this type of fiber is jute. Along with being available as a byproduct and readily accessible, jute has many other advantages. These advantages include being renewable, porous, hydroscopic, viscoelastic, biodegradable, combustible, compostable, and reactive [4]. Some may consider biodegradable and combustible as disadvantages but these features provide a path for predictable and programmable disposal not easily seen with other materials [4]. Nature is programmed to recycle jute back to basic building blocks; carbon dioxide and water [4]. However, in order to interrupt the deterioration of jute, there has been research to introduce chemicals to increase the lifetime of the natural fiber. One such chemical is acetic anhydride [4]. One contribution to the deterioration of jute fibers is the susceptibility to moisture in the environment. However, in a study done on composite materials made from starch-based biopolymers and jute with 10%, 20%, and 30 % fiber reinforcement, the absorbed humidity was very low [5]. All three samples were between 0.95 -1.15% humidity absorption [5]. The resin used in these experiments reduced the moisture diffusion into the fibers from the environment. The matrix has a number of critical functions: (1) it binds the reinforcement together, (2) maintains the shape of a component and transfers the applied load to the reinforcing fibers, and (3) protects the reinforcing fibers from degradation due to abrasion and the environment [6]. Along with

these functions, the resin system resists delamination between plies of reinforcement and inhibits fiber buckling due to compressive loads [6].

One of the major drawbacks of natural fibers, when compared to synthetic fibers, is the poor adhesion between the natural fibers and the matrix [7]. This brings down the tensile properties of natural composites because interfacial bonding is the most important aspect that transfers stresses from the matrix to the fibers. The fiber/matrix interface is impaired in natural laminates because of surface impurities present in natural fibers which are not present in manufactured fibers [5]. In order to increase the mechanical properties in a natural composite, the process of bonding the matrix and the fibers must be optimized. Research has been aimed to condition the fiber surface with alkali treatment which has been shown to help increase fiber/matrix interface bonding [8]. As lignin is removed from jute fibers, the middle lamella joining the ultimate cells is expected to be more plastic and homogeneous due to the elimination of imperfections due to alkali treatment [5]. In one study, jute fibers were exposed to alkali treatment with 5% NaOH solution for 0, 2, 4, 6, and 8 hours at 30°C [9]. The modulus of elasticity of the jute fibers increased by 12%, 68%, and 79% after 4, 6, and 8 hours, respectively [9]. This study shows that alkali treatment improves the interfacial bond between the fiber and the matrix, in turn, increasing the tensile properties. Along with alkali treatment, work has been done to modify jute fibers with oleoyl chloride which is a fatty acid able to react with the –OH groups of jute fibers [10]. This process may improve the wettability and decrease water absorption when used as reinforcement for polymeric matrices [10]. Wettability is also a large concern when dealing with “dry” fibers. If the resin is not spread properly, pools of resin can form throughout the composite causing weaknesses.

There may also be spots of dry fibers where resin was not able to spread. However, properly treating jute fibers will allow for optimal axial mechanical properties. After fiber treatment is complete, an acceptable resin that bonds the fiber and matrix must be considered. Polyester and some phenolic resins are suitable for bonding with natural fibers because they are compatible with cellulose [11].

Different studies have been conducted to compare the mechanical properties of synthetic fibers and other natural fibers to jute fibers. It has been shown that the specific modulus of jute is superior to fiberglass [12]. Since jute has a higher specific modulus than fiberglass, an equal stiffness should be maintained with less weight. Table 1 shows a comparison of properties for selected natural fibers and synthetic fibers.

Table 1: Mechanical properties of synthetic and natural fibers [7].

Properties of selected natural and manmade fibers [adapted from 3, 8].

Fiber	Density (g/cm^3)	Elongation (%)	Tensile strength (MPa)	Elastic modulus (GPa)	Refs.
Cotton	1.5–1.6	7.0–8.0	400	5.5–12.6	[6,7]
Jute	1.3	1.5–1.8	393–773	26.5	[6]
Flax	1.5	2.7–3.2	500–1500	27.6	[4]
Hemp	1.47	2–4′	690	70	[4]
Kenaf	1.45	1.6	930	53	[4]
Ramie	N/A	3.6–3.8	400–938	61.4–128	[8]
Sisal	1.5	2.0–2.5	511–635	9.4–22	[8]
Coir	1.2	30	593	4.0–6.0	[9]
Softwood kraft pulp	1.5	4.4	1000	40	[9]
E-glass	2.5	0.5	2000–3500	70	[9]
S-glass	2.5	2.8	4570	86	[9]
Aramid (Std.)	1.4	3.3–3.7	3000–3150	63.0–67.0	[9]
Carbon (Std. PAN-based)	1.4	1.4–1.8	4000	230–240	[9]

Another important aspect that measures a composites performance is the ability to absorb impacts. In tests conducted by several authors, impact-fatigue testing was done on jute/vinylester composites treated and untreated with alkali solutions. The impact-fatigue testing was set up similar to a Charpy Impact Test. The specimen was placed between two plates and struck repeatedly with a mass attached to the end of a pendulum [13]. In one set of tests, jute composites were soaked for 0, 4, and 8 hours to test the E-N fatigue curves (impact energy – number of impacts until failure) [13]. The E-N curve for these laminates is shown in Figure 1 with a summary of the values shown in Table 2.

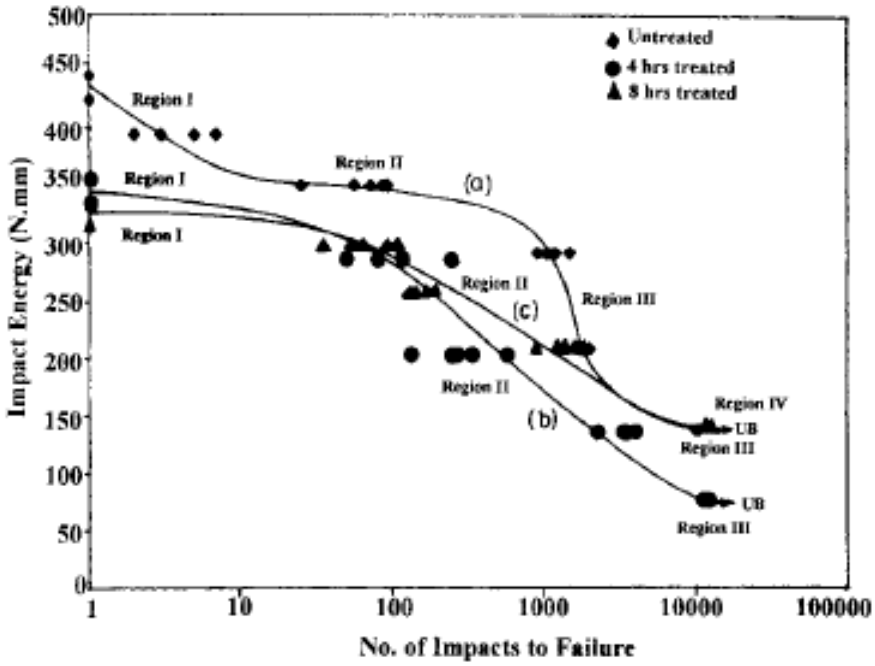

Figure 1: E-N curve for jute/vinylester composites [13].

Table 2: Summary of E-N values for jute/vinylester composites [13].

Fatigue property of composites reinforced with untreated and alkali treated jute fibres

Type of sample	Single impact energy (N mm)	Endurance limit (N mm)	Toughness (kJ/m^2)	Fatigue ratio (endurance limit/ single impact energy)
35% Composite (untreated)	438.750	137.24	17.80	0.312
35% Composite (4 h alkali treated)	342.124	79.36	13.88	0.232
35% Composite (8 h alkali treated)	327.044	140.77	13.27	0.430

The laminate that recorded the highest single impact energy were the untreated fibers. However, the laminate with the highest fatigue strength is greatest for the fibers soaked for 8 hours in an alkali solution. It was reported above that the maximum tensile properties were obtained after 8 hours of soaking as well. Therefore, an 8 hour soak in an alkali solution with 5% NaOH will optimize both the endurance limit and tensile properties for jute reinforced composites.

2.2 Material Characterization of Composites

Many materials are characterized by their mechanical properties such as strength, stiffness, thermal conductivity, etc. In many materials, such as steel and aluminum, these

properties are not a function of a single direction within the material. These materials are isotropic and are characterized by global properties which are independent of the orientation of the material. An anisotropic material has an infinite number of directions you can travel within the material and each one will correspond to a different value for the same material property. Composite orthotropic materials are in the middle of the two extreme cases (isotropic and anisotropic) due to the three planes of material symmetry. In composites, the intersection of these three planes creates three axes which are defined as the principal material axes.

There are many different types of composite materials but most can be classified into three major categories. The three categories are particulate filler composites, discontinuous fiber composites, and continuous fiber composites which are shown in Figure 2.

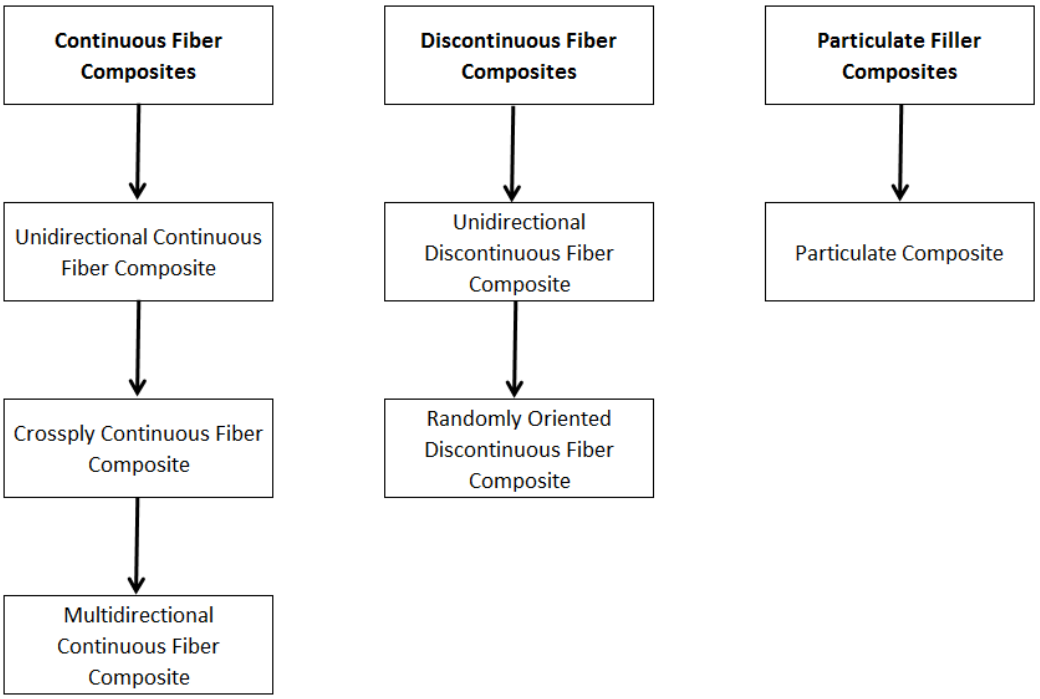

Figure 2: Composite material classification.

Particulate composites consist of randomly placed particles in a matrix with different sizes. These composites can be assumed as quasi-homogeneous and quasi-isotropic on a macroscopic scale [14]. A good example of this type of composite is concrete. Discontinuous fiber composites use short fibers for reinforcement which are oriented unidirectional or randomly within the matrix. Unidirectional discontinuous fibers tend to have orthotropic material behavior while randomly placed discontinuous fibers are considered quasi-isotropic on the macroscopic level [14]. Continuous fiber composites use a continuous fiber through the length of the composite as its reinforcement. Since fibers are the constituent that give a composite its strength and stiffness, continuous fiber composites are the most efficient type of composite when these mechanical characteristics are of concern. As seen from Figure 2 there are different classifications within the continuous fiber category. Unidirectional continuous fiber composites consist of a composite where the fibers are oriented in a single direction. Crossply continuous fiber composites have fibers in two directions that are perpendicular to each other. These composites can be created by weaving the fibers together or by placing two unidirectional composites on top of each other with the principal axes at 90°. Laminated composites are created by different weave patterns or by placing unidirectional composites on top of each other with the principal axes randomly oriented.

Two terms that should be defined are lamina and laminate. When describing composites, a lamina refers to one layer of unidirectional fibers or woven fabric in a matrix [14]. Lamina are orthotropic with one principal axis (two principal axes for woven lamina) oriented along the fiber direction (longitudinal) and the other two axes

(one axis for woven lamina) normal to the fibers in the plane of the lamina (in-plane) and normal to the plane of the lamina (out-of-plane) [14]. This is shown in Figure 3.

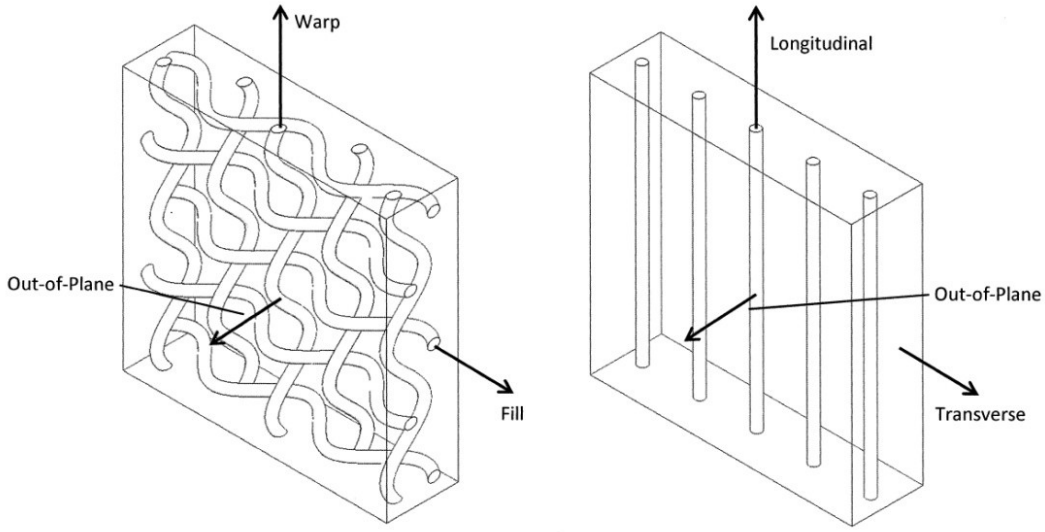

Figure 3: Woven and unidirectional lamina.

A lamina is the building block for laminates and composites in general. A laminate consists of two or more lamina placed on top of each other. The orientation of each lamina depends on what the composite will be used for and the type of material properties that should be obtained. Since a laminate is composed of different lamina stacked on top of each other, their individual principal axes will not align in most cases. Therefore, a global coordinate system is established for the laminate and the orientation of a given lamina is given by the angle between the longitudinal principal axis and the global x-axis measured in a counterclockwise direction [14].

There are different ways to analyze a structure made from composite materials. In many instances an engineer is only concerned about the global characteristics on the macroscopic level so a structural analysis can be performed. However, to understand what is happening on the large scale, it is important to understand what is happening on the microscopic scale and how different characteristics on this level can influence the

entire structure. There are three different analyses that can be investigated to predict the performance of a composite. These are the study of the micromechanics, macromechanics, and a structural analysis. It takes an understanding of each level to gain insight into the performance on a structural scale.

Micromechanics is concerned with each constituent and how the interaction of each material influences the properties. A micromechanics analysis concentrates on local failures of the matrix, fiber, and the fiber/matrix interface [14]. Strength, fatigue, and fracture toughness are greatly influenced at the microscopic level [14]. Also, in this type of analysis, each material is considered individually with their own set of mechanical properties.

Macromechanics is the study of what is happening at the lamina level. Average mechanical properties are used in this analysis and the composite is now considered homogeneous. Failure in this analysis is concerned with average stresses in the lamina and the exact behavior at the fiber/matrix interface is not of concern [14]. However, it can be seen that the average properties used in the macromechanics analysis are greatly influenced by the mircomechanics. If the mechanical properties can be increased in the micromechanics analysis, different average values can be used for mechanical properties in the macromechanics analysis. If laminates are being studied at the macromechanic level, Classical Lamination Plate Theory that deals with the overall behavior of the laminate as a function of the lamina properties is used [14].

At the structural level, Classical Lamination Plate Theory is used along with common techniques such as the finite element method to analyze how a structure will behave [14]. However, it can be seen that the overall structural behavior is dependent on the

interactions at the microscopic level. Imperfections that can be seen and analyzed at the microscopic level will have a large impact on the overall structural behavior.

Both the micromechanics and macromechanics approaches will be looked at in the analysis of jute fiber composites throughout this thesis. The micromechanics approach will use the finite element method to analyze what is happening at the microscopic level while the macromechanics approach will use average mechanical properties assuming the material is orthotropic. Some common material properties that are used for such an analysis are listed below.

- E_1, E_2, E_3 = Modulus of Elasticity
- G_{12}, G_{23}, G_{13} = Shear Modulus
- ν_{12}, ν_{23}, ν_{13} = Poisson's Ratio

This is the ground work for characterizing composites to determine how and when they can be used for structural applications. This thesis will characterize jute composites and look for ways to optimize their performance on both the microscopic and macroscopic levels.

2.3 Microstructural Finite Element Analysis Methods

To help characterize composites without performing experimental testing, the finite element method can be used. The finite element method is a cost effective way to analyze a composite without setting up expensive experiments. A unit cell is the smallest volume cut from a composite that when placed next to other unit cells, creates the entire composite. A unit cell is usually proposed when dealing with a micromechanical model [15]. Representative volume elements are used to bridge the gap between the micro-scale damage (inherent at unit cell) and macroscopic failure (assembly of representative

volume elements to macro-structure) [15]. Figure 4 shows a meshed representative volume element with and without isolated fibers.

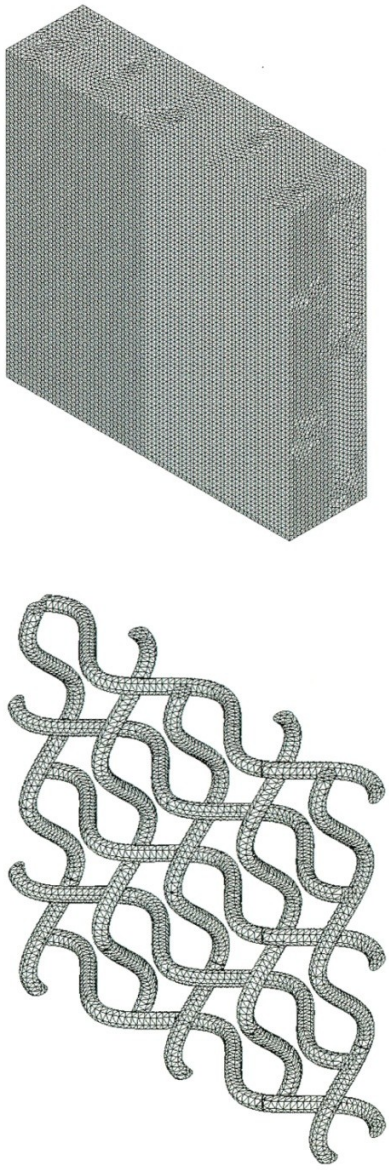

Figure 4: Meshed representative volume element.

A major advantage of micromechanical modeling is the possibility to incorporate damage processes and to follow the progressive degradation of the overall properties [16]. An assembly of unit cells creates a representative volume element and an assembly

of representative volume elements creates the laminate. For many composites, the macrostructure can be seen as a periodic array of a repeated unit cell [17]. This is the case with plain weave composites and textile composites. A unit cell can be thought of as a heterogeneous object of two volumes A and B with two distinct material properties [18]. The fiber volume is subtracted from the matrix volume after which the two are merged together to form the composite [18]. This is shown in Figure 5 where M_A and M_B are the material properties of volume A and volume B, respectively.

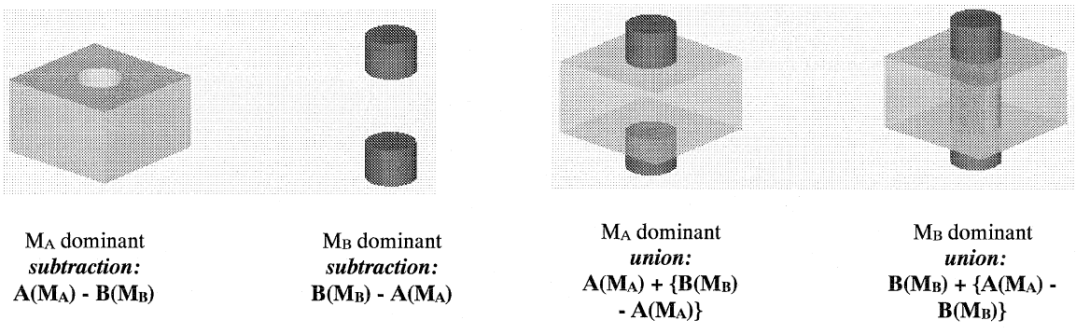

Figure 5: Fiber and matrix subtraction and merging [18].

The models proposed in Figure 5 are the basis for modeling more complex unit cells and representative volume elements which could contain more fibers and different weave patterns. It is also seen in Figure 5 that the solid model of the fibers are circular in cross-section. This is an idealization of the geometry of fiber cross-sections in composites. Woven composite panels show clearly that tows deform and twist due to the weave [19]. Therefore, the semi-axes of the ellipse as well as its orientation in space are variables which are spline-interpolated from nodal values [19]. Typical fiber cross-sections are shown in Figure 6.

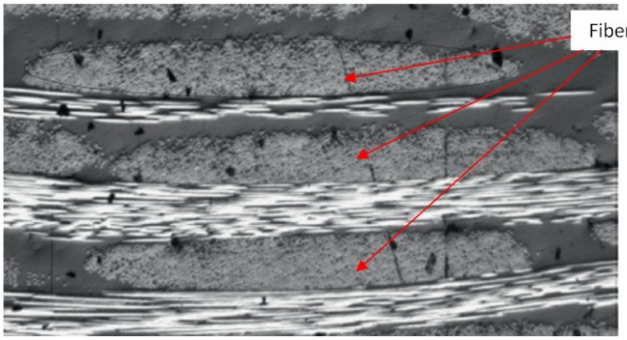

Figure 6: Elliptical cross-sections of fibers [19].

Another aspect that must be accounted for is the path the fiber takes through the composite. A spline comprised of 3rd order polynomials will allow for correct continuities, and maintain a low order for acceptable interpolation errors and algorithm efficiency [19]. This type of approach is an idealization that will make the finite element models easier to mesh.

Meshing of the solid model is then considered. This process allows different material properties to be assigned to the different constituents. Voxel meshing for analysis has many positive features, such as: (1) possibility to automate mesh generation due to regularity of the mesh, (2) ease and possibility to automate application of boundary conditions due to the regularity of node distribution at the boundary, and (3) ease of automation inclusion of defects and deformities within weaves [19].

After meshing, the loads and constraints can be applied. One approach is a "plane-remains-plane" condition. This type of constraint is only valid for symmetrically repeated unit cells subjected to normal tractions [17]. Many researchers have indicated that the "plane-remains-plane" boundary conditions are over-constrained for other types of finite element models that are not symmetrical [17]. A finite element model with proper loads and constraints is shown below in Figure 7.

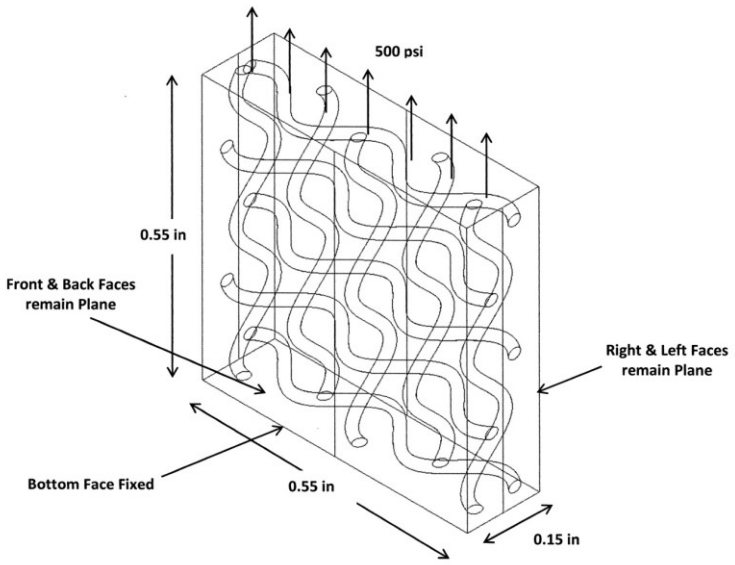

Figure 7: Finite element model with loading and constraints.

2.4 Analytical Method (Classical Lamination Plate Theory and Fiber Undulation Model)

The characterization of jute fiber composites are handled in different ways throughout this thesis. The final technique used to characterize jute composites was analytical modeling using a combined Classical Lamination Plate Theory and fiber undulation model. Analytical models to predict failure of woven composites can be broadly divided into meso- and macro-scale models [20]. Macro-scale models regard the composite as an orthotropic material without any distinction made between the fibers and matrix [20]. The main disadvantage here is that the reinforcement is not modeled explicitly, and actual damage mechanisms are not captured, nor is the physical representation [20]. Meso-scale models represent the geometry of the internal reinforcement explicitly, and failure prediction is usually made using failure criteria applied at the constituent level [20]. Previous work has been done by other researchers (Ishikawa and Chou) to develop three analytical models for two-dimensional woven composites based on Classical Lamination Plate Theory [21]. These models are the

mosaic model, fiber undulation model, and the fiber bridging model [21]. When compared to experimental data, the mosaic model shows appropriate estimates of elastic properties of composites, the tow undulating model is useful for the modeling of plain weave fabrics, and the bridging model is desirable for satin weave fabrics [21]. A meso-scale, tow undulating model using Classical Lamination Plate Theory was applied with mechanical properties being used from physical experimentation. This type of approach helped verify the behavior of the material and the mechanical properties observed through physical testing and finite element analysis because fiber undulation models correlate well with plain weave fabrics. The analytical modeling was set up to calculate the modulus of elasticity of a laminate consisting of four layers. Previous authors assume the load-aligned tow has a sinusoidal shape and mechanical properties are based on this idealization [20]. The modeling parameters are fiber volume ratio, wave amplitude, wavelength, lamina thickness, modulus of elasticity of the fiber and matrix, and the Poisson's ratio of the fiber and matrix. These parameters helped calibrate the tool to match the mechanical properties observed for a specific laminate created for experimental analysis. Once a model was calibrated, parameters were adjusted to study the influence of specific variables which could then be correlated back to experimental evaluation and the finite element analysis.

In this model, the total stiffness of the analytical model is composed of four separate composite layers. Each layer consists of one lamina oriented at a specified angle from the global coordinate axis. The elastic mechanical properties of each layer are obtained by using the rule of mixtures or by experimental measurements to obtain the ply-level properties. Each layer of the composite is considered to be made of a transversely

isotropic material. The crimp effect of the yarns is taken into account by applying the following sinusoidal function [22] [23]:

$$\tan(\beta) = \frac{\pi A}{L}\cos\left(\frac{\pi x'}{L}\right) \quad (1)$$

The local coordinates of an undulating yarn along a ply is defined by the 1-2-3 local coordinates [22]. Two rotations are used for considering the crimp effect and the second set is for the bias angles that are shown in equations 2-6 respectively:

$$\dot{T}_1 = \begin{vmatrix} \cos(\theta)^2 & 0 & \sin(\theta)^2 & 0 & 2\cos(\theta)\sin(\theta) & 0 \\ 0 & 1 & 0 & 0 & 0 & 0 \\ \sin(\theta)^2 & 0 & \cos(\theta)^2 & 0 & -2\cos(\theta)\sin(\theta) & 0 \\ 0 & 0 & 0 & \cos(\theta) & 0 & -\sin(\theta) \\ -\cos(\theta)\sin(\theta) & 0 & \cos(\theta)\sin(\theta) & 0 & \cos(\theta)^2 - \sin(\theta)^2 & 0 \\ 0 & 0 & 0 & \sin(\theta) & 0 & \cos(\theta) \end{vmatrix} \quad (2)$$

$$\dot{T}_2 = \begin{vmatrix} \cos(\theta)^2 & 0 & \sin(\theta)^2 & 0 & \cos(\theta)\sin(\theta) & 0 \\ 0 & 1 & 0 & 0 & 0 & 0 \\ \sin(\theta)^2 & 0 & \cos(\theta)^2 & 0 & -\cos(\theta)\sin(\theta) & 0 \\ 0 & 0 & 0 & \cos(\theta) & 0 & -\sin(\theta) \\ -2\cos(\theta)\sin(\theta) & 0 & 2\cos(\theta)\sin(\theta) & 0 & \cos(\theta)^2 - \sin(\theta)^2 & 0 \\ 0 & 0 & 0 & \sin(\theta) & 0 & \cos(\theta) \end{vmatrix} \quad (3)$$

The stress-strain relation can be obtained by using the average transformed local stiffness calculated over one wave-length [23]:

$$\{\sigma\} = \frac{1}{2l}\int_0^{2l}[\dot{T}_1]^{-1}[C][\dot{T}_2]dx\{\epsilon\} \quad (4)$$

The second rotation is given by [22]:

$$T_1 = \begin{vmatrix} \cos(\theta)^2 & \sin(\theta)^2 & 0 & 0 & 0 & 2\cos(\theta)\sin(\theta) \\ \sin(\theta)^2 & \cos(\theta)^2 & 0 & 0 & 0 & -2\cos(\theta)\sin(\theta) \\ 0 & 0 & 1 & 0 & 0 & 0 \\ 0 & 0 & 0 & \cos(\theta) & -\sin(\theta) & 0 \\ 0 & 0 & 0 & \sin(\theta) & \cos(\theta) & 0 \\ -\cos(\theta)\sin(\theta) & \cos(\theta)\sin(\theta) & 0 & 0 & 0 & \cos(\theta)^2 - \sin(\theta)^2 \end{vmatrix} \quad (5)$$

$$T_2 = \begin{vmatrix} \cos(\theta)^2 & \sin(\theta)^2 & 0 & 0 & 0 & \cos(\theta)\sin(\theta) \\ \sin(\theta)^2 & \cos(\theta)^2 & 0 & 0 & 0 & -\cos(\theta)\sin(\theta) \\ 0 & 0 & 1 & 0 & 0 & 0 \\ 0 & 0 & 0 & \cos(\theta) & -\sin(\theta) & 0 \\ 0 & 0 & 0 & \sin(\theta) & \cos(\theta) & 0 \\ -2\cos(\theta)\sin(\theta) & 2\cos(\theta)\sin(\theta) & 0 & 0 & 0 & \cos(\theta)^2 - \sin(\theta)^2 \end{vmatrix} \quad (6)$$

The stress-strain relation in the global stiffness axes is given as [23]:

$$\{\sigma\} = [T_1]^{-1}[\overline{C}][T_2]\{\epsilon\} \quad (7)$$

where $[\overline{C}]$ is the stiffness matrix obtained from rotation around the y-axis. After calculating the stiffness matrix of each layer, the stiffness matrix of the entire composite can be determined as [23]:

$$[C^{RUC}] = t^{+\theta}[C_{global}]^{+\theta} + t^{-\theta}[C_{global}]^{-\theta} + t^{0}[C_{global}]^{0} \quad (8)$$

where $t^{+\theta}$, $t^{-\theta}$ and t^0 are specified as the thickness of each layer to the thickness of the laminate. Equation 8 is set up for a braided tri-axial composite. Since the composite used in the analytical modeling for this thesis have four layers, an additional term must be added to equation 8 to account for the additional layer. Previous studies [23] have considered all layer thicknesses to be equal, however, in this thesis actual thickness values obtained from microstructural examinations are used.

3. Mechanical Characterization

3.1 Manufacturing and Classifying Recycled Materials

The natural composite fibers used in this research were obtained from recycled jute fiber woven bags used to transport coffee beans from the production sites. As a result of using recycled products, the production of the fabric was not controlled to be used as a structural member in a natural composite. Therefore, classifying different jute fabric is the best way of characterizing the different options available.

After obtaining burlap sacks at random, two different plain weave patterns were observed. One weave had considerably more fibers packed into the fabric than the other. The two weave densities are shown in Figure 8.

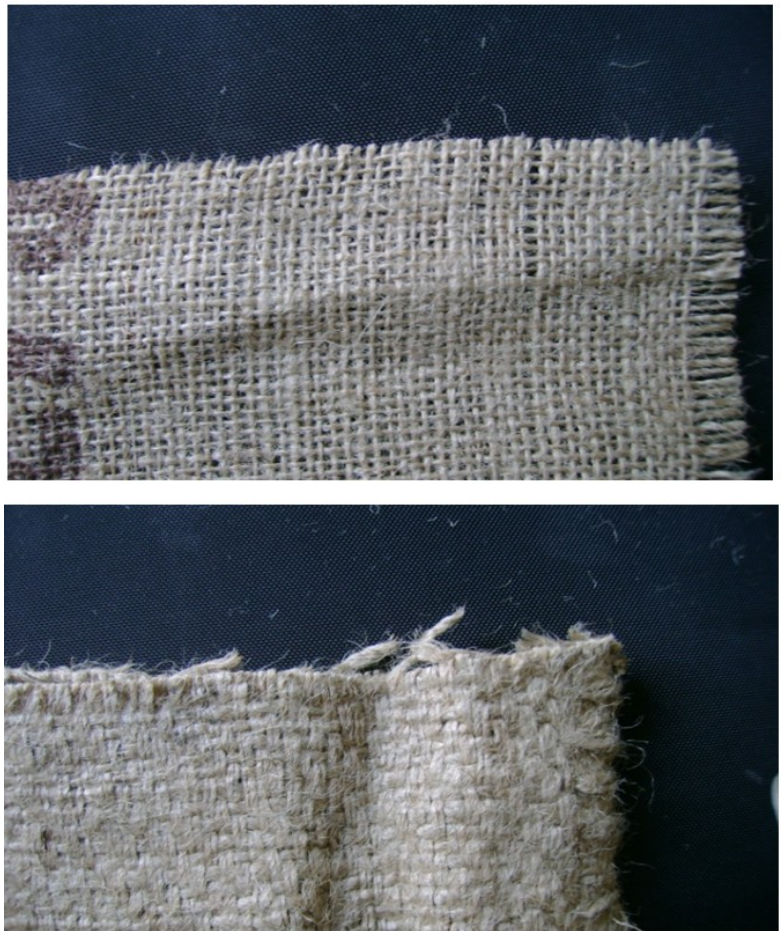

Figure 8: Two different jute fabric densities.

The fabrics have different densities but share the same weave pattern. They are both plain weave fabrics which correlate to each yarn being interlaced over every other yarn in the opposite direction. However, each sack has different amounts of fibers per yarn, and different amounts of yarns per unit length which corresponds to different densities. The less dense fabric was denoted as "Fabric A" and the more dense fabric was denoted as "Fabric B". The two different fabrics were classified based on their densities and mass per area. Five measurements of each were taken with the average being the accepted value. Aside from density, another useful physical property is the mass per area (oz/yd^2). This is important for comparing different natural fabrics obtained for this project to fabrics already being used in the industry. The industry has adapted to identifying different fabrics by their mass per area instead of the fabrics density. Table 3 and Table 4 show the properties for Fabric A and Fabric B, respectively. Also, Figure 9 and Figure 10 show the densities and mass per area with the standard deviations, respectively.

Table 3: Properties of Fabric A.

Fabric A				
Sample	Mass (oz)	Density (oz/in^3)	Area (yd^2)	Mass/Area (oz/yd^2)
1	0.81	0.23	0.11	7.30
2	0.83	0.23	0.11	7.46
3	0.81	0.23	0.11	7.30
4	0.79	0.22	0.11	7.14
5	0.81	0.23	0.11	7.30
Average	**0.81**	**0.23**	**0.11**	**7.30**
Standard Deviation	**0.01**	**0.01**	**0.00**	**0.11**
Coefficient of Variation	**0.02**	**0.02**	**0.00**	**0.02**

Table 4: Properties of Fabric B.

Fabric B				
Sample	Mass (oz)	Density (oz/in^3)	Area (yd^2)	Mass/Area (oz/yd^2)
1	1.57	0.26	0.11	14.13
2	1.43	0.29	0.11	12.86
3	1.36	0.31	0.11	12.22
4	1.66	0.23	0.11	14.92
5	1.66	0.26	0.11	14.92
Average	**1.53**	**0.27**	**0.11**	**13.81**
Standard Deviation	**0.14**	**0.03**	**0.00**	**1.22**
Coefficient of Variation	**0.09**	**0.11**	**0.00**	**0.09**

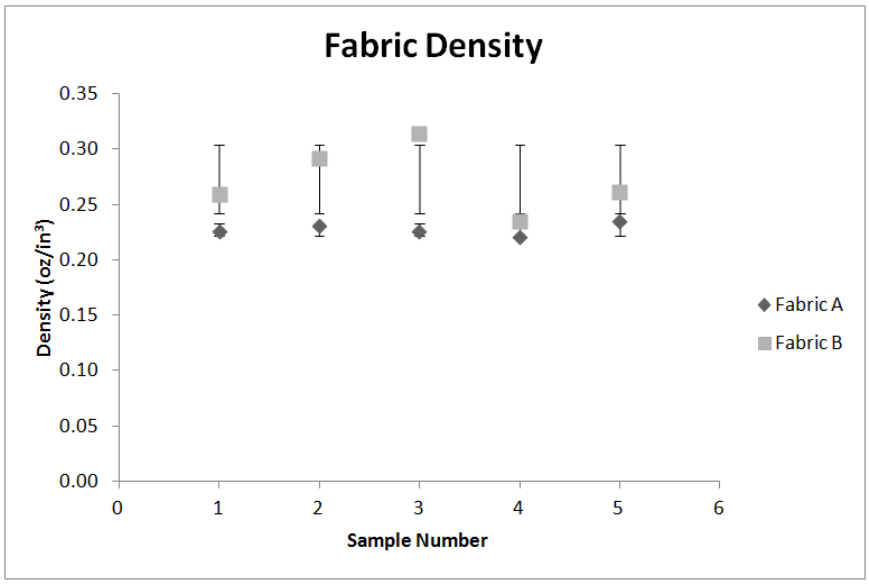

Figure 9: Fabric A & Fabric B densities with standard deviations.

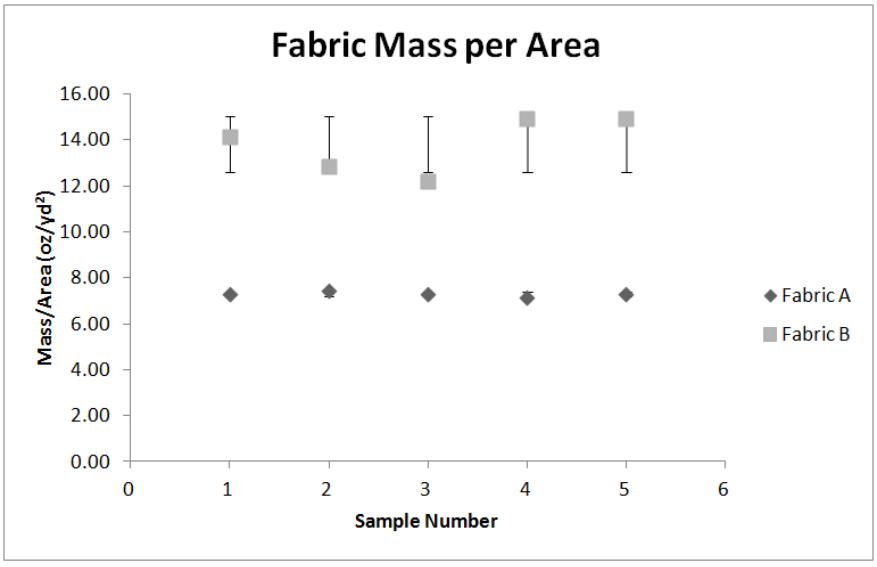

Figure 10: Fabric A & Fabric B mass per area with standard deviations.

To classify any given jute fabric into one of the two categories, a sample must be taken to measure its mass per area. The sample can then be classified into Fabric A or Fabric B if the mass per area measurement comes within two standard deviations of the mean value. This will capture approximately 95% of the data.

3.2 Fiber Bundle Testing

In order to perform a finite element analysis, the material properties for the individual constituents must be determined. Common properties applied to cured resin can be determined via literature however, the modulus of elasticity for jute fiber bundles must be determined through experimentation. To obtain the modulus of elasticity for jute fiber bundles, 11 different tensile tests were performed in accordance with ASTM Standard D3822-07 [24] (Standard Test Method for Tensile Properties of Single Textile Fibers). The tensile testing was done in the UW-Milwaukee Mechanics of Materials lab on the Instron 3369 machine (Dual Column Tabletop Universal Testing System) with a load cell capacity of 11,250 lb (50 kN). To perform the analysis, fiber bundles from Fabric A were cut into 10 inch pieces and fastened to a cardboard backing. The cardboard backing is used to provide support for the fiber bundles near the clamps and it also helps prevent failure from occurring near the clamps due to fiber pull out. To create samples with the same 10 inch gauge length, a large piece of cardboard must be obtained from which 10 inch slots can be cut out. The fiber bundles were then placed over the hole in one inch increments and fastened in place with epoxy. The ten inch hole ensures that each fiber bundle had the same gauge length. A representative specimen is shown in Figure 11.

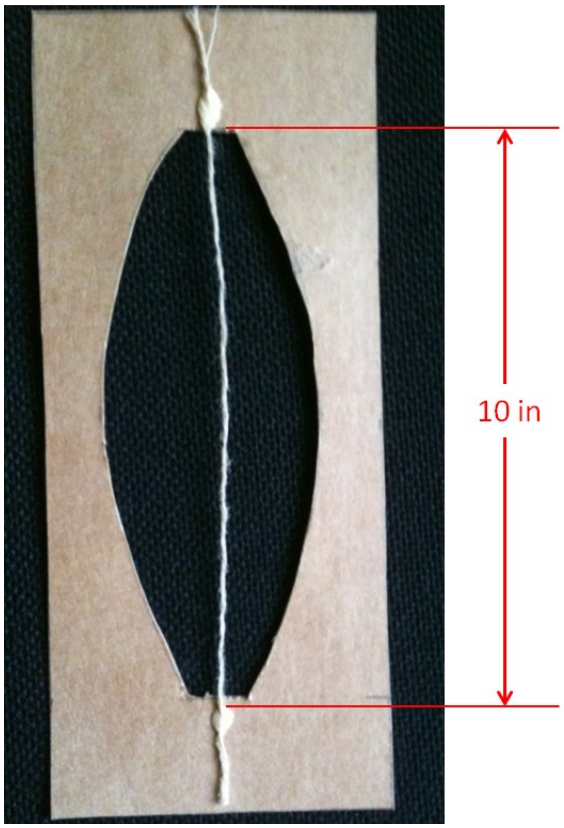

Figure 11: Fiber bundle test specimen.

The specimen was then mounted into the Instron 3369 and was fastened to the clamps. Once fastened to the clamps, the cardboard was cut so only the fiber bundles were tested. The machine was set up to apply a constant rate of extension. ASTM D3822-07 gives guidelines on the rate of extension that should be applied for an estimated elongation at break. The three different categories used for extension rates are 'Under 8%', '8% to 100%', and 'Over 100%' [24]. Since jute fibers are relatively stiff, an extension rate that corresponds to 'Under 8%' elongation was used. This corresponds to a constant rate of extension of 10% of the initial gauge length per minute [24]. Since the initial gauge lengths were 10 inches, a constant rate of extension was applied at 1 inch per minute.

After all the data was acquired, it was analyzed to determine the initial modulus as stated in ASTM D3822-07 [24]. The initial modulus is determined by finding the largest slope of any line that is tangent to the stress-strain curve. The data was obtained through testing for extension and load every tenth of a second. These data points were converted to strain and stress by dividing the extension and load by gauge length and cross-sectional area, respectively. Therefore a large number of stress-strain data points exist with no particular equation to obtain an initial modulus from. However, the slope at any point can be found by finding the slope of an interval directly to the left of the point and averaging it with the slope of an interval directly to the right of the point. The starting interval used for this analysis was 1 second. Since the data points do not follow a smooth curve, the slope at the same point is found in the same manner, except now the interval is extended to 2 seconds. An approximate error can be determined because there are two initial modulus calculations for one data point. If the error is greater than 5%, the slope at the same point is obtained using an interval of 3 seconds. This process was done until two consecutive approximate error measurements of less than 5% were obtained. Using this process, the slope at any one point can be captured using a numerical method approach. In the end, a command was used to extract the maximum slope for all data points using this method. For the eleven different specimens tested, the results for the initial modulus are shown in Table 5 and Figure 12.

Table 5: Initial modulus of jute fiber bundles.

Specimen	Initial Modulus (psi)
Fiber 1	407,479
Fiber 2	336,593
Fiber 3	346,253
Fiber 4	367,632
Fiber 5	344,723
Fiber 6	341,457
Fiber 7	366,218
Fiber 8	350,157
Fiber 9	345,076
Fiber 10	338,215
Fiber 11	346,444
Average	**353,659**
Standard Deviation	**20,496**
Coefficient of Variation	**0.058**

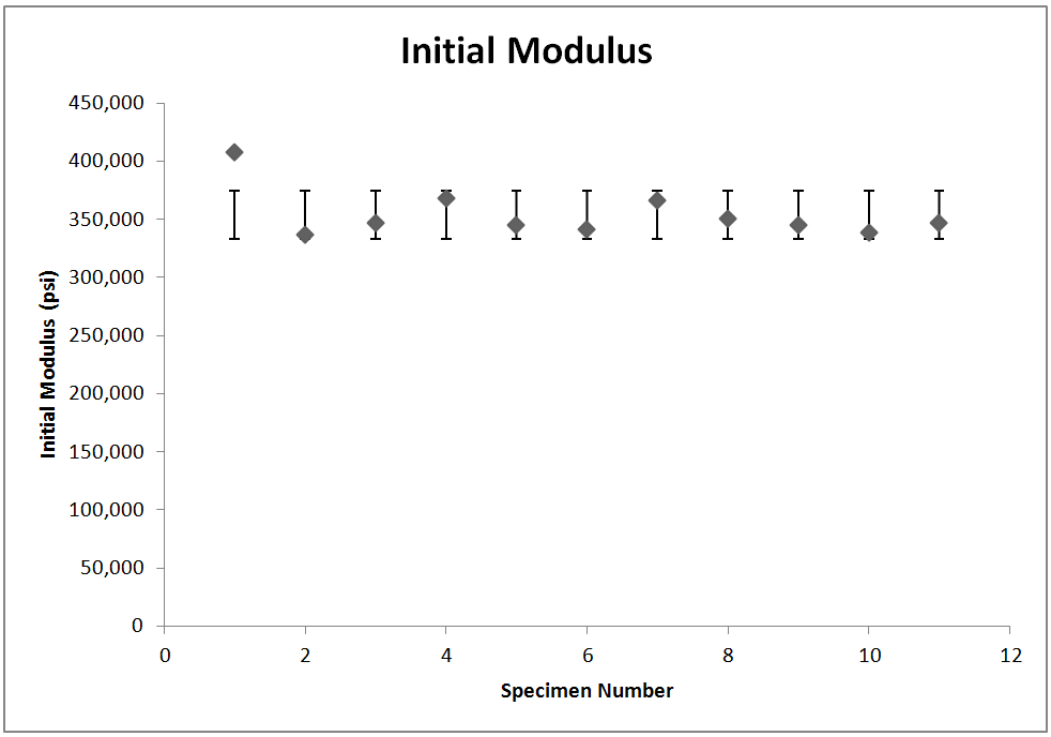

Figure 12: Initial modulus of jute fiber bundles.

The average value obtained from fiber bundle testing was used as the value for the modulus of elasticity for the fibers in the finite element analysis. This value is 353,659

psi. The modulus of elasticity for the matrix used in the finite element analysis was a value taken from literature and will be specified in the 'Finite Element Analysis' section.

3.3 Lamina/Laminate Testing

The goal of this study was to determine the strength of different laminates made from jute fabric. These tests helped characterize the natural fibers on a macroscopic scale giving useful global mechanical properties. The result of this testing gave modulus of elasticity values for different laminates in the longitudinal and transverse directions. A sample of a tension test coupon and panel is shown in Figure 13.

Figure 13: Tension test coupon and panel.

Each of the laminates were made from different combinations of Fabric A and Fabric B material. First, 12 in^2 pieces of Fabric A or Fabric B were cut out depending on the type of laminate being created. The jute fiber bundles ran longitudinally, transversely, or diagonally depending on the angle of the specific ply. From here, lamina were placed on top of each other in the order specified by the type of laminate. The fabric making up the laminate was then placed on non-stick plastic on a smooth surface in preparation for the resin to be poured. This is shown in Figure 14.

Figure 14: Creation of a laminate.

After the resin was poured and distributed evenly throughout the laminate, another piece of non-stick plastic was placed on top of the laminate. The non-stick plastic was used as protection from the environment and foreign objects. After the laminate was protected, a 100 pound force was applied evenly on top of the laminate. The force applied to the laminate serves a couple purposes: (1) it further distributes the resin throughout the laminate to decrease resin pooling and dry pockets, (2) it compresses the laminate to increase the fiber volume ratio, and (3) it helps standardize the conditions that each of the laminates were cured with.

The resin used in the laminates was polyester. This resin was chosen because of its accessibility and compatibility with natural fibers. The mechanical properties of polyester resin is also established in literature which means results from physical testing should be easier to correlate back to analytical and numerical models.

Below is a description of each laminate and the results from each tensile test. Table 12 and Table 13 at the end of this section compare the mechanical properties and strength for each layup.

Layup 1 ($0°_B$, $45°_A$, $0°_B$)

Layup 1 was configured with two Fabric B lamina and one Fabric A lamina. The layers from bottom to top are: 0° Fabric B, 45° Fabric A, 0° Fabric B. This is shown in Figure 15. The average mechanical properties obtained from tension testing are listed in Table 6.

Figure 15: Layup 1 ($0°_B$, $45°_A$, $0°_B$).

Table 6: Average mechanical properties of Layup 1.

Layup 1		
Modulus of Elasticity(psi)	Ultimate Stress (psi)	Ultimate Load (lbs)
E_1 = 975,592	σ_1 = 4,203	P_1 = 619
E_2 = 626,025	σ_2 = 4,279	P_2 = 628

Figure 16 shows a microscopic image of a cross-section of Layup 1. This image shows evidence of voids within the matrix along with other discontinuities. The image was generated using a 2.25 magnification factor. Areas on the image that appear white are due to light reflecting off the fibers that are exposed to the surface.

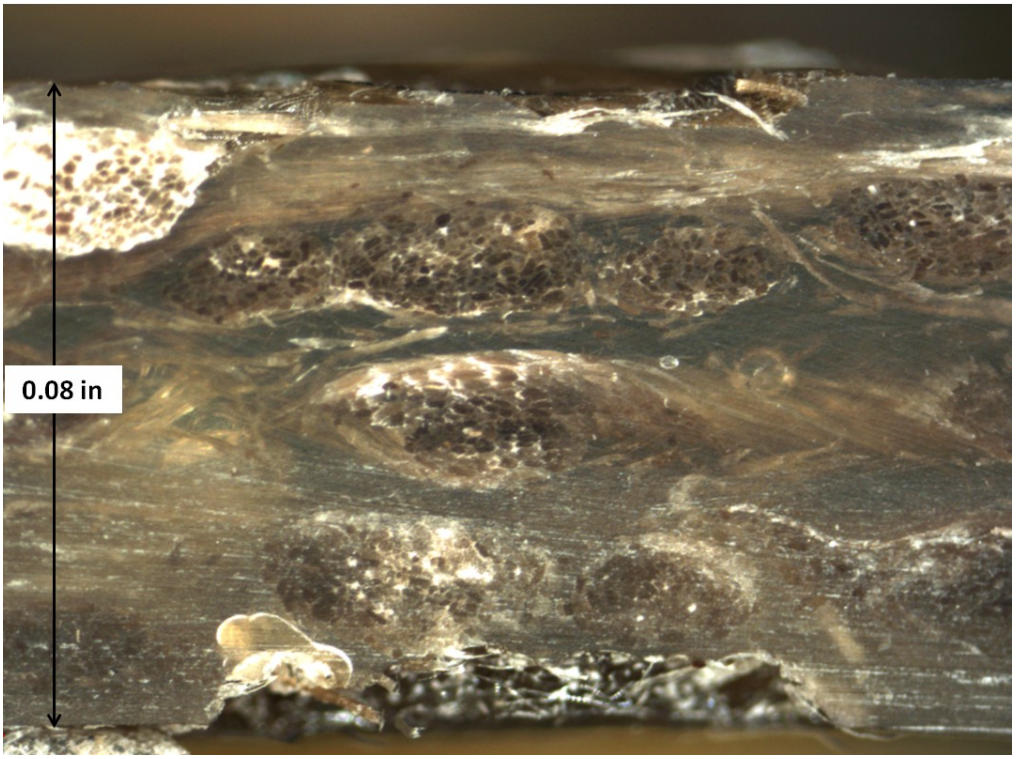

Figure 16: Microscopic view of Layup 1.

Layup 2 ($0°_A$, $45°_A$, $0°_A$)

Layup 2 was configured with three Fabric A lamina. The layers from bottom to top are: 0° Fabric A, 45° Fabric A, 0° Fabric A. This is shown in Figure 17. The average mechanical properties obtained from tension testing are listed in Table 7.

Figure 17: Layup 2 ($0°_A$, $45°_A$, $0°_A$).

Table 7: Average mechanical properties of Layup 2.

Layup 2		
Modulus of Elasticity(psi)	Ultimate Stress (psi)	Ultimate Load (lbs)
E_1 = 661,604	σ_1 = 3,811	P_1 = 521
E_2 = 499,005	σ_2 = 4,640	P_2 = 476

Figure 18 shows a microscopic image of a cross-section of Layup 2. This image shows evidence of discontinuities within the matrix. It also shows a variation in composite thickness from one side of the image to the other. Fibers in the upper, right location of the image appear not to have been completely saturated by resin during curing. This is one of the concerns when dealing with dry, coarse fibers. The image was generated using a 2.25 magnification factor.

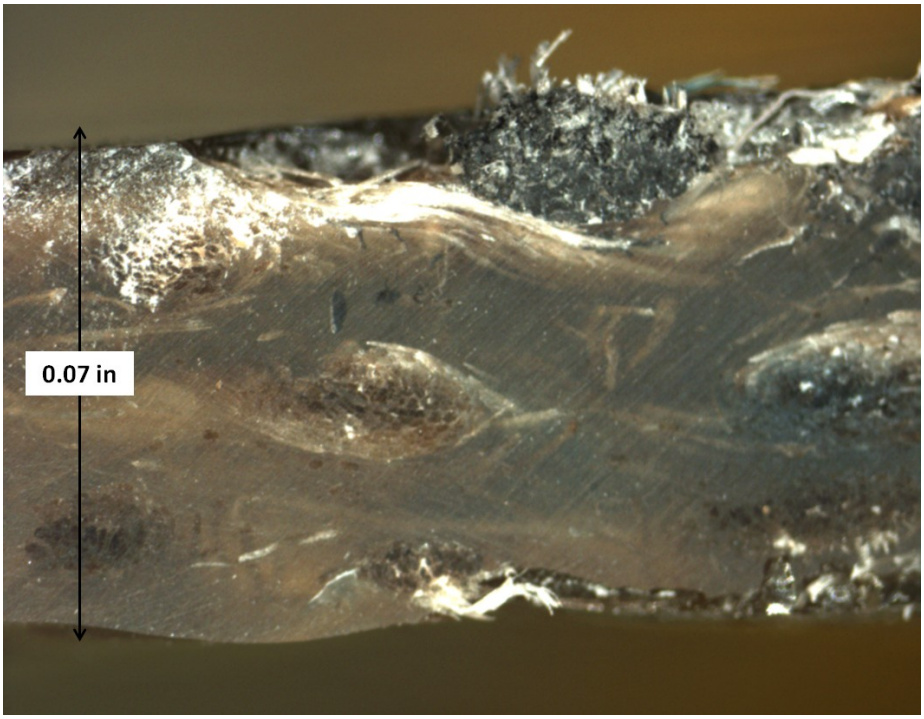

Figure 18: Microscopic view of Layup 2.

Layup 3 ($0°_B$)

Layup 3 was configured with one Fabric B lamina. There is only one biaxial layer with fibers running in the longitudinal and transverse directions. This is shown in Figure 19. The average mechanical properties obtained from tension testing are listed in Table 8.

Figure 19: Layup 3 ($0°_B$).

Table 8: Average mechanical properties of Layup 3.

Layup 3		
Modulus of Elasticity(psi)	Ultimate Stress (psi)	Ultimate Load (lbs)
E_1 = 255,425	σ_1 = 3,541	P_1 = 232
E_2 = 171,462	σ_2 = 3,165	P_2 = 188

Figure 20 shows a microscopic image of a cross-section of Layup 3. This image shows evidence of discontinuities within the matrix. This image also shows the sinusoidal nature of the fiber bundles as they run through the composite. The jute fiber bundle appears lighter than the matrix due to the reflection of light. This image was generated using a 2.25 magnification factor.

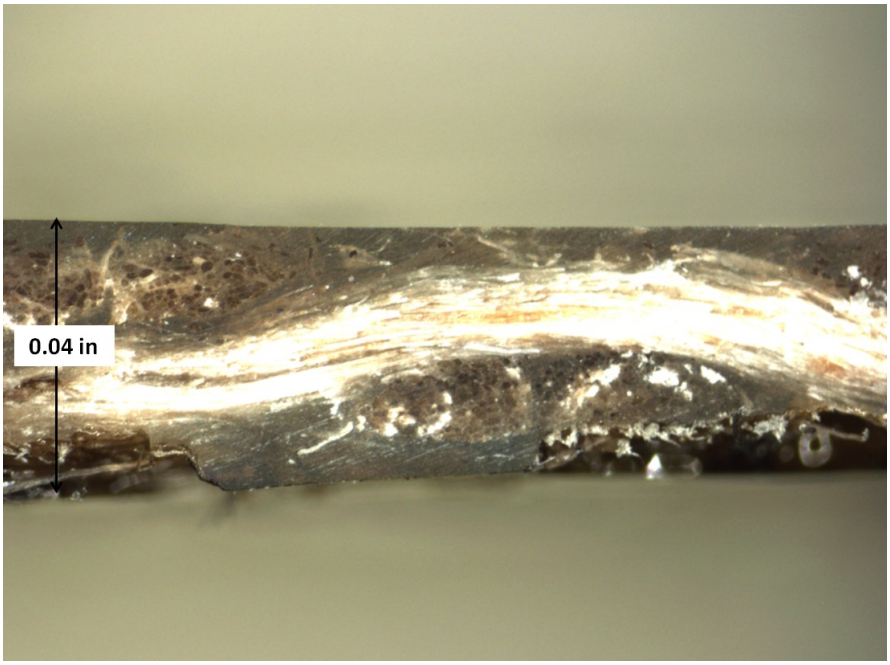

Figure 20: Microscopic view of Layup 3.

Layup 4 ($0°_A$, $45°_A$)

Layup 4 was configured with two Fabric A lamina. The layers from bottom to top are: 0° Fabric A, 45° Fabric A. This is shown in Figure 21. The average mechanical properties obtained from tension testing are listed in Table 9.

Figure 21: Layup 4 ($0°_A$, $45°_A$).

Table 9: Average mechanical properties of Layup 4.

Layup 4		
Modulus of Elasticity(psi)	Ultimate Stress (psi)	Ultimate Load (lbs)
E_1 = 342,884	σ_1 = 3,862	P_1 = 294
E_2 = 209,402	σ_2 = 2,478	P_2 = 211

Figure 22 shows a microscopic image of a cross-section of Layup 4. This image shows evidence of matrix voids however, there appears to be less discontinuity when compared to the previous layups. Parts of the composite that appear to be "grainy" are the jute fibers on the surface of this particular cross-section. The image was generated using a 2.25 magnification factor.

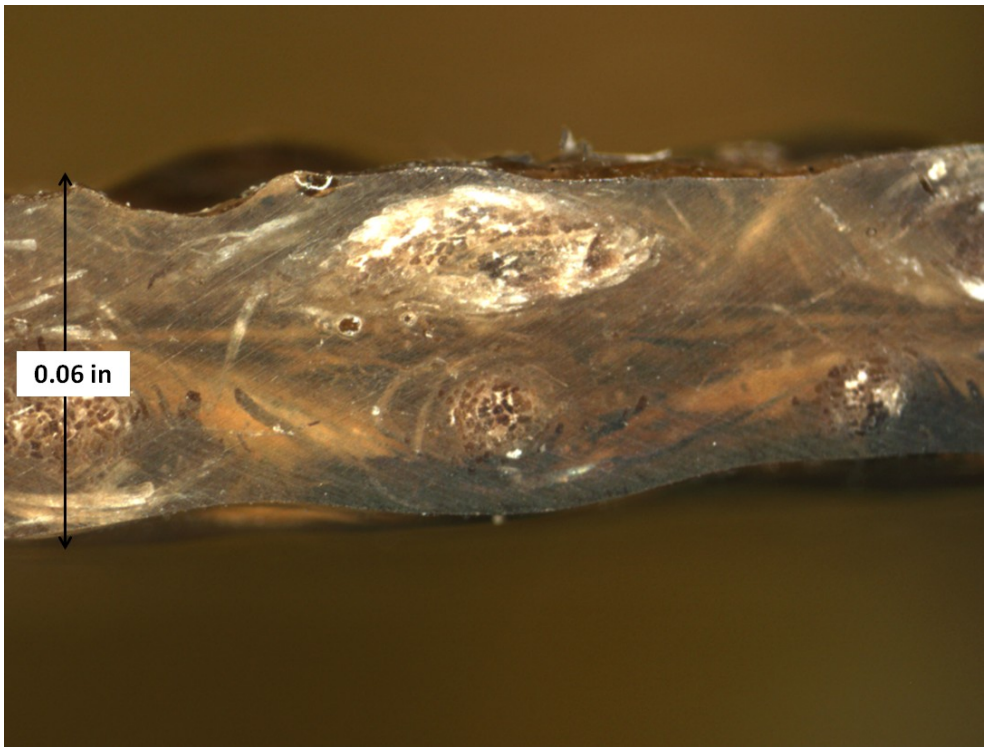

Figure 22: Microscopic view of Layup 4.

Layup 5 ($0°_A$, $0°_A$)

Layup 5 was configured with two Fabric A lamina. The layers from bottom to top are: 0° Fabric A, 0° Fabric A. This is shown in Figure 23. The average mechanical properties obtained from tension testing are listed in Table 10.

Figure 23: Layup 5 ($0°_A$, $0°_A$).

Table 10: Average mechanical properties of Layup 5.

Layup 5		
Modulus of Elasticity(psi)	Ultimate Stress (psi)	Ultimate Load (lbs)
E_1 = 371,610	σ_1 = 5,294	P_1 = 431
E_2 = 307,012	σ_2 = 4,557	P_2 = 393

Figure 24 shows a microscopic image of a cross-section of Layup 5. This image shows evidence of air pockets within the matrix. Parts of the composite that appear to be "grainy" are the jute fibers on the surface of this particular cross-section. The image was generated using a 2.25 magnification factor.

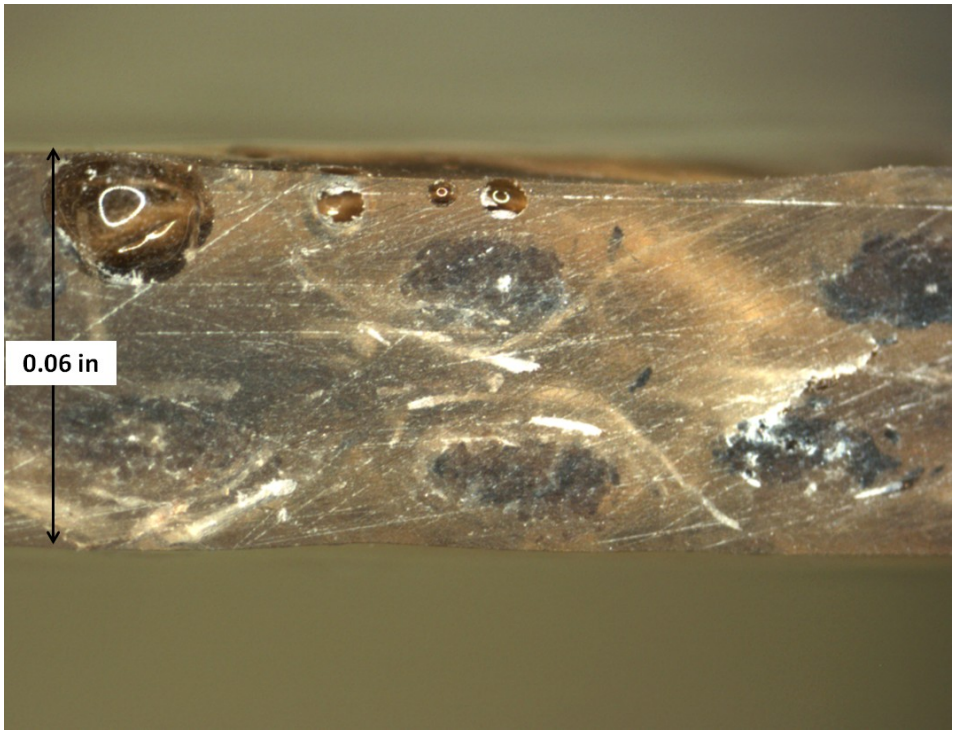

Figure 24: Microscopic view of Layup 5.

Fiberglass/Polyester Composite

The fiberglass/polyester composite used for this project contained one plain weave E-glass lamina with a mass per area of 6 oz/yd^2. This is shown in Figure 25. The average mechanical properties obtained from tension testing are listed in Table 11.

Figure 25: Fiberglass/polyester composite.

Table 11: Average mechanical properties of fiberglass/polyester composite.

Fiberglass/Polyester Composite		
Modulus of Elasticity(psi)	Ultimate Stress (psi)	Ultimate Load (lbs)
E_1 = 948,047	σ_1 = 20,006	P_1 = 364
E_2 = 918,770	σ_2 = 21,652	P_2 = 325

Comparison

The microscopic views of the laminates show a different side of the experimental evaluation. Wettability was a major factor in creating each of the laminates. The extent of this became evident under the microscope when a number of voids were observed. Each of these voids caused weaknesses throughout the laminate. The elimination of such voids would greatly improve the mechanical properties of the laminates.

These voids can cause major problems when predicting failure and are not a desirable characteristic to have in any composite. The voids present in the laminates made up for this research were likely the product of the manufacturing process. If the laminates would have been made in a press or using vacuum resin infusion, the number of voids per laminate would have been reduced which would correlate to higher tensile properties.

The finite element analysis takes a closer look at how these imperfections influence the composite.

The results of mechanical properties are presented in Table 12 for comparison. Each coupon is labeled with two numbers. The first number indicates the longitudinal or transverse direction (1 or 2) and the second number identifies between each coupon (coupon 1, coupon 2, or coupon 3). The properties that were calculated are the modulus of elasticity (E), longitudinal specific modulus, longitudinal specific strength, and density. All properties are compared to the biaxial fiberglass lamina with a mass per area of 6 oz/yd^2.

Table 12: Comparison of mechanical properties.

	Layup 1	**Layup 2**	**Layup 3**	**Layup 4**	**Layup 5**	**Fiberglass**
Density (lb/yd^3)	2,016	2,013	1,591	1,654	1,731	2,800
Specific Modulus (yd^2/s^2) (Longitudinal)	6,724,553	4,567,695	2,231,582	2,883,070	2,982,578	4,708,146
Specific Strength (lb_f*yd/lb_m) (Longitudinal)	2,701	2,454	2,885	3,028	3,962	9,264
oz/yd^2	36	22	14	15	15	6
E_{11} (psi)	1,356,123	620,977	266,381	384,372	393,674	932,356
E_{12} (psi)	376,575	702,230	288,916	289,138	371,639	963,737
E_{13} (psi)	1,194,078	-	210,977	355,141	349,517	-
E_1 Avg. (psi)	**975,592**	**661,604**	**255,425**	**342,884**	**371,610**	**948,047**
Standard Dev.	**525,053**	**57,455**	**40,108**	**48,786**	**22,079**	**22,190**
Coef. of Variation	**0.54**	**0.09**	**0.16**	**0.14**	**0.06**	**0.02**
E_{21} (psi)	711,749	402,418	200,191	266,316	334,853	900,927
E_{22} (psi)	556,282	595,592	197,246	185,232	288,656	936,612
E_{23} (psi)	610,044	-	116,949	176,659	297,526	-
E_2 Avg. (psi)	**626,025**	**499,005**	**171,462**	**209,402**	**307,012**	**918,770**
Standard Dev.	**78,956**	**136,595**	**47,233**	**49,475**	**24,516**	**25,233**
Coef. of Variation	**0.13**	**0.27**	**0.28**	**0.24**	**0.08**	**0.03**

The densities for the natural composite laminates are all lower than the fiberglass laminate. This is a desirable property in which natural fiber composites have the

advantage. The specific modulus for each layup varied with the highest value coming from Layup 1. The specific strengths of the natural fiber composites were all below the fiberglass. The highest natural fiber composite specific strength came from Layup 5. The specific strength of the fiberglass laminate is about 2.3 times higher than this value. The modulus of elasticity varied between each of the different laminates. In general, the fiberglass/polyester composite had the highest modulus of elasticity with exception of the longitudinal modulus of elasticity for Layup 1. Figure 26 shows the average modulus of elasticity for each of the natural fiber composites. In general, the composites with more layers and greater thickness had higher modulus of elasticity values due to the increased fibers in the longitudinal direction.

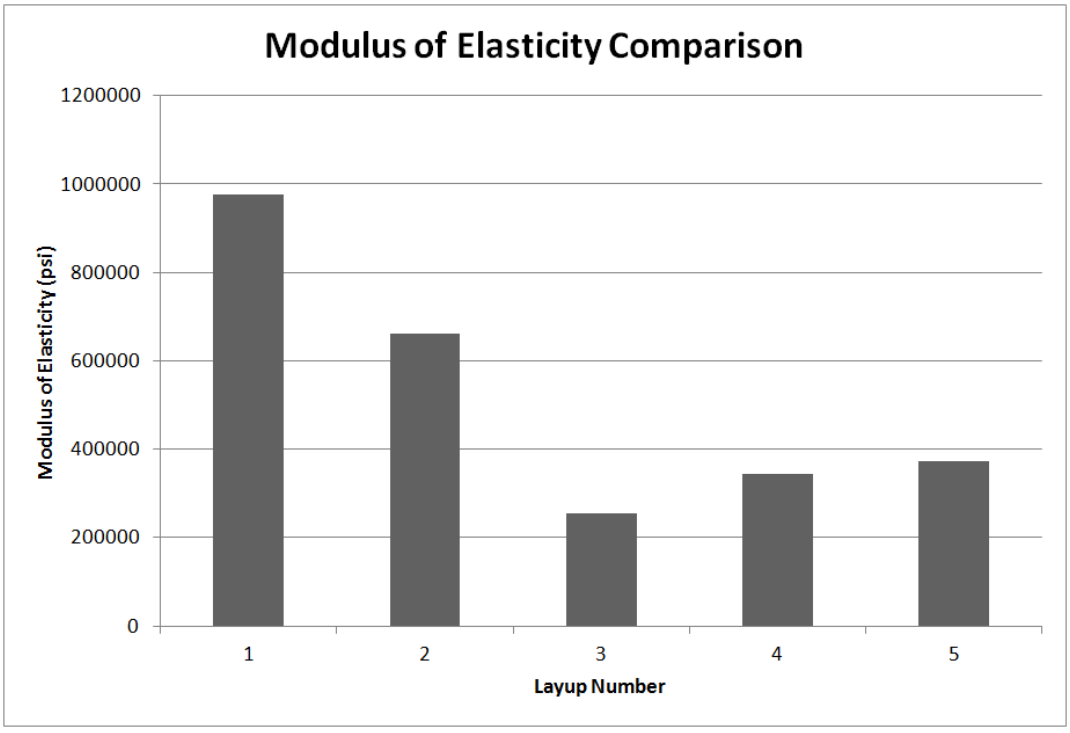

Figure 26: Modulus of elasticity comparison.

The results of strength are presented in Table 13 for comparison. Each coupon is labeled with two numbers. The first number indicates the longitudinal or transverse direction (1 or 2) and the second number identifies between each coupon (coupon 1,

coupon 2, or coupon 3). The properties that were calculated are the ultimate stresses (U.S.) and the ultimate loads (U.L). All properties are compared to the biaxial fiberglass lamina with a mass per area of 6 oz/yd^2.

Table 13: Comparison of ultimate strength values.

	Layup 1	Layup 2	Layup 3	Layup 4	Layup 5	Fiberglass
$U.S._{11}$ (psi)	4,760	4,228	4,072	4,626	5,837	20,210
$U.S._{12}$ (psi)	3,496	3,395	2,928	3,462	5,300	19,802
$U.S._{13}$ (psi)	4,353	-	3,625	3,498	4,745	-
$U.S._1$ Avg. (psi)	**4,203**	**3,811**	**3,541**	**3,862**	**5,294**	**20,006**
Standard Dev.	**645**	**589**	**576**	**662**	**546**	**288**
Coef. of Variation	**0.15**	**0.15**	**0.16**	**0.17**	**0.10**	**0.01**
$U.S._{21}$ (psi)	4,515	4,542	3,358	2,284	5,209	22,255
$U.S._{22}$ (psi)	4,461	4,737	3,625	2,921	3,593	21,049
$U.S._{23}$ (psi)	3,861	-	2,513	2,229	4,870	-
$U.S._2$ Avg. (psi)	**4,279**	**4,640**	**3,165**	**2,478**	**4,557**	**21,652**
Standard Dev.	**363**	**138**	**580**	**385**	**852**	**853**
Coef. of Variation	**0.08**	**0.03**	**0.18**	**0.16**	**0.19**	**0.04**
$U.L._{11}$ (lbs)	657	554	299	352	479	308
$U.L._{12}$ (lbs)	503	489	179	244	460	420
$U.L._{13}$ (lbs)	697	-	218	285	356	-
$U.L._1$ Avg. (lbs)	**619**	**521**	**232**	**294**	**431**	**364**
Standard Dev.	**102**	**46**	**61**	**54**	**66**	**79**
Coef. of Variation	**0.16**	**0.09**	**0.26**	**0.19**	**0.15**	**0.22**
$U.L._{21}$ (lbs)	609	432	191	201	444	331
$U.L._{22}$ (lbs)	669	521	213	234	305	319
$U.L._{23}$ (lbs)	606	-	158	198	429	-
$U.L._2$ Avg. (lbs)	**628**	**476**	**188**	**211**	**393**	**325**
Standard Dev.	**36**	**63**	**28**	**20**	**76**	**8**
Coef. of Variation	**0.06**	**0.13**	**0.15**	**0.09**	**0.19**	**0.03**

The ultimate stresses of the natural fiber composites were all below the fiberglass/polyester composite. This was anticipated and was compensated for by using additional lamina for the natural fiber laminates to increase strength. The ultimate load calculations are very important. Since it is known that the ultimate stresses of jute fibers are below fiberglass, which is a property that cannot be changed, we can look at the

ultimate loads as another way to compare the strengths i.e. ultimate loads can be controlled more than ultimate stresses by adding more layers. If there is an ultimate load of a natural laminate that compares well with the ultimate load of the fiberglass, it should be expected that the natural laminate could take the place of the fiberglass composite. The ultimate loads varied from laminate to laminate with Layup 5 being the best match for the fiberglass.

4. Finite Element Analysis

4.1 Control Geometry

The finite element analysis was used to compare the influence different imperfections had on natural fiber composites. Two different material properties based on the constituents that make up the composite were applied to each model. The modulus of elasticity for the jute fiber bundles were obtained from the previous section in 'Fiber Bundle Testing'. The average value from fiber bundle testing is the value used in the finite element analysis (353,659 psi). The modulus of elasticity for the polyester resin is taken from literature [6]. Table 14 shows the values for the fiber and matrix used in this analysis. Modulus of rigidity values were obtained by using relations relating the modulus of elasticity and Poisson's ratio to the modulus of rigidity.

Table 14: Mechanical properties of fibers and matrix [6].

Material	Modulus of Elasticity (psi)	Poisson's Ratio	Modulus of Rigidity (psi)
Fiber Bundle	353,659	0.30	136,023
Polyester Resin	145,038	0.35	53,718

The finite element analysis used different geometries to evaluate the behavior at the microscopic level. A control geometry was used based on the actual composite laminates that were previously made. The control geometry was assumed to be free of imperfections and each fiber bundle was assumed to be a perfect sinusoidal wave with a wavelength of approximately 0.24 inches and amplitude of approximately 0.04 inches. A value of 0.02 inches was used as an approximation for the diameter of each fiber bundle based on the measured diameter in the microscopic views. Once results for the control geometry were obtained, the geometry was altered to simulate different imperfections (addition of voids, change in sine wave function, and addition of fiber damage). Figure 27 shows a schematic of the control geometry.

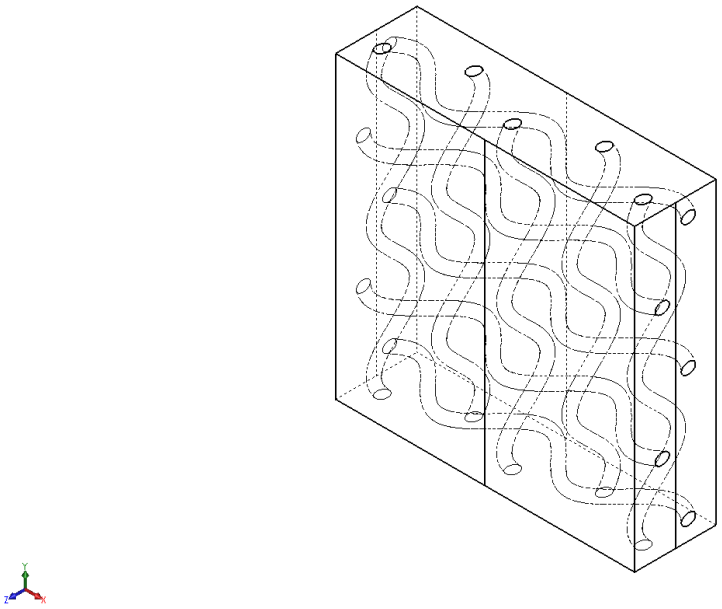

Figure 27: Finite element control geometry.

The CAD models for each of the laminates were created in *SolidWorks 2012* (Dassault Systèmes SolidWorks Corporation, Waltham, MA, USA). The fiber bundles and matrix were modeled as individual parts and then brought together as an assembly. To create the fiber/matrix interface, the matrix was edited in the context of the assembly. This was done so the exact fiber model could be used to subtract material where the fiber and matrix intersect. A "Cavity" feature was used to subtract the matrix out of the model which created a perfect interface between the matrix and fiber bundles. The models that had imperfections were modeled the same way with the only difference being the addition of features to model fiber damage and matrix porosity.

After the models were complete, they were brought into the *SolidWorks Simulation Premium* environment for analysis. Since models being analyzed were assemblies, a global contact had to be specified. A bonded contact was imposed for all contact taking place within the model. Other constraints allowed the model to expand or contract

transversely while being fixed at the opposite end from where the pressure was applied. Faces on the finite element model were also constrained to remain plane.

Loading of the model was similar to models from other research. In these models a known pressure was applied normal to the top face. This pressure was applied to both the fiber bundles and the matrix on that face. The pressure applied was 500 psi in the positive y-direction. The control geometry with applied loads and constraints is shown in Figure 28.

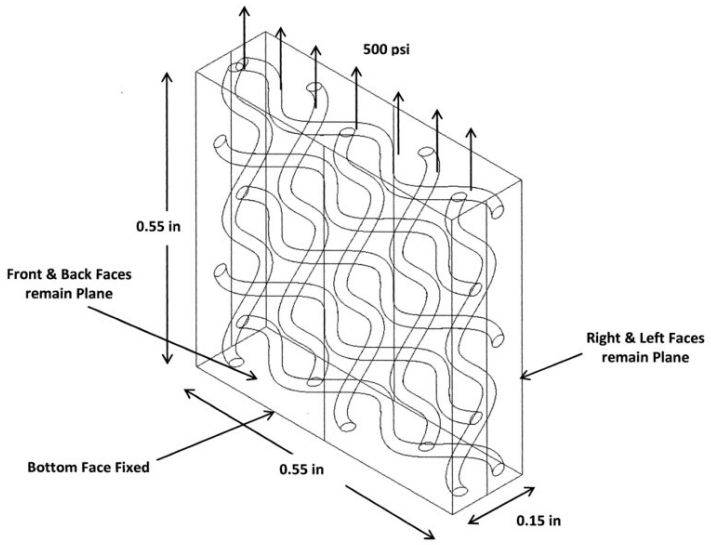

Figure 28: Applied loads and constraints.

Once the loading and constraints were applied, the model was meshed. Tetrahedral elements were used to mesh the fiber bundles and matrix. The global element size was 0.0075 inches. Smaller element sizes resulted in longer computational times with little (less than 5%) difference in results. Mesh refinement was used on the model that included fiber damage. Refinement was used on this model because the imperfections were on the same scale as the elements being used throughout the rest of the model. Mesh refinement allowed results to be more accurate at points of interest while not taking

up an extended amount of computational time as compared to refining the whole model. After the models were set up they were solved using a linear analysis.

The first model was the control geometry. It was based off the observed parameters of microscopic images from Layup 5 from 'Lamina/Laminate Testing" shown in Figure 29. However, the control geometry had an amplitude twice as high as the observed parameters. This increase in amplitude helped highlight differences in stress between each of the finite element models

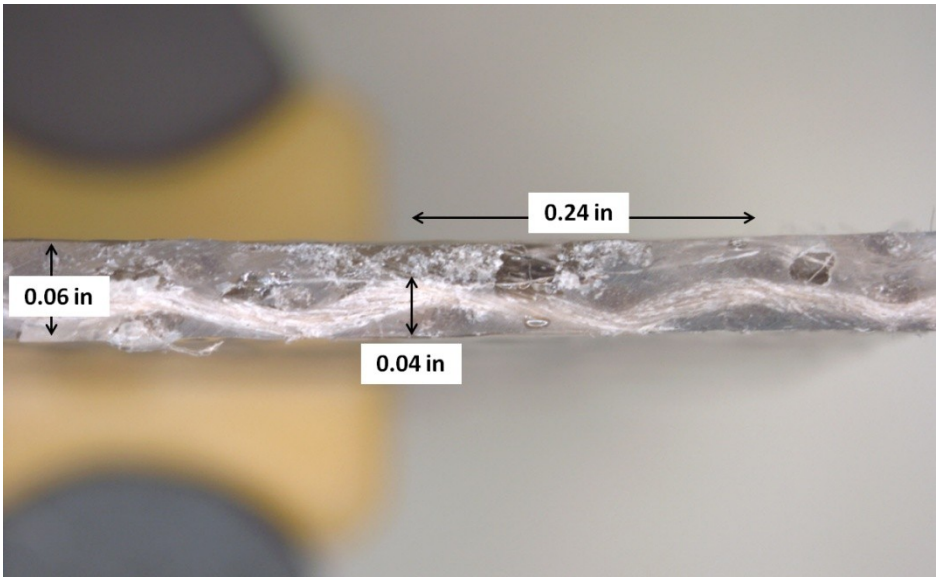

Figure 29: Microstructural details and dimensions of Layup 5.

Figure 30 shows the geometry of the finite element model and the fiber. Table 15 was the function used to estimate the sinusoidal fiber wave. Figure 31 shows the matrix and fiber bundles after being meshed. Mesh size was based on convergence and further mesh refinement was not applied to this model. Mesh details are listed in Table 16.

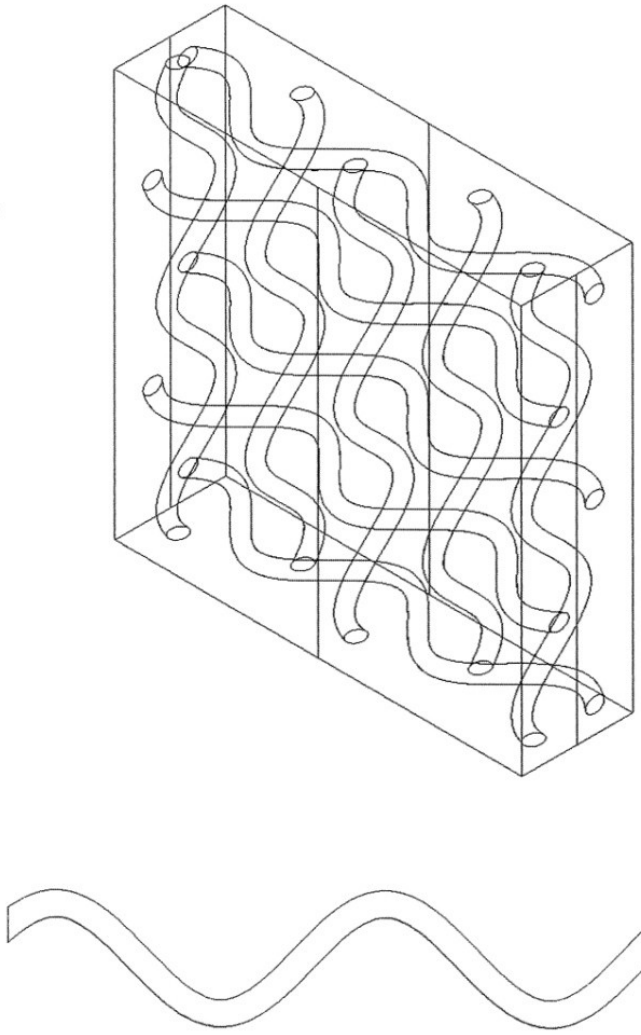

Figure 30: Finite element and fiber bundle model (Control Geometry).

Table 15: Wave function (Control Geometry).

Fiber Wave Function
$y = 0.04\sin(26.18x + \pi/2)$

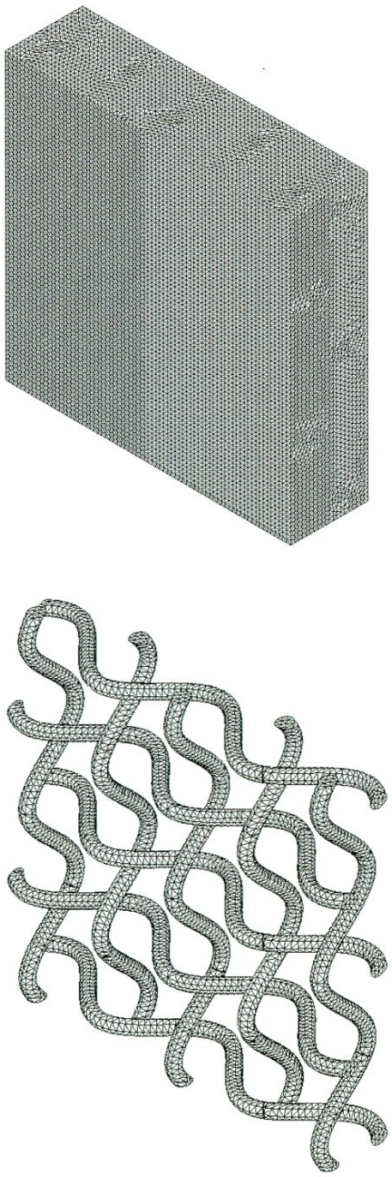

Figure 31: Matrix and fiber bundle mesh (Control Geometry).

Table 16: Mesh details (Control Geometry).

Control Geometry	
Element Size (in)	0.0075
Tolerance (in)	0.000375
Total Nodes	870,519
Total Elements	623,494
Max Aspect Ratio	17.23
% of Elements with Aspect Ratio < 3	99.6

Figure 32 shows a plot of σ_1 (first principal stress) for the fiber bundles. A point of interest is the maximum amplitude on the fiber sine wave and is defined as location A. The local maximum for σ_1 at location A is 3,921.5 psi.

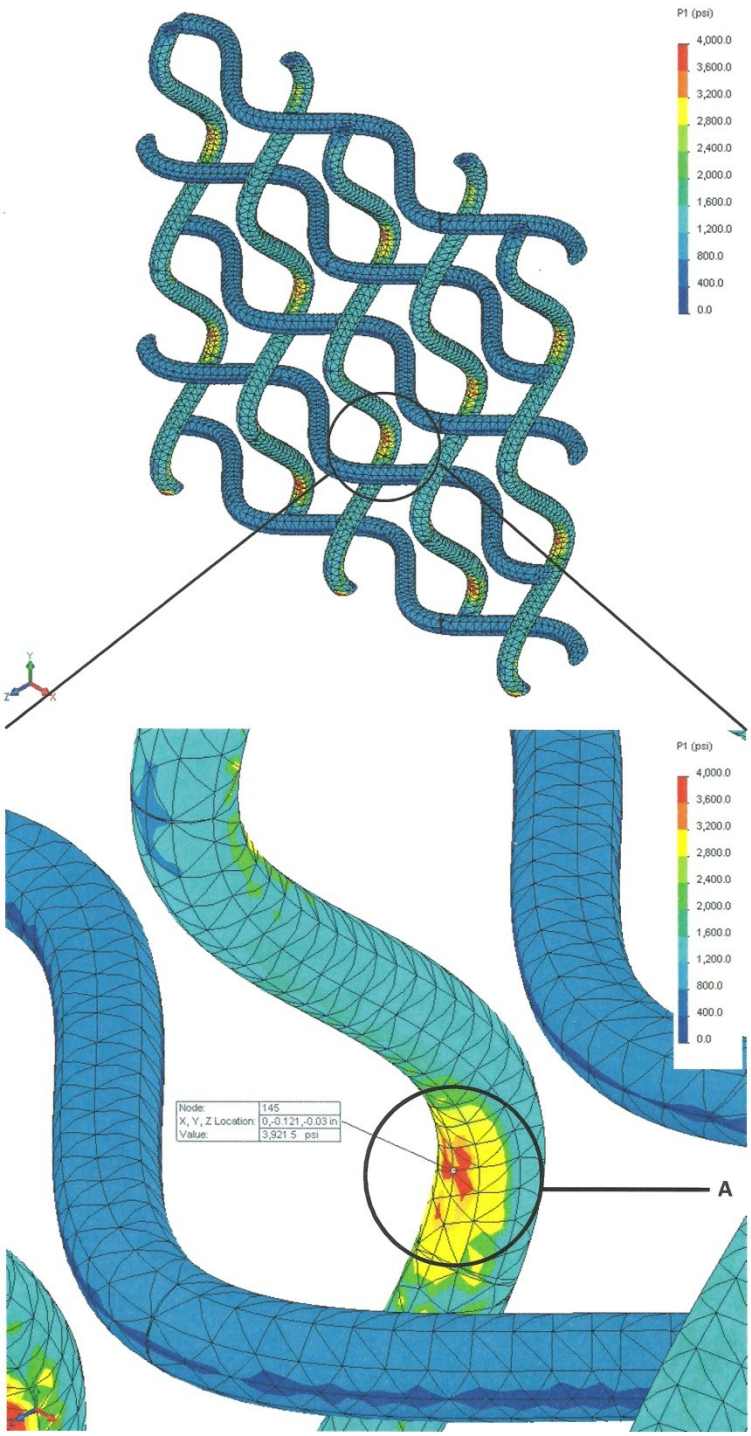

Figure 32: σ_1 of the fiber bundles (Control Geometry).

Figure 33 shows a plot of σ_1 for the matrix. A point of interest is the area between the longitudinal fiber bundle and transverse fiber bundle amplitudes and is defined as location B. The nominal value for σ_1 at location B is 438.2 psi.

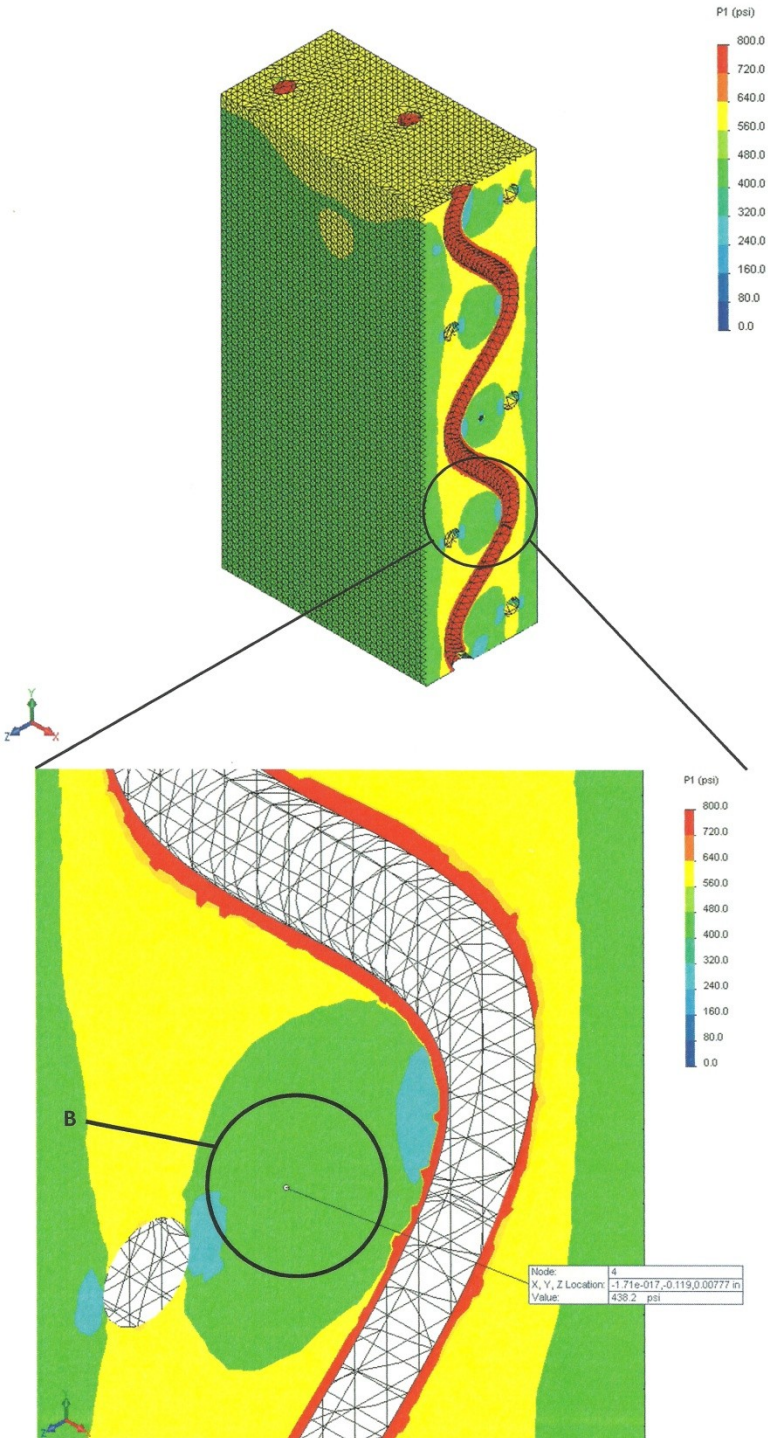

Figure 33: σ_1 of the matrix (Control Geometry).

Figure 34 shows a plot of τ_{yz} for the fiber bundles. A point of interest is around the maximum amplitude which is defined as location C. The maximum and minimum values for τ_{yz} at location C are 966.2 psi and -933.6 psi, respectively.

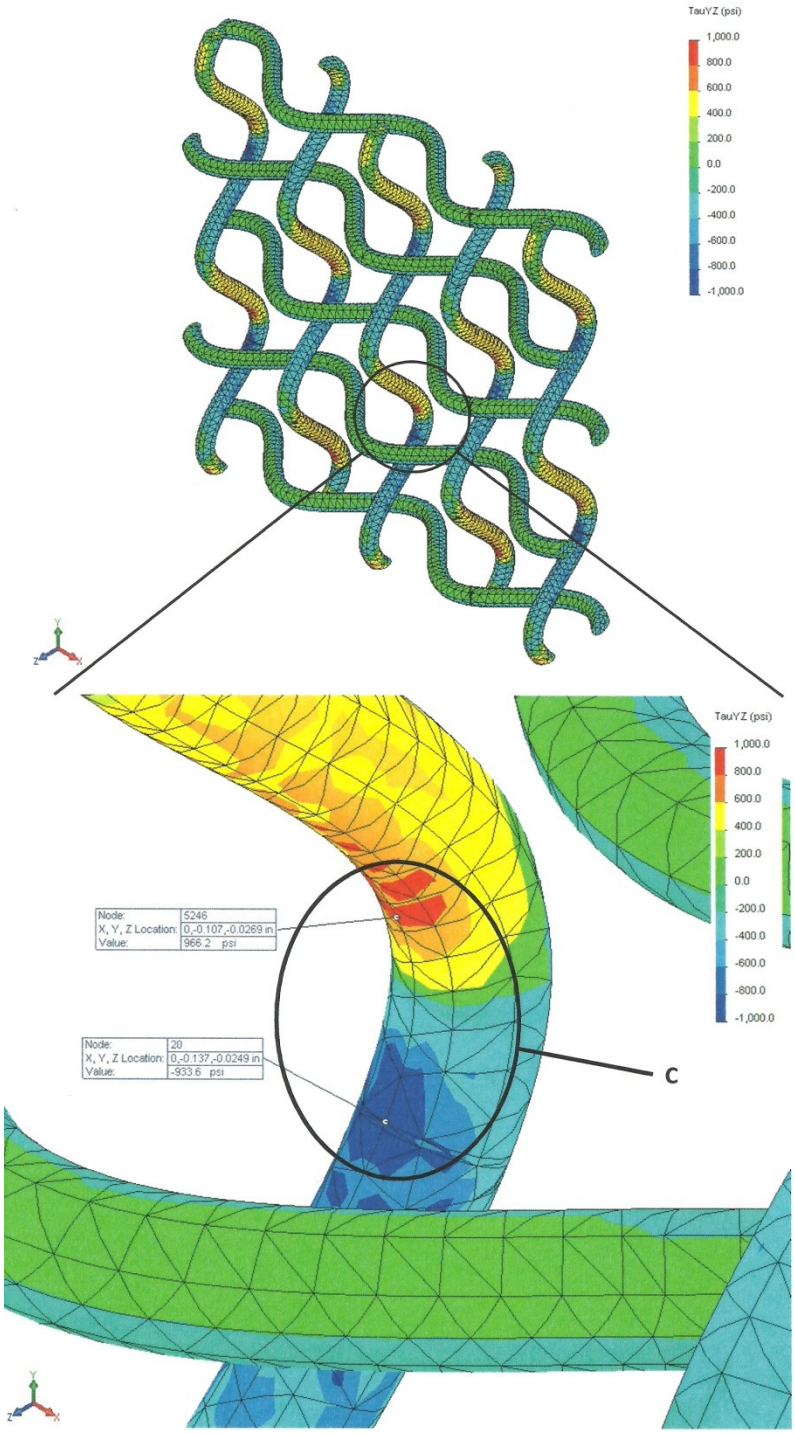

Figure 34: τ_{yz} of the fiber bundles (Control Geometry).

Figure 35 shows a plot of τ_{yz} for the matrix. A point of interest occurs around the maximum amplitude of the fiber bundles and is defined as location D. The maximum and minimum values for τ_{yz} at location D are 120.8 psi and -128.3 psi, respectively.

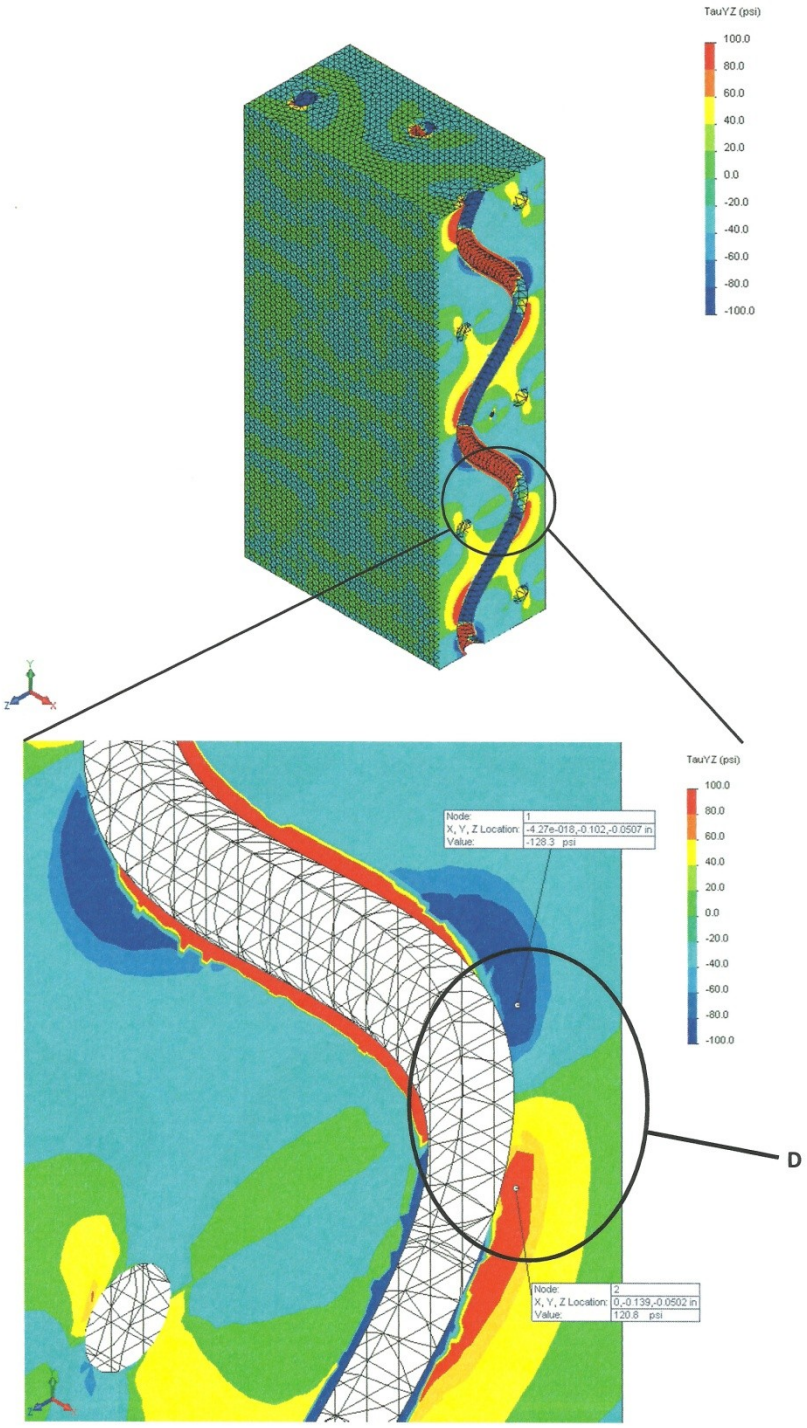

Figure 35: τ_{yz} of the matrix (Control Geometry).

The model presented in this section serves as a baseline to compare other models to. Points of interest were identified for comparison purposes. It is seen from the shear stress plots above that the forces are being transferred from the matrix to the fiber bundles via shearing stresses. It can also be seen that there is a stress concentration around the maximum amplitude of the fiber bundles when looking at the first principal stress plot.

4.2 Fiber Undulation Effects

The second geometry decreases the fiber wave amplitude to match Layup 5 which is an amplitude reduction of half. This geometry can be seen in Figure 29 above. Figure 36 shows the geometry of the finite element model and the fiber bundle. Table 17 is the function used to estimate the sinusoidal fiber wave. Figure 37 shows the fiber bundles after being meshed. Mesh size was based on convergence and further mesh refinement was not applied to this model. Mesh details are listed in Table 18.

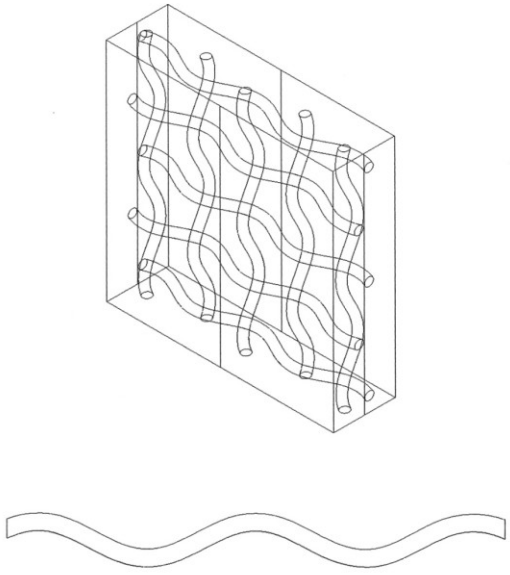

Figure 36: Finite element and fiber bundle model (Fiber Undulation).

Table 17: Wave function (Fiber Undulation).

Fiber Wave Function
$y = 0.02\sin(26.18x + \pi/2)$

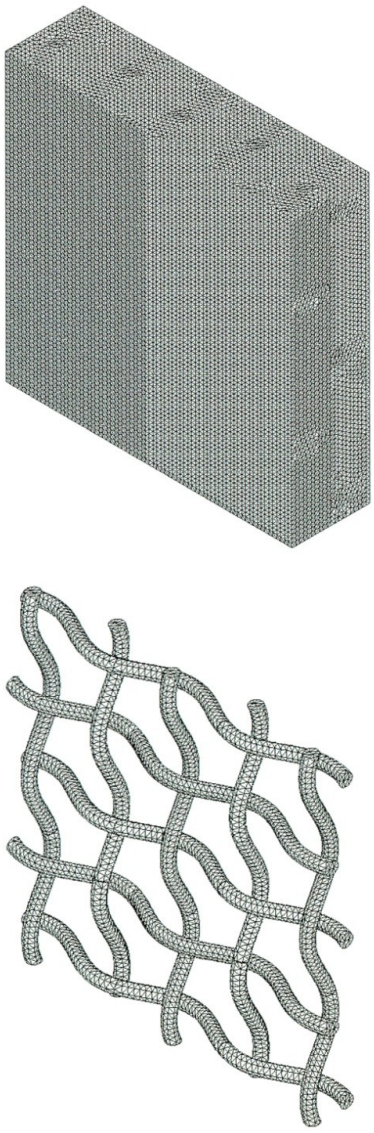

Figure 37: Matrix and fiber bundle mesh (Fiber Undulation).

Table 18: Mesh details (Fiber Undulation).

Fiber Undulation	
Element Size (in)	0.0075
Tolerance (in)	0.000375
Total Nodes	845,830
Total Elements	609,776
Max Aspect Ratio	13.05
% of Elements with Aspect Ratio < 3	99.7

Figure 38 shows a plot of σ_1 for the fiber bundles. The local maximum for σ_1 at location A is 4,030.0 psi. This represents an increase of 2.8% when compared to the control geometry.

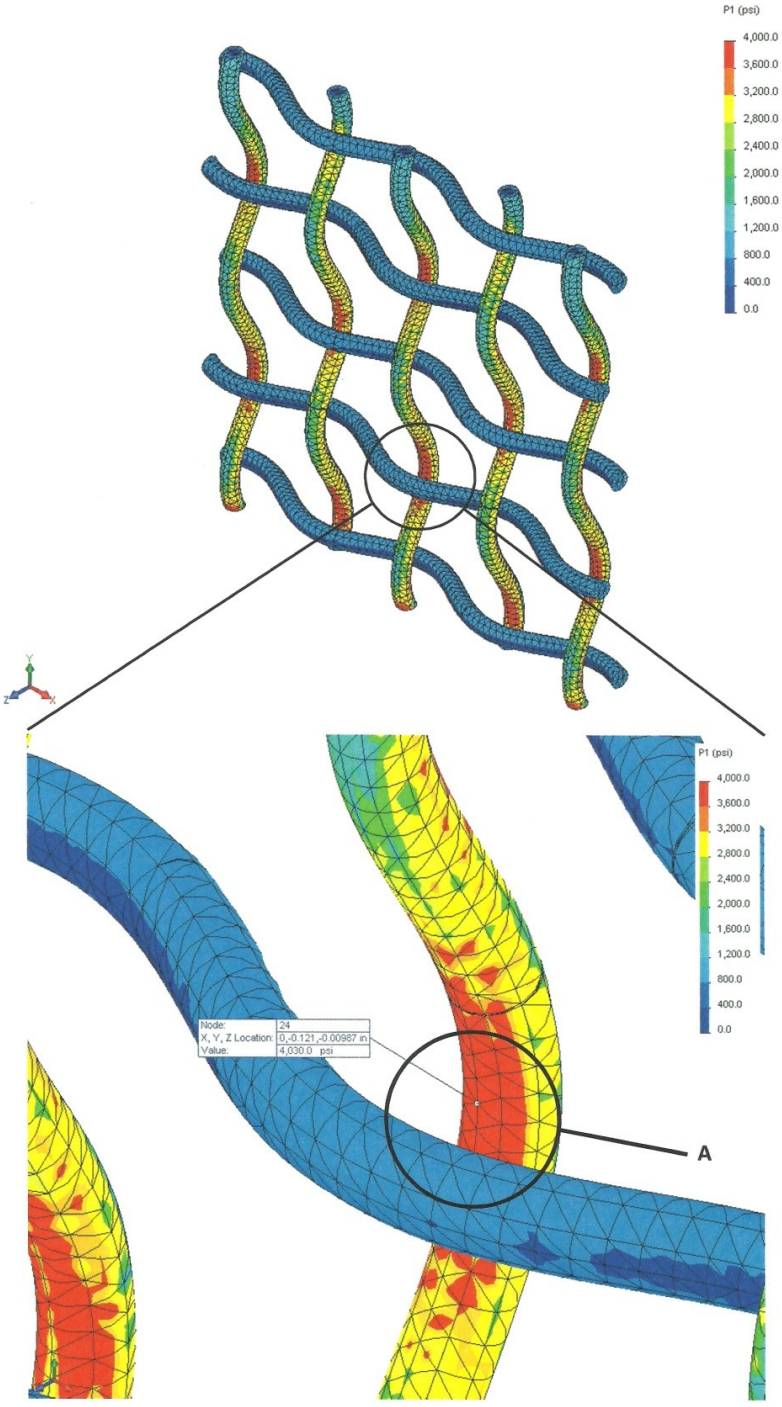

Figure 38: σ_1 of the fiber bundles (Fiber Undulation).

Figure 39 shows a plot of σ_1 for the matrix. The nominal value for σ_1 at location B is 302.4 psi. This represents a decrease of 31.1% when compared to the control geometry.

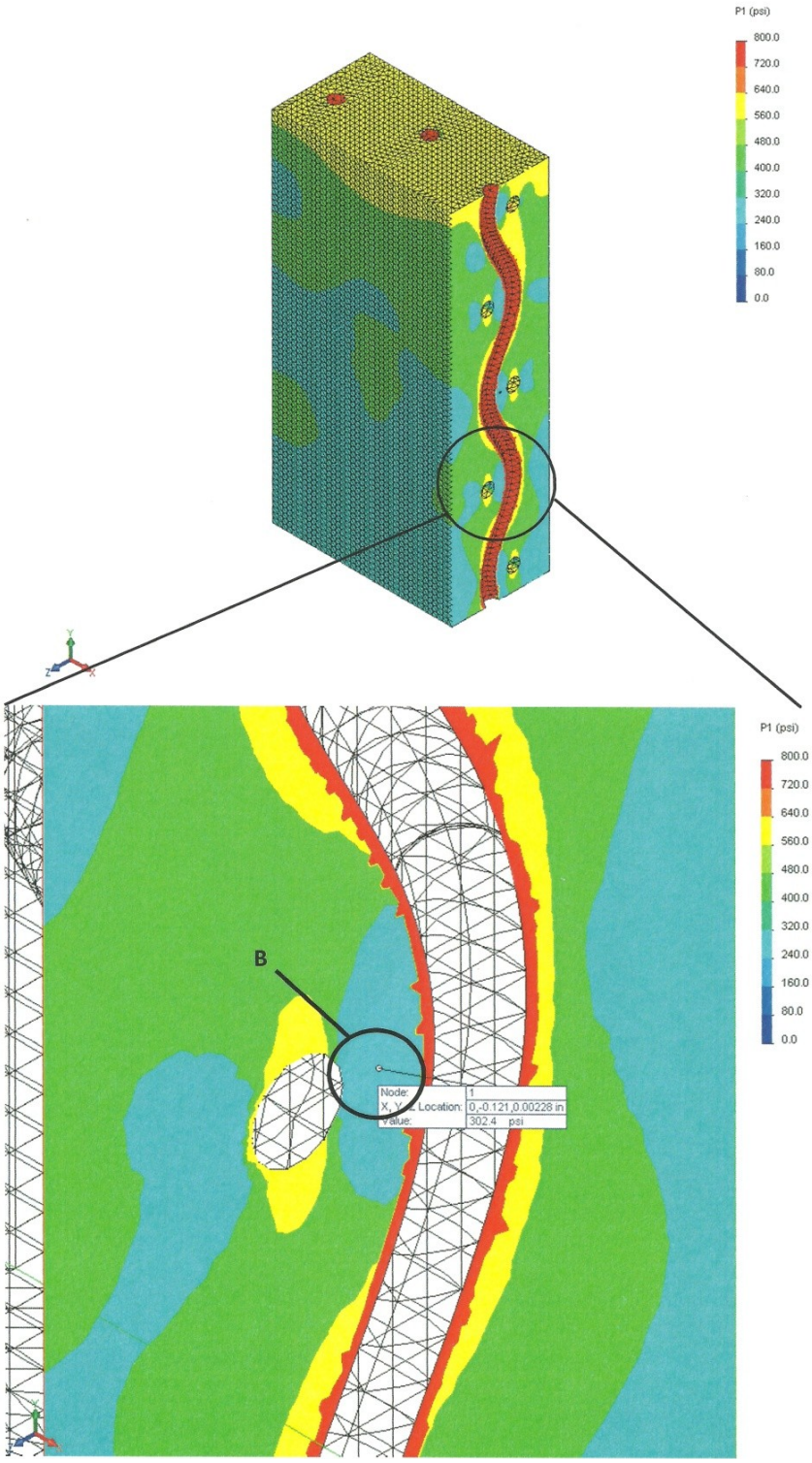

Figure 39: σ_1 of the matrix (Fiber Undulation).

Figure 40 shows a plot of τ_{yz} for the fiber bundles. The maximum and minimum values for τ_{yz} at location C are 1,267.9 psi and -1,085.5 psi, respectively. This represents an increase of 31.2% and 16.3% when compared to the control geometry, respectively.

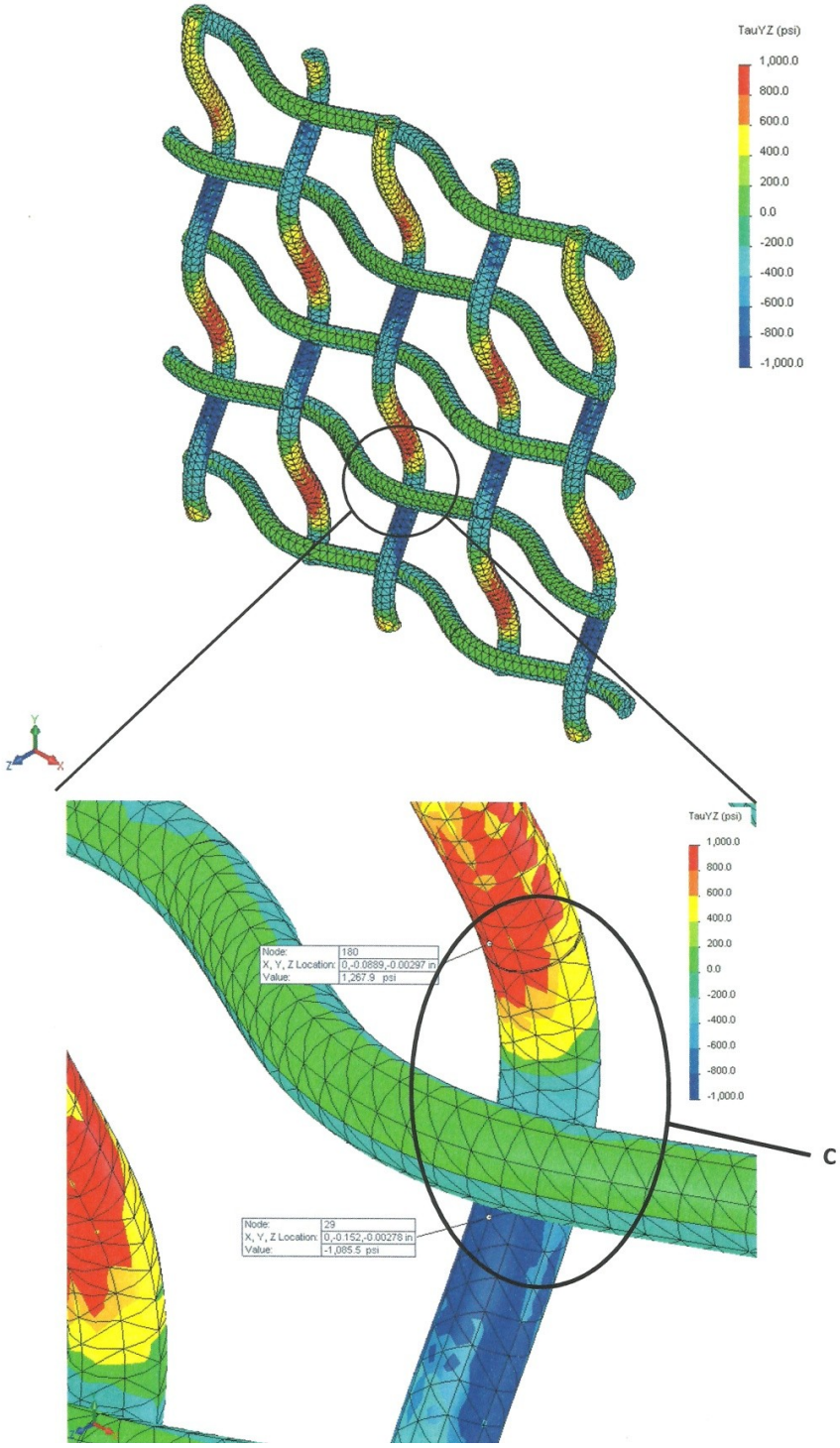

Figure 40: τ_{yz} of the fiber bundles (Fiber Undulation).

Figure 41 shows a plot of τ_{yz} for the matrix. The maximum and minimum values for τ_{yz} at location D are 99.4 psi and -99.7 psi, respectively. This represents a decrease of 17.7% and 22.3% when compared to the control geometry, respectively.

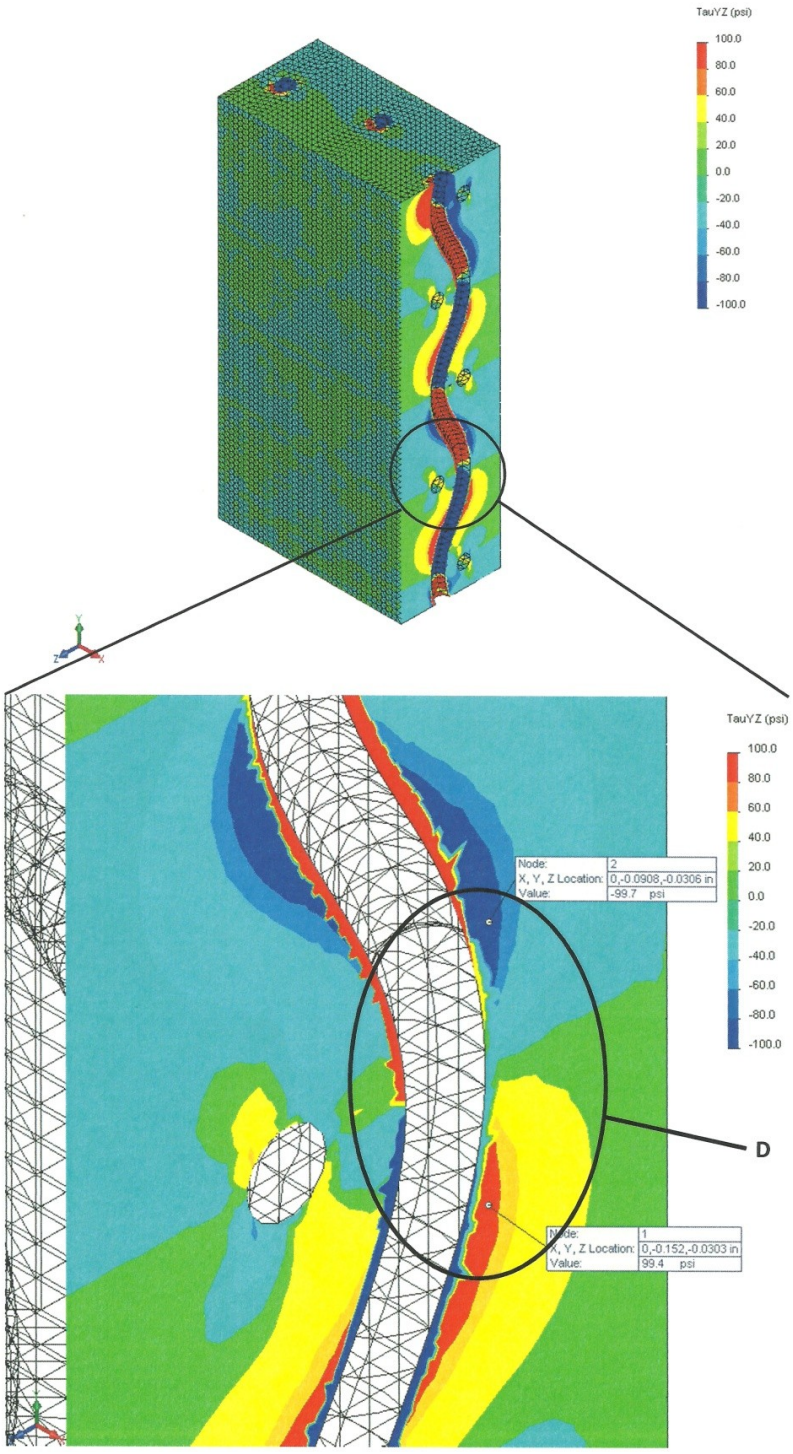

Figure 41: τ_{yz} of the matrix (Fiber Undulation).

A decrease in fiber amplitude has a negligible influence on the peak σ_1 in the fibers. However, there is a substantial influence on σ_1 in the matrix. A 31.1% decrease in stress was observed at location B in the matrix. This result shows composites with less pronounced fiber waves transfer normal stresses to the fibers more efficiently. This was accompanied by an increase in shear stress in the fibers and a decrease in shear stress in the matrix. The results are tabulated in Table 19.

Table 19: Stress comparison (Control Geometry vs. Fiber Undulation).

	Location A	Location B	Location C		Location D	
	σ_1 (psi)	σ_1 (psi)	$\tau_{yz,\,max}$ (psi)	$\tau_{yz,\,min}$ (psi)	$\tau_{yz,\,max}$ (psi)	$\tau_{yz,\,min}$ (psi)
Control Geometry	3,921.5	438.2	966.2	-933.6	120.8	-128.3
Fiber Undulation	4,030.0	302.0	1,267.9	-1,085.5	99.4	-99.7
Percent Δ	**2.8**	**-31.1**	**31.2**	**16.3**	**-17.7**	**-22.3**

4.3 Fiber Damage Effects

The third geometry introduces fiber damage at the maximum amplitude on the fiber function. This configuration used the same fiber function as the control geometry. Figure 42 shows the geometry of the finite element model and the damaged fiber bundles. Table 20 is the function used to estimate the sinusoidal fiber wave. Figure 43 shows the fiber bundles after being meshed. Mesh refinement was used near the fiber damage with element sizes of 0.0025 inches. Refinement was used on this model because the fiber damage is on a smaller scale than the rest of the model. Normal elements used in this area would become distorted and the influence of damage would not be captured as accurately if mesh refinement was not used. Mesh details are listed in Table 21.

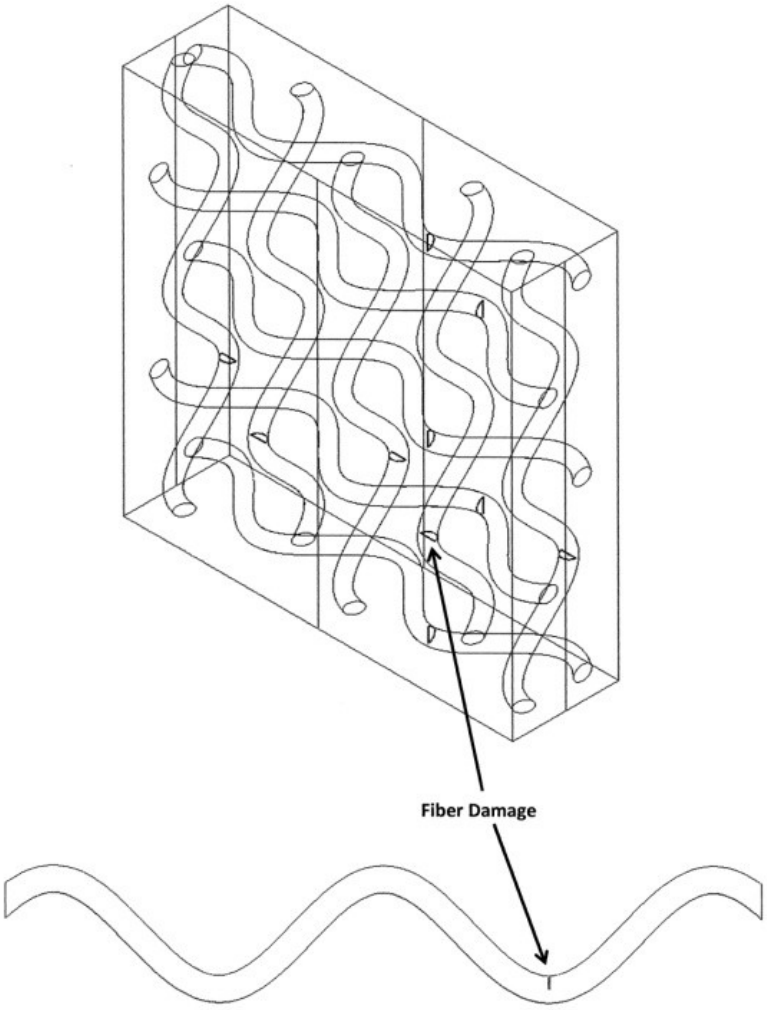

Figure 42: Finite element and fiber bundle model (Fiber Damage).

Table 20: Wave function (Fiber Damage).

Fiber Wave Function
$y = 0.04\sin(26.18x + \pi/2)$

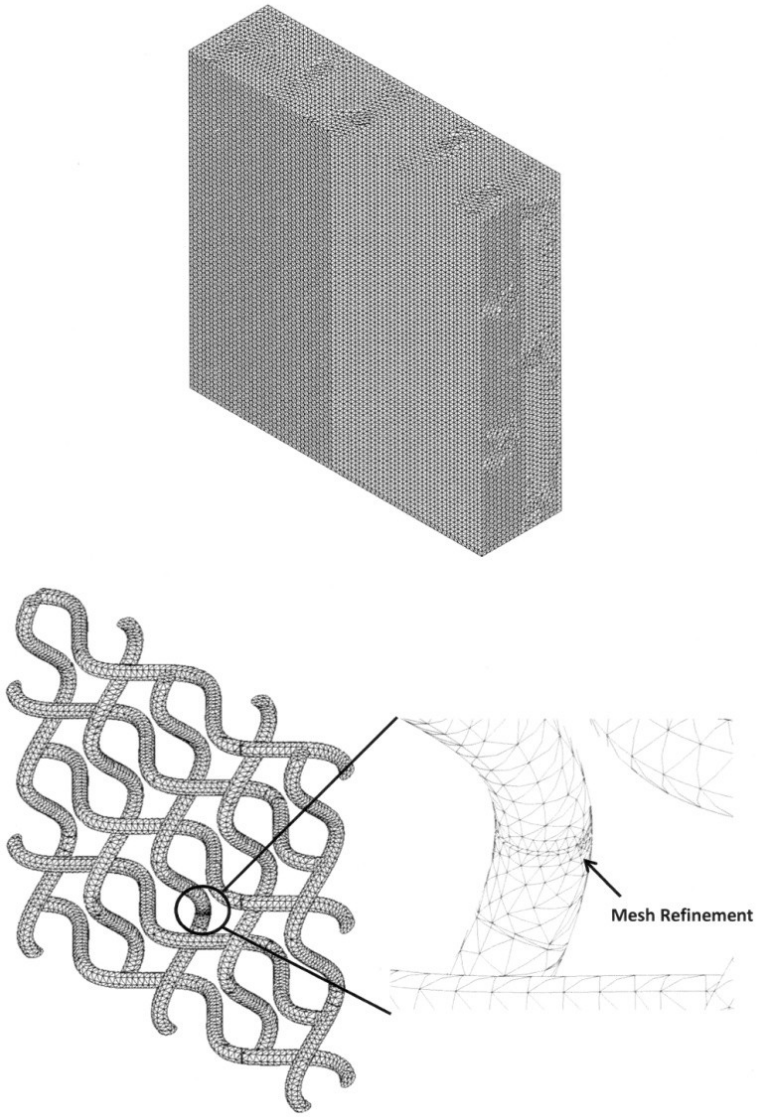

Figure 43: Matrix and fiber bundle mesh (Fiber Damage).

Table 21: Mesh details (Fiber Damage).

Fiber Damage	
Element Size (in)	0.0075
Tolerance (in)	0.000375
Total Nodes	880,843
Total Elements	631,955
Max Aspect Ratio	17.54
% of Elements with Aspect Ratio < 3	99.4

Figure 44 shows a plot of σ_1 for the fiber bundles. The local maximum for σ_1 at location A is 6,119.7 psi. This represents an increase of 56.1% when compared to the control geometry.

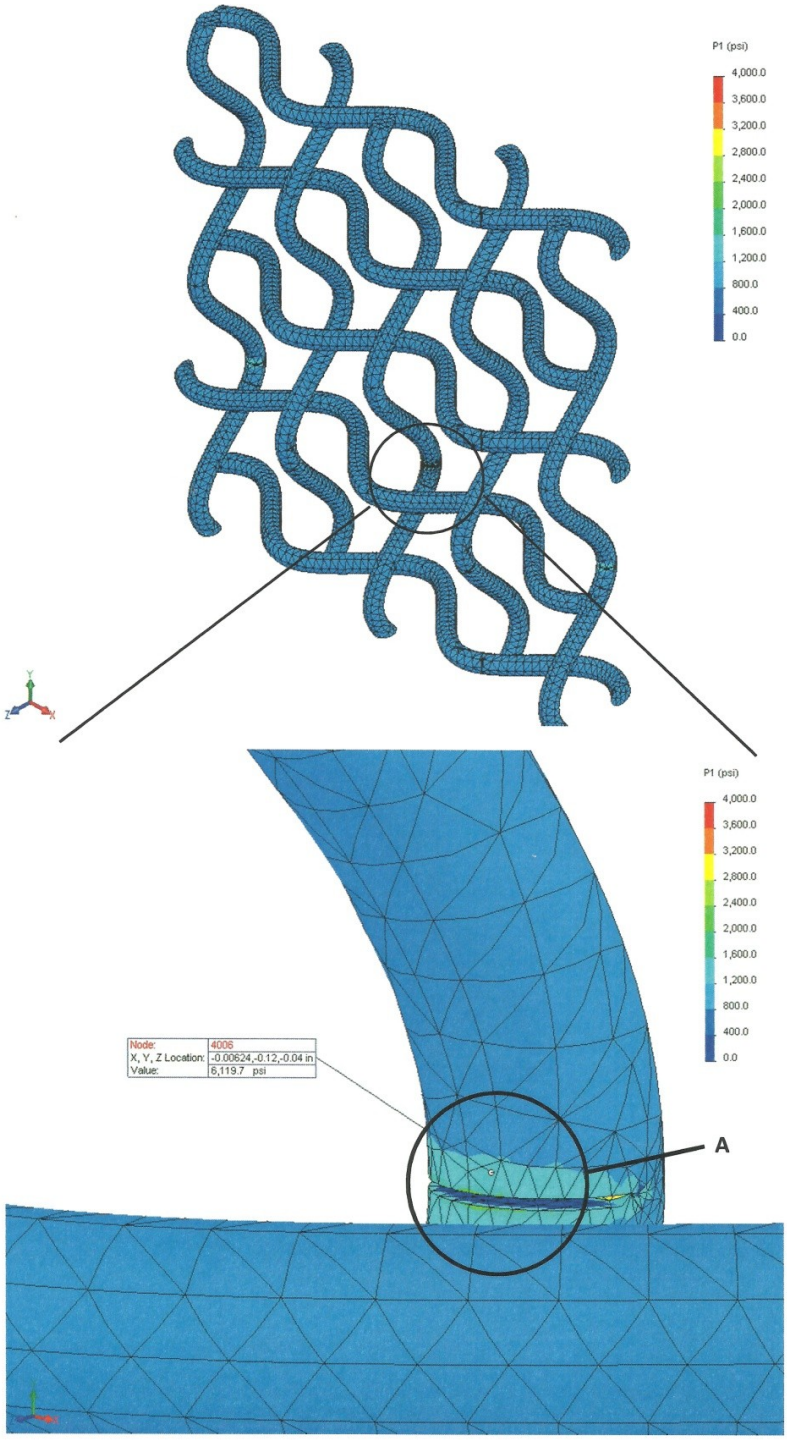

Figure 44: σ_1 of the fiber bundles (Fiber Damage).

Figure 45 shows a plot of σ_1 for the matrix. The nominal value for σ_1 at location B is 502.8 psi. This represents an increase of 14.7% when compared to the control geometry.

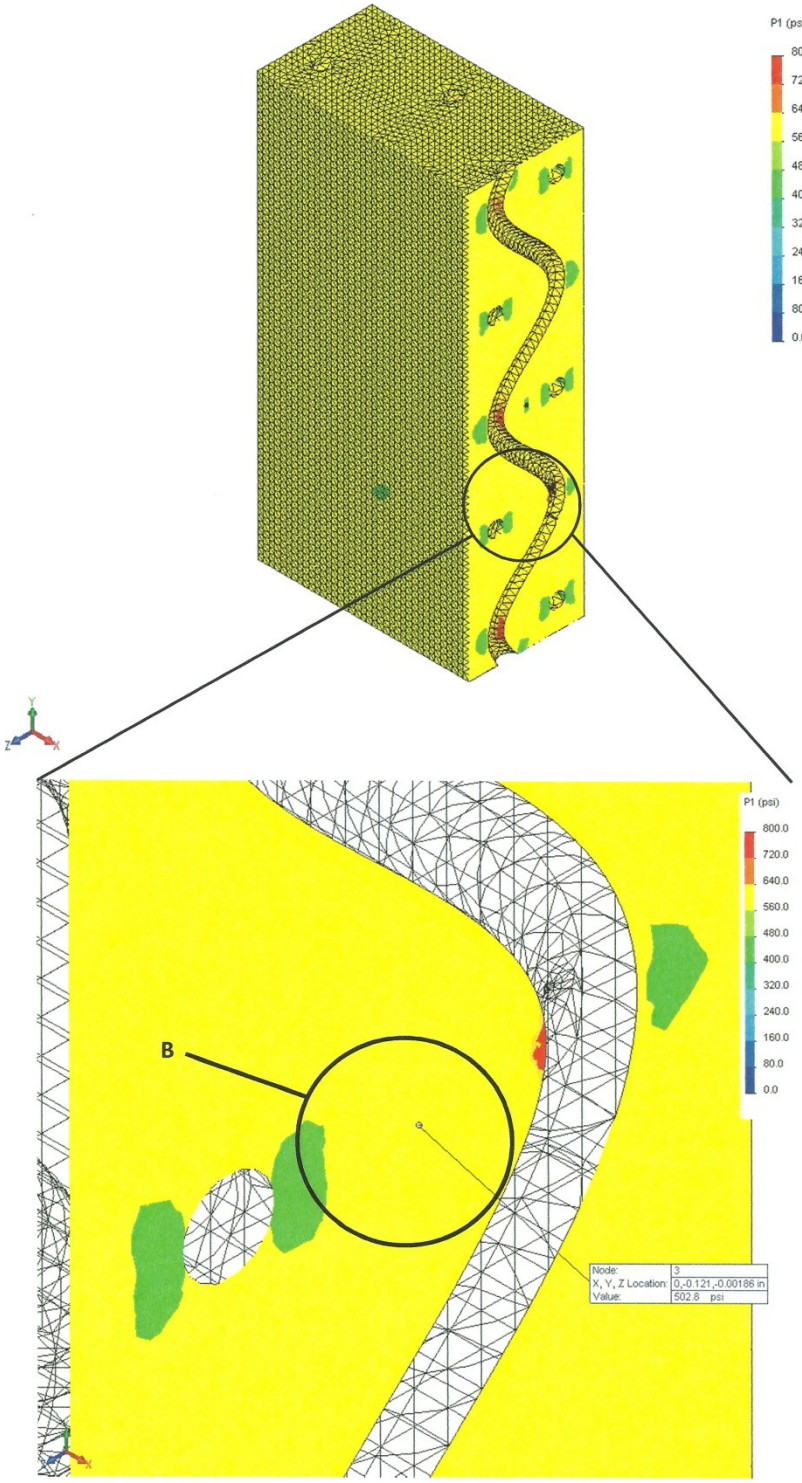

Figure 45: σ_1 of the matrix (Fiber Damage).

Figure 46 shows a plot of τ_{yz} for the fiber bundles. The maximum and minimum values for τ_{yz} at location C are 49.3 psi and -40.5 psi, respectively. This represents a decrease of 94.9% and 95.7% when compared to the control geometry, respectively.

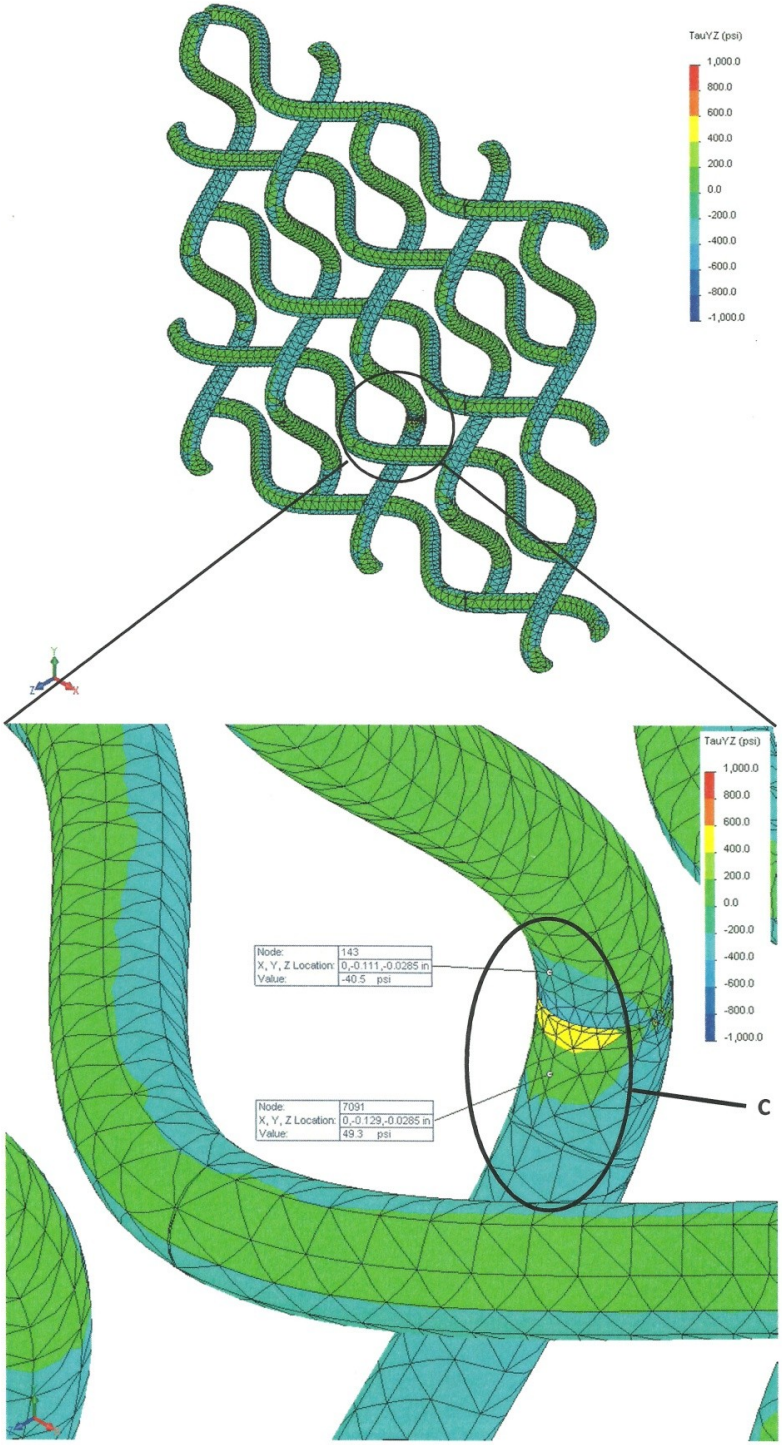

Figure 46: τ_{yz} of the fiber bundles (Fiber Damage).

Figure 47 shows a plot of τ_{yz} for the matrix. The maximum and minimum values for τ_{yz} at location D are 23.0 psi and -20.4 psi, respectively. This represents a decrease of 81.0% and 84.1% when compared to the control geometry, respectively.

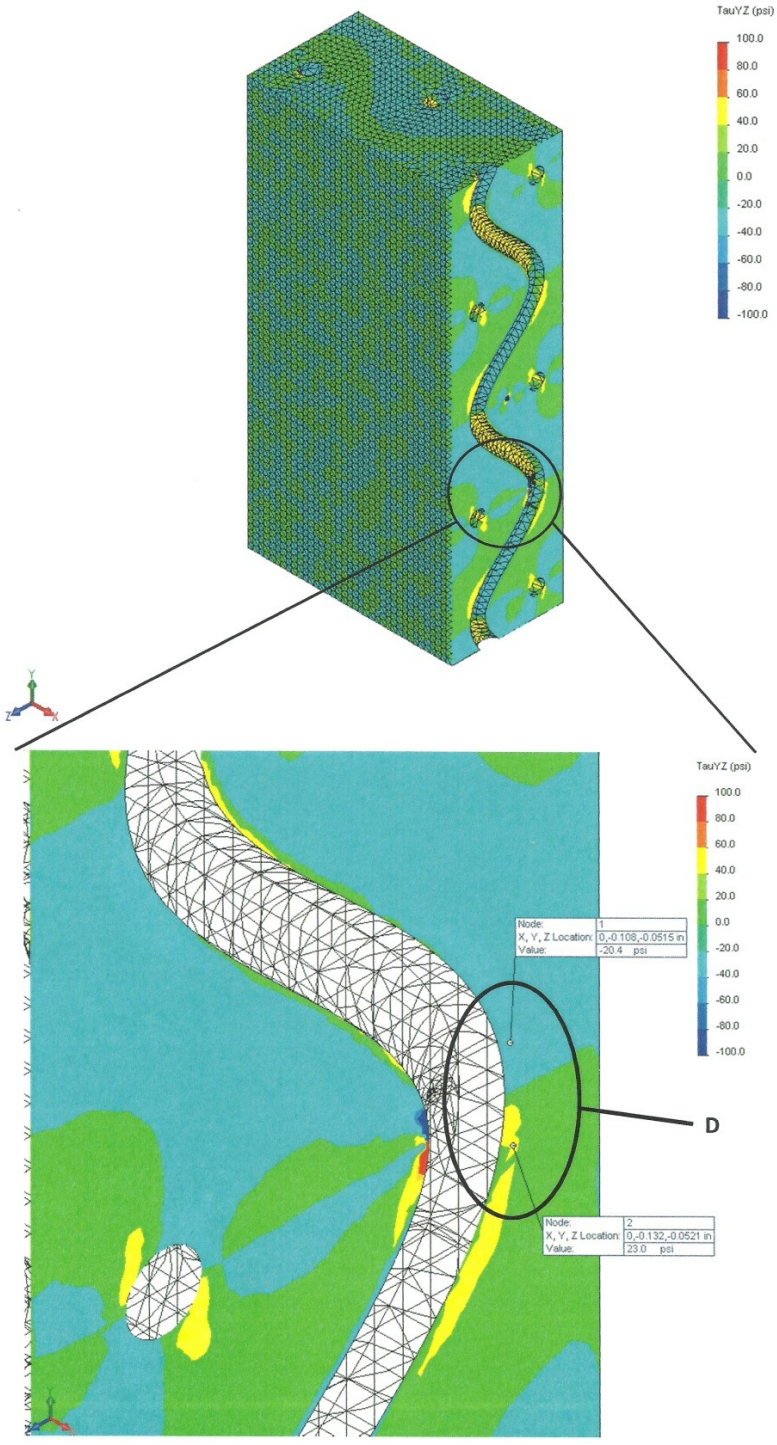

Figure 47: τ_{yz} of the matrix (Fiber Damage).

Fiber damage introduced at the peak amplitude on the fiber wave has a large impact on σ_1 in the fibers. A 56.1% increase in σ_1 in the fibers could compromise an entire structure. This increase in stress is a local concentration around the fiber damage. The matrix also had an increase in σ_1. Shear stresses for the fibers and the matrix all had a decrease in magnitude on a global scale. However, there are spikes in shear stresses in both the fiber and the matrix centralized around the fiber damage. These results indicate that stresses are not being transferred to the fibers as uniformly as models without fiber damage. This can be seen from the increase in normal stresses and decrease in shear stresses around the fiber/matrix interface. The results are tabulated in Table 22.

Table 22: Stress comparison (Control Geometry vs. Fiber Damage).

	Location A	Location B	Location C		Location D	
	σ_1 (psi)	σ_1 (psi)	$\tau_{yz,\,max}$ (psi)	$\tau_{yz,\,min}$ (psi)	$\tau_{yz,\,max}$ (psi)	$\tau_{yz,\,min}$ (psi)
Control Geometry	3,921.5	438.2	966.2	-933.6	120.8	-128.3
Fiber Damage	6,119.7	502.8	49.3	-40.5	23.0	-20.4
Percent Δ	**56.1**	**14.7**	**-94.9**	**-95.7**	**-81.0**	**-84.1**

4.4 Porosity/Fiber Interaction Effects

The fourth geometry introduces matrix porosity into the composite. This finite element model uses the same fiber function as the control geometry. Figure 48 shows the geometry of the finite element model and fiber bundles. Table 23 is the function used to estimate the sinusoidal fiber wave. Figure 49 shows the fiber bundles after meshing. Mesh size was based on convergence and further mesh refinement was not applied to this model. Mesh details are listed in Table 24.

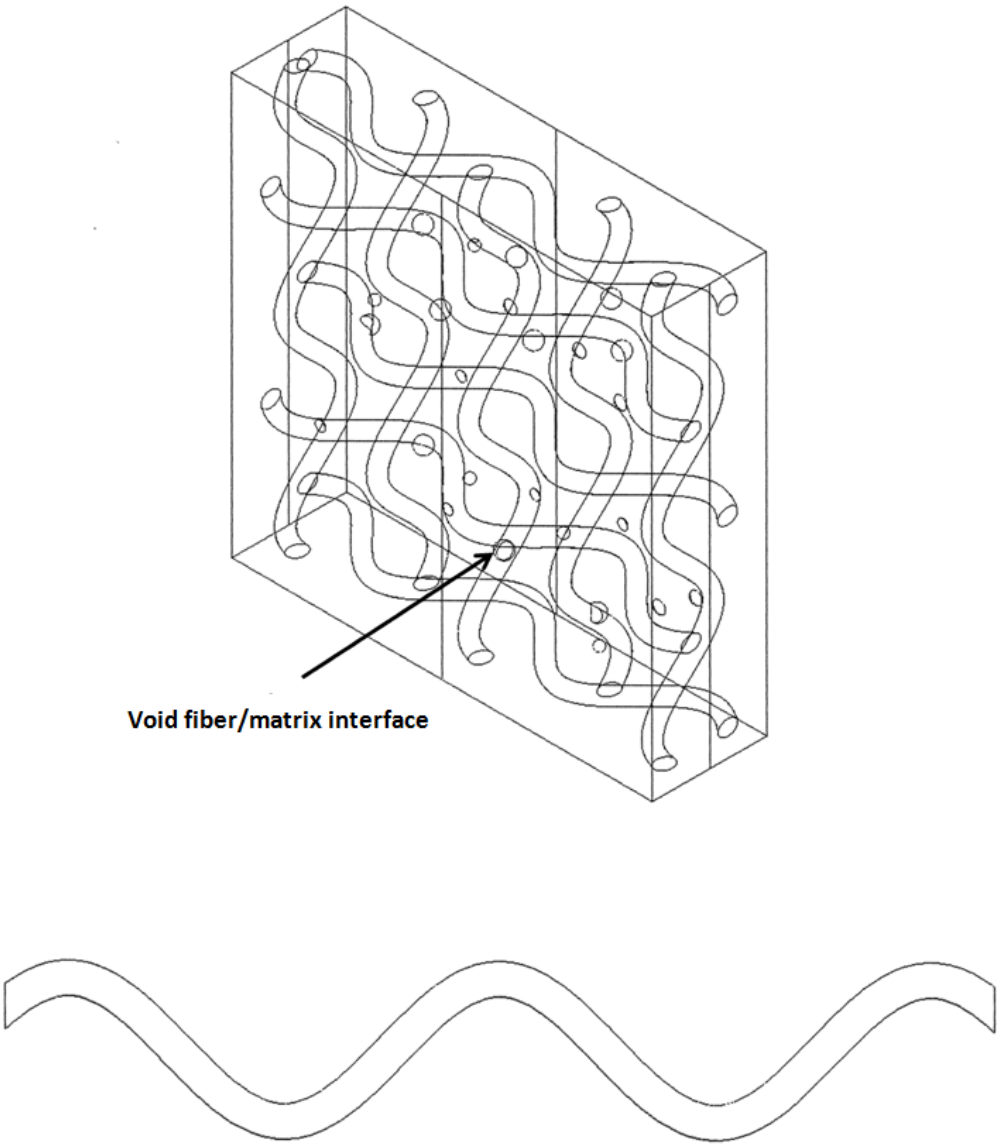

Figure 48: Finite element and fiber bundle model (Matrix Porosity).

Table 23: Wave function (Matrix Porosity).

Fiber Wave Function
$y = 0.04\sin(26.18x + \pi/2)$

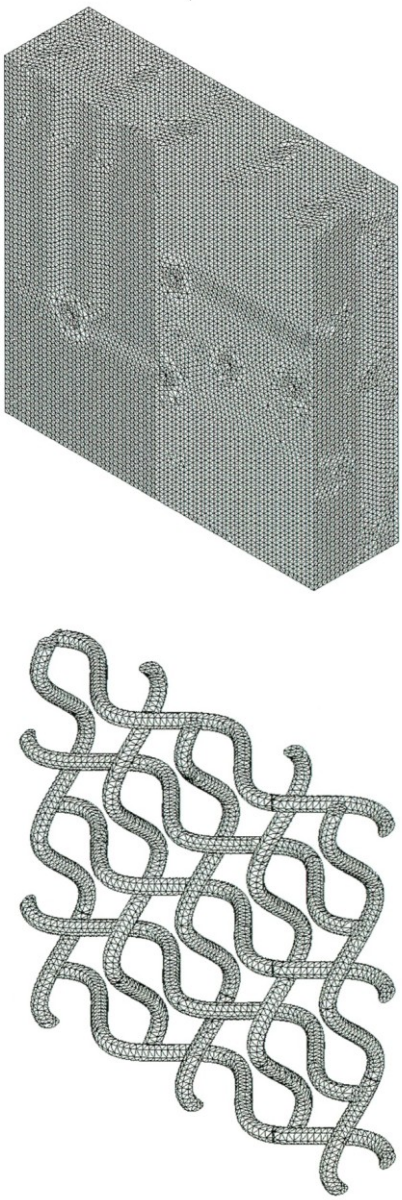

Figure 49: Matrix and fiber bundle mesh (Matrix Porosity).

Table 24: Mesh details (Matrix Porosity).

Matrix Porosity	
Element Size (in)	0.0075
Tolerance (in)	0.000375
Total Nodes	901,601
Total Elements	645,294
Max Aspect Ratio	16.52
% of Elements with Aspect Ratio < 3	99.6

Figure 50 shows a plot of σ_1 for the fiber bundles. The local maximum for σ_1 at location A is 3,809.6 psi. This represents a 2.9% decrease when compared to the control geometry.

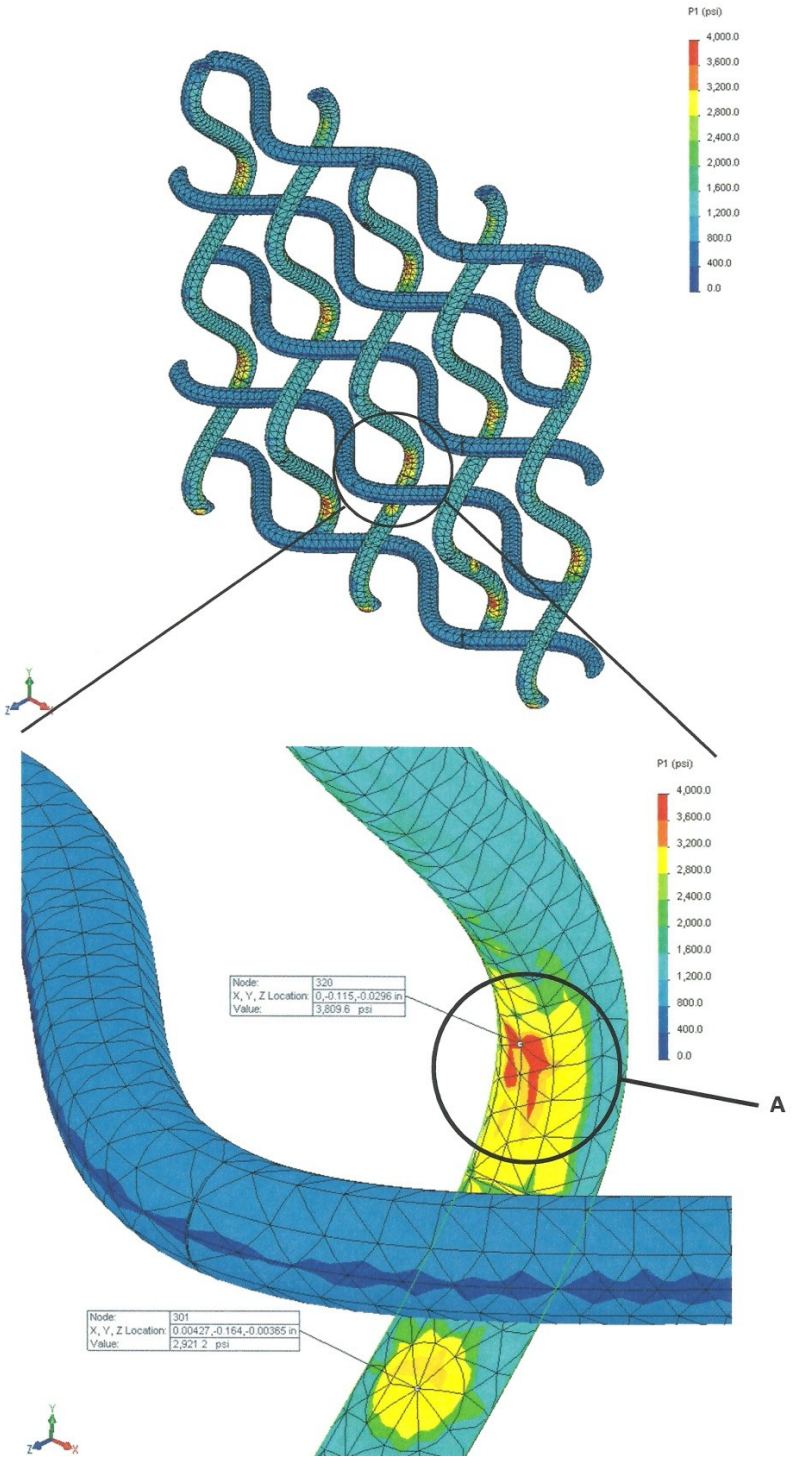

Figure 50: σ_1 of the fiber bundles (Matrix Porosity).

Figure 51 shows a plot of σ_1 for the matrix. The nominal value for σ_1 at location B is 428.0 psi. This represents a 2.3% decrease when compared to the control geometry.

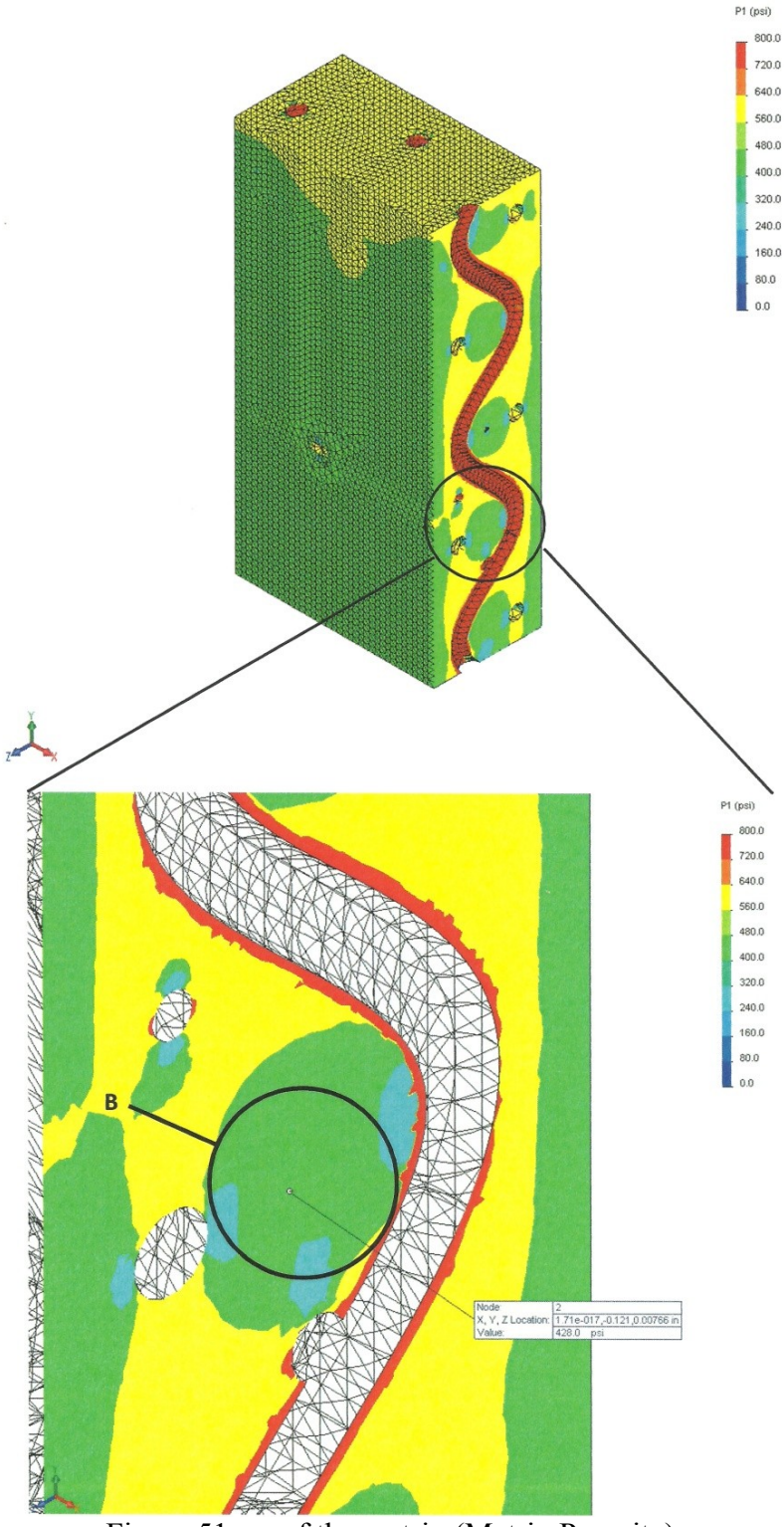

Figure 51: σ_1 of the matrix (Matrix Porosity).

Figure 52 shows a plot of τ_{yz} for the fiber bundles. The maximum and minimum values for τ_{yz} at location C are 1,012.4 psi and -1,050.7 psi, respectively. This represents an increase of 4.8% and 12.5% when compared to the control geometry, respectively.

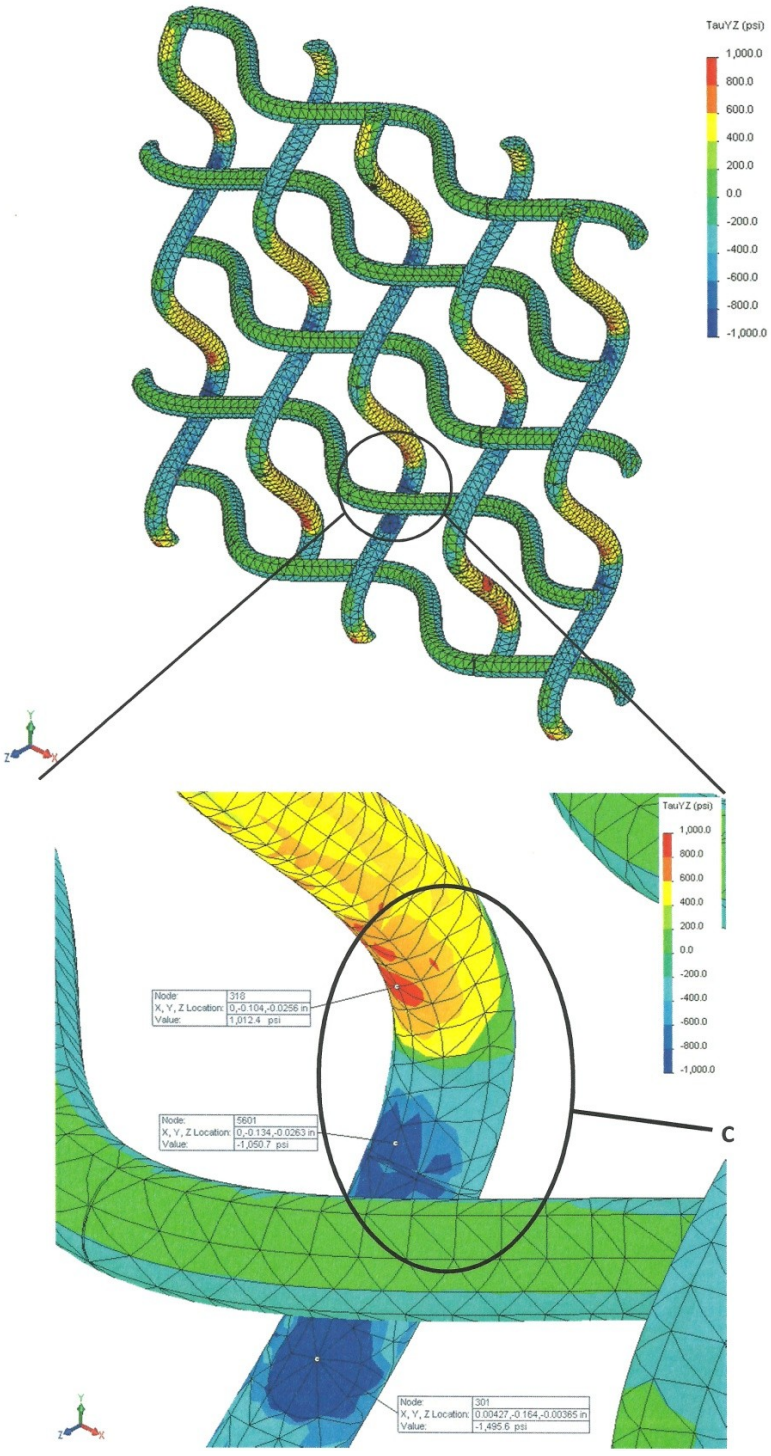

Figure 52: τ_{yz} of the fiber bundles (Matrix Porosity).

Figure 53 shows a plot of τ_{yz} for the matrix. The maximum and minimum values for τ_{yz} at location D are 122.4 psi and -123.0 psi, respectively. This represents an increase of 1.3% and a decrease of 4.1% when compared to the control geometry, respectively.

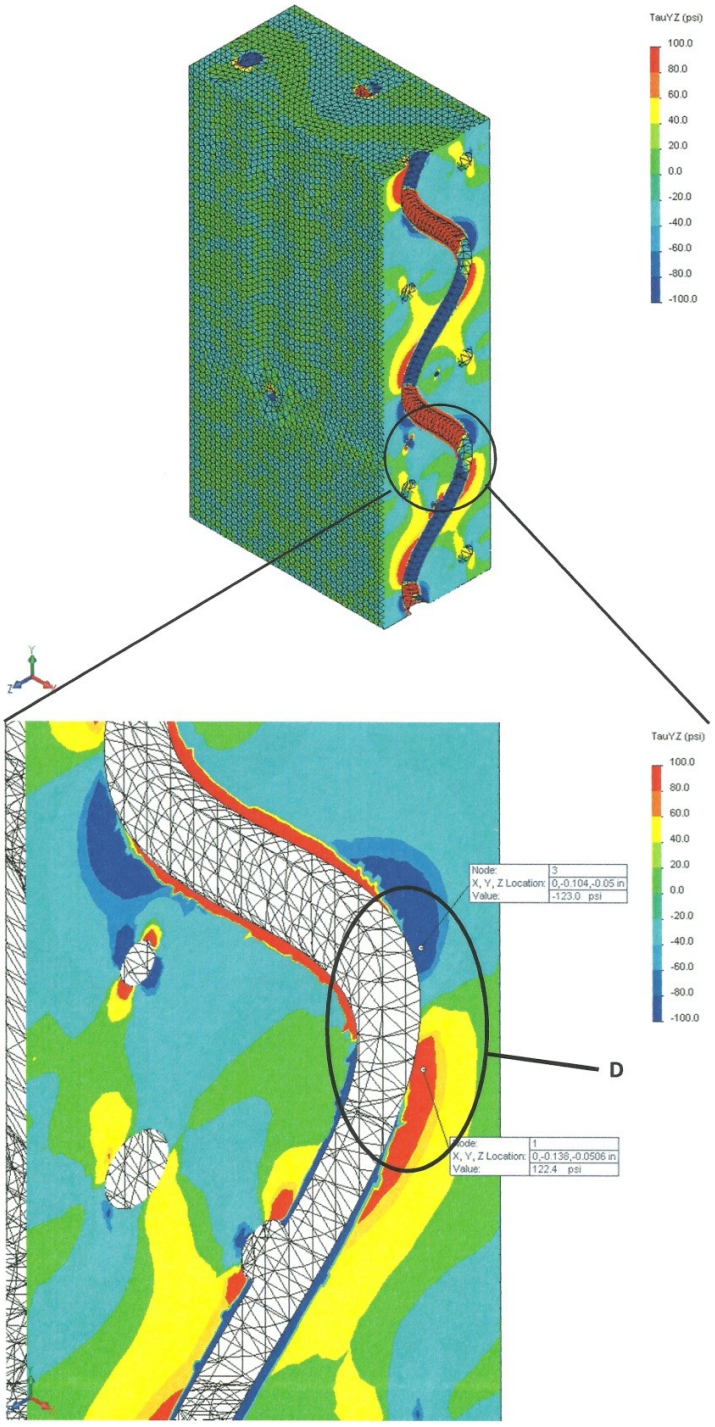

Figure 53: τ_{yz} of the matrix (Matrix Porosity).

Voids introduced into the matrix had negligible effects at the four points of interest. First principal stresses in the fibers and matrix remained relatively the same. Shear stresses were largely unchanged except for the minimum τ_{yz} on the fiber bundles at location C. A discontinuity at the fiber/matrix interface will see an increase in the local shear stress. The minimum shear stress value at location C can be attributed to the void in the matrix located in the vicinity of location C. However, there were stress concentrations located at the void that are cause for concern. The fiber bundles had increases in both normal and shear stresses at the void while the matrix only had an increase in shear stress at this location. An increase in voids will deteriorate a composite even further and larger localized stress concentrations can be expected as voids become larger or coalesce. The results are tabulated in Table 25.

Table 25: Stress comparison (Control Geometry vs. Matrix Porosity).

	Location A	Location B	Location C		Location D	
	σ_1 (psi)	σ_1 (psi)	$\tau_{yz,\,max}$ (psi)	$\tau_{yz,\,min}$ (psi)	$\tau_{yz,\,max}$ (psi)	$\tau_{yz,\,min}$ (psi)
Control Geometry	3,921.5	438.2	966.2	-933.6	120.8	-128.3
Matrix Porosity	3,809.6	428.0	1,012.4	-1,050.7	122.4	-123.0
Percent Δ	**-2.9**	**-2.3**	**4.8**	**12.5**	**1.3**	**-4.1**

4.5 Results

Results obtained from the finite element analysis lead to a number of conclusions. The jute fibers used earlier in this project were very coarse and dry. These characteristics lead to a composite that contains voids and other areas where resin pools together. The manufacturing process used for these layups was not adequate in optimizing the number of defects that were found. Another process that could have been used to remove voids is vacuum resin infusion. This process starts with dry fibers sealed in an air tight bag. The

vacuum removes air from the bag while compacting the laminate. Finally, resin is infused through the system before it is left to cure. This vacuum process helps pull air pockets out of the composite and minimize the defects. However, voids were modeled in a finite element analysis to see how they influenced the stress levels in the composite microstructure. It was shown voids introduced at the fiber/matrix interface produce higher localized stresses in the composite. If there are enough voids present, the composite as a whole will have less than desirable effective properties and an accumulation of voids may greatly compromise a composites performance. This conclusion would need further physical testing for validation.

It was also shown that in a plain weave pattern, the fibers are not linear. Since the fibers in the longitudinal direction have to weave around fibers in the transverse direction, the fibers follow a sinusoidal curve through the composite laminate. The curvature of these fibers causes stress concentrations in the composite. It was shown that models with greater linearity were more desirable than models having fibers with large amplitudes due to the decrease in the nominal first principal stresses in the matrix. From a manufacturing standpoint, this can be achieved by pre-tensioning the fibers before they are cured. The fibers will never be 100% linear but the closer fibers are to this idealization, the more optimum the design will be. One drawback that the finite element models create is the fiber volume ratio becomes dependent on the wavelength of the fibers since the amplitudes of longitudinal and transverse fibers must match. Therefore, a smaller wavelength will produce a composite with a larger fiber volume ratio. In composites, fiber volume ratio is not dependent on the wavelength of the fibers. Therefore, the finite element analysis will not isolate the fiber volume ratio as a single

variable and these effects are explored in the 'Natural Fiber Analytical Modeling' section. However, the goal of the finite element analysis was to show how the geometry of the fiber influences stress and not how the fiber volume ratio influences stress.

Finally, it was shown that fiber damage can be detrimental to the composite. Stress concentrations around damaged fibers can be remarkably high and can cause failure of the fiber even under small loading. When one fiber is damaged, it puts additional stress on other fibers in the composite. If these stresses get to large, the composite will eventually fail. Therefore, proper handling and weaving operations may influence the final strength of the composite.

5. Natural Fiber Analytical Modeling

5.1 Description of Models

The previous sections have focused on characterization of jute fibers and laminates using physical testing methods along with finite element modeling. This section focuses on bringing that information into a closed-form solution by correlating the behavior from physical testing and finite element analyses to analytical solutions. The analytical modeling in this section uses a combined Classical Lamination Plate Theory and fiber undulation model to calculate global modulus of elasticity and Poisson's ratio values. Similar to the finite element analysis, the analytical models assume the fibers follow a perfect sine wave and are also dependent on the amplitude and wave length in mechanical calculations. The modeling parameters are fiber volume ratio, wave amplitude, wavelength, lamina thickness, modulus of elasticity of the fibers and matrix, and the Poisson's ratio of the fibers and matrix. The model parameters are shown in Figure 54.

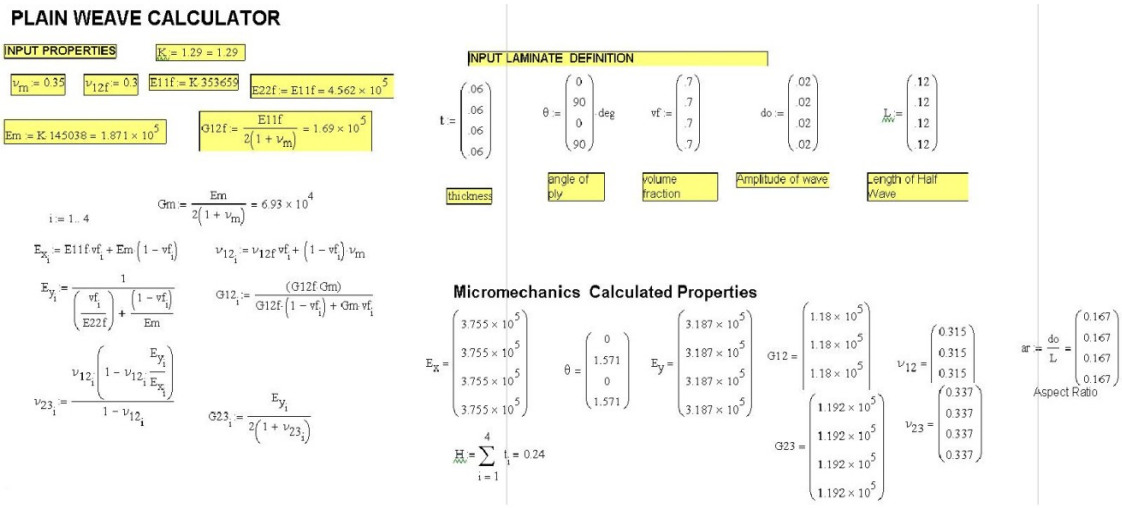

Figure 54: Analytical model input parameters.

The models were set up to calculate the modulus of elasticity of a laminate consisting of four layers. The model calculates mechanical properties for each ply and then uses the

correct transformations to calculate the modulus of elasticity for a global x and y direction. Calculations for the first ply are shown in Figure 55.

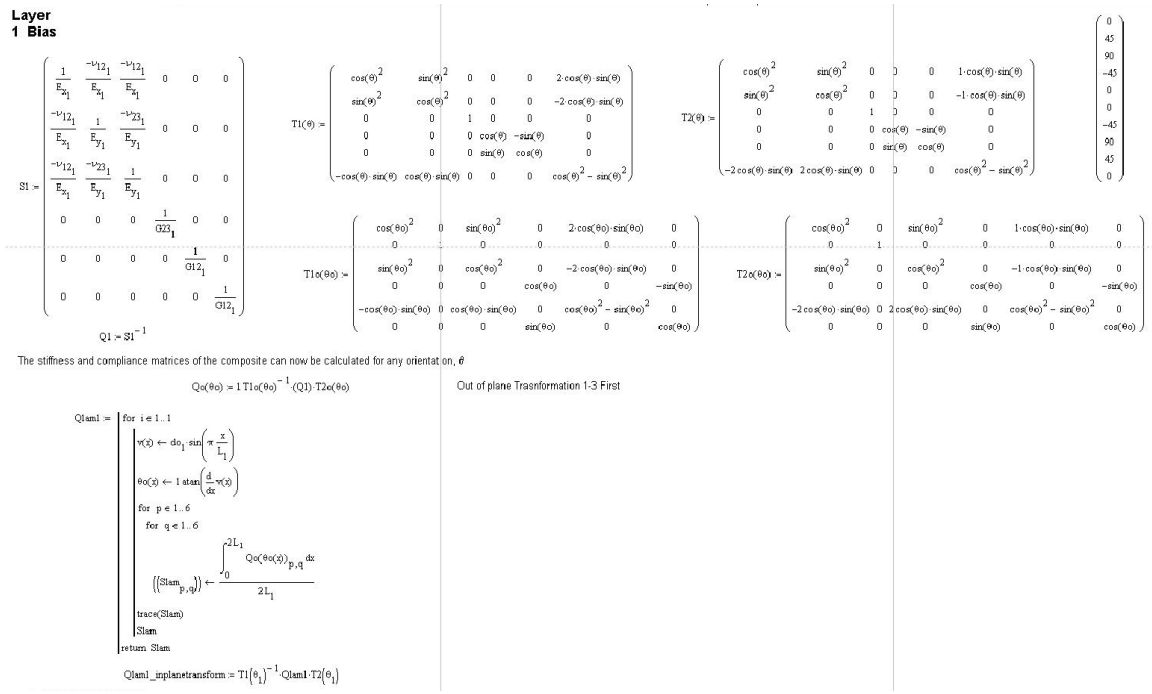

Figure 55: Calculation of mechanical properties for single ply.

Using the parameters above, a model can be calibrated to match the mechanical properties of a specific test coupon used during experimental analysis. The model that helped calibrate the analytical tool is Layup 5 from Section 3.3 'Lamina/Laminate Testing'. This is the same layup that was used in the 'Finite Element Analysis' section. Once a model was calibrated, parameters were adjusted to study the influence of specific variables. This was then correlated with the finite element analysis to verify the influence specific variables have.

5.2 Calibration

The analytical model is prone to display results that differ from results obtained from physical laminate testing. Initially, physical and mechanical properties that were gathered in 'Fiber Bundle Testing' and from Layup 5 in 'Lamina/Laminate Testing' were

inserted as variables into the analytical model. The properties inserted into the analytical model are listed below in Table 26.

Table 26: Initial analytical model parameters.

Mechanical Properties		Layer Thickness		Angle of Ply	
$E_{11f} = E_{22f}$ (psi) =	353,659	t_1 (in) =	0.06	Θ_1 (deg) =	0
E_m (psi) =	145,038	t_2 (in) =	0.06	Θ_2 (deg) =	90
v_{12f} =	0.30	t_3 (in) =	0.06	Θ_3 (deg) =	0
v_m =	0.35	t_4 (in) =	0.06	Θ_4 (deg) =	90
Volume Fraction		Fiber Amplitude		Half Wavelength	
v_{f1} =	0.70	A_1 (in) =	0.02	L_1 (in) =	0.12
v_{f2} =	0.70	A_2 (in) =	0.02	L_2 (in) =	0.12
v_{f3} =	0.70	A_3 (in) =	0.02	L_3 (in) =	0.12
v_{f4} =	0.70	A_4 (in) =	0.02	L_4 (in) =	0.12

The analytical model gave global modulus of elasticity values below the calculated values from experimental analysis. Physical testing for Layup 5 gave modulus of elasticity values for the longitudinal and transverse directions of 371,610 psi and 307,012 psi, respectively. However, the analytical model will be calculating the same value for both directions because the inputs are the same for each. A satisfactory value for the global modulus of elasticity for the analytical model is the mean value calculated from physical testing (339,000 psi). The analytical model gave a value of 262,500 psi for both the longitudinal and transverse directions when the original values were used. The analytical model values and the physical testing values were not equal but they were the same magnitude which is good for calibration purposes.

Since the modulus of elasticity for the analytical model was below the value from experimental testing, some of the parameters were calibrated to obtain a more acceptable value. To obtain the accepted mean value of 339,000 psi, the model had a “Calibration Factor” (K) that could be adjusted to obtain values observed during testing. The initial

calculations had K set equal to 1. The calibration factor was only applied to the modulus of elasticity of the fibers and matrix. A calibration factor of 1.29 was applied to obtain global modulus of elasticity values of 338,600 psi for both the longitudinal and transverse directions. The modified analytical model parameters with K equal to 1.29 are shown below in Table 27.

Table 27: Calibrated analytical model parameters.

Mechanical Properties		Layer Thickness		Angle of Ply	
$E_{11f} = E_{22f}$ (psi) =	456,200	t_1 (in) =	0.06	Θ_1 (deg) =	0
E_m (psi) =	187,100	t_2 (in) =	0.06	Θ_2 (deg) =	90
v_{12f} =	0.30	t_3 (in) =	0.06	Θ_3 (deg) =	0
v_m =	0.35	t_4 (in) =	0.06	Θ_4 (deg) =	90
Volume Fraction		Fiber Amplitude		Half Wavelength	
v_{f1} =	0.70	A_1 (in) =	0.02	L_1 (in) =	0.12
v_{f2} =	0.70	A_2 (in) =	0.02	L_2 (in) =	0.12
v_{f3} =	0.70	A_3 (in) =	0.02	L_3 (in) =	0.12
v_{f4} =	0.70	A_4 (in) =	0.02	L_4 (in) =	0.12

These modified parameters helped achieve global modulus of elasticity values that were acceptable. The calibrated model can now be used to help give insight to how different parameters will influence the stiffness of a plain weaved composite.

5.3 Modulus of Elasticity vs. Fiber Aspect Ratio

Two of the main parameters that have large influences on the modulus of elasticity of a composite are the amplitude and wavelength of the fiber. The influence of the amplitude was demonstrated in the finite element analysis in previous sections. In analytical modeling, the aspect ratio is the value of the amplitude divided by the half wavelength. Therefore, the aspect ratio and amplitude can both be investigated to determine their influences on the laminate. To be consistent with the finite element analysis, only the amplitude was varied to calculate different aspect ratios. This value

was then used to calculate the global modulus of elasticity for the longitudinal and transverse directions. The amplitude (which consequently changes the aspect ratio) was the only variable that was changing, while all other parameters were set to the calibrated analytical model parameters previously assigned. Figure 56 shows how the aspect ratio influences the global modulus of elasticity.

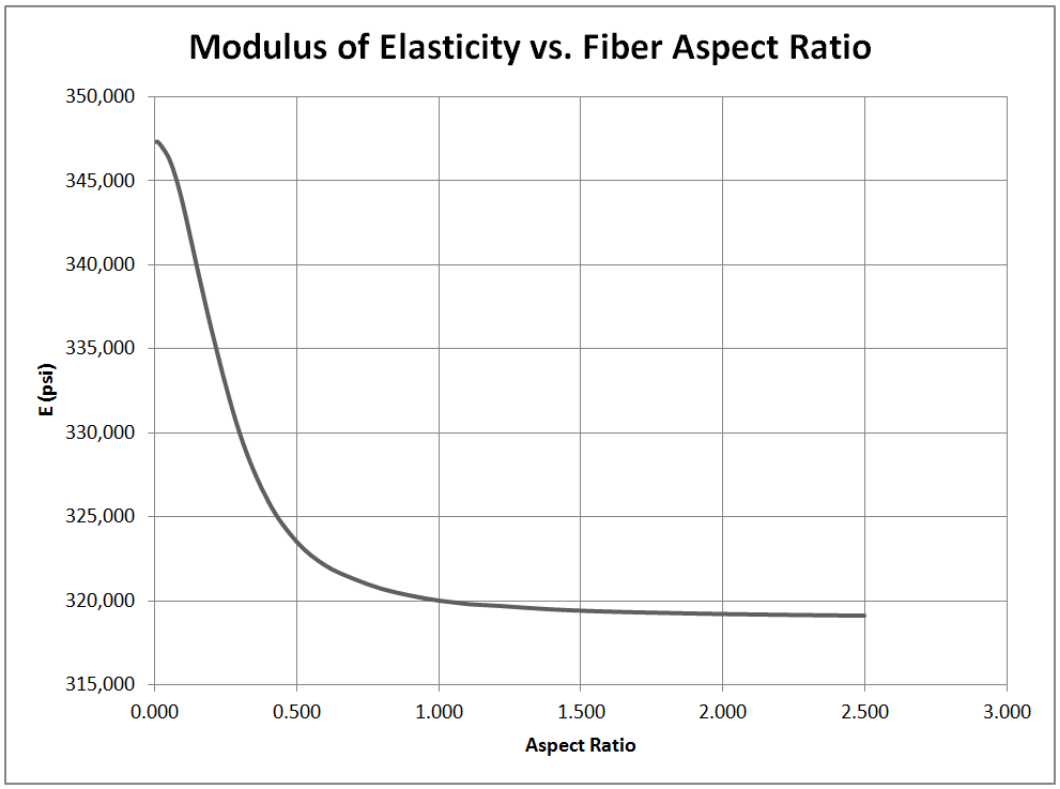

Figure 56: Modulus of elasticity vs. aspect ratio.

It can be seen that the modulus of elasticity does not change linearly with a change in aspect ratio. The modulus of elasticity drops off very steep with little change in aspect ratio and eventually converges on a lower limit of 319,000 psi. This indicates that controlling the aspect ratio is a very important characteristic in determining the stiffness of the composite. A small change in aspect ratio will result in a relatively large change in stiffness.

This can be correlated back to the finite element models. When the control geometry was compared to the finite element model with a less pronounced fiber bundle wave, the first principal stresses in the matrix were higher in the model with a greater aspect ratio (control geometry). The first principal stresses in the fibers were equal in overall magnitude but the less pronounced fibers had a larger area of stress distribution. This provided evidence that stresses were being transferred to the fibers more efficiently when the fibers were more linear. This is also evidence that the matrix is not taking as much load in the model with a smaller fiber wave and that the fibers are providing a higher percentage of stiffness to the overall composite. This is equivalent to saying the model with a lower aspect ratio had a higher global stiffness which is a positive correlation to the trend shown in Figure 56.

5.4 Modulus of Elasticity vs. V_f (Fiber Volume Ratio)

Another parameter that has a large influence on the modulus of elasticity is the fiber volume ratio. Analytical solutions provide an effective method to isolate and interrogate this variable. During experimental analysis, it is extremely hard to control the fiber volume ratio of the composite during manufacturing. It is only after testing is done can an engineer go back and determine the fiber volume ratio for analysis. A finite element analysis also provides a means of isolating the fiber volume ratio but it is more time consuming than an analytical solution. For these reasons, the influences of fiber volume ratio have been left for analytical solutions. Figure 57 shows how the fiber volume ratio influences the global modulus of elasticity. The two trends calculated in Figure 57 are the analytical model (Classical Lamination Plate Theory and fiber undulation model)

values and the rule of mixture values. The rule of mixtures is shown in the equation below:

$$E = E_f V_f + E_m V_m \quad (9)$$

where E is the global modulus of elasticity, E_f is the modulus of elasticity of the fibers, E_m is the modulus of elasticity of the matrix, V_f is the volume ratio of the fibers, and V_m is the volume ratio of the matrix.

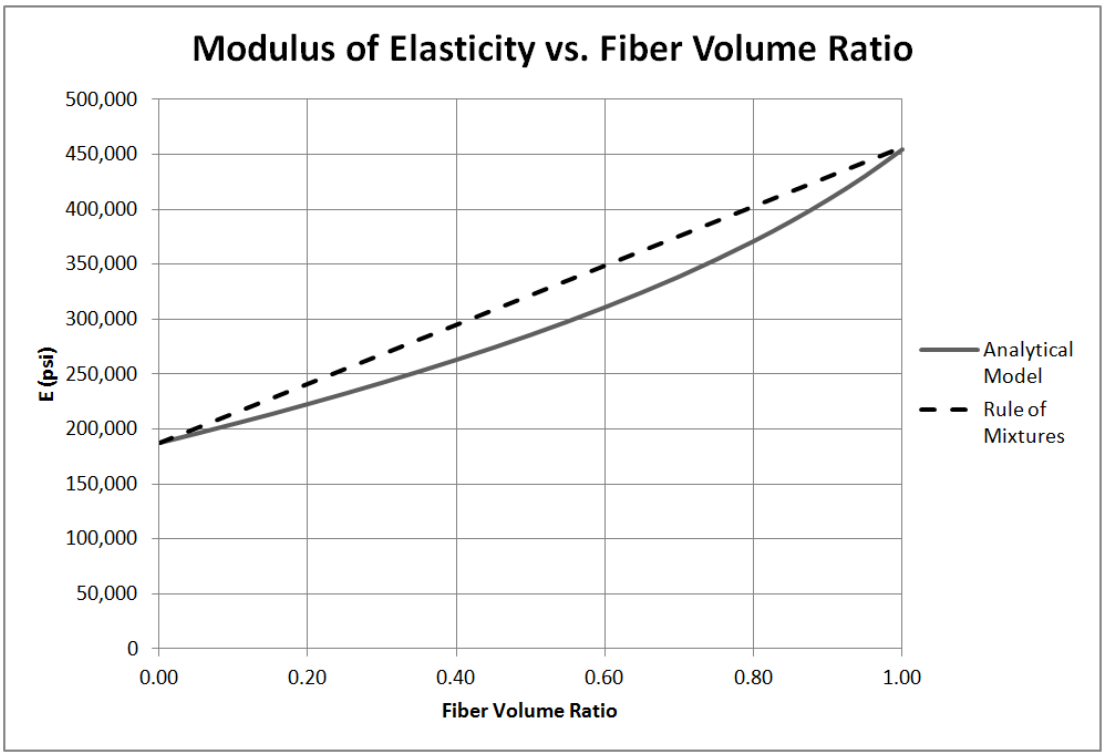

Figure 57: Modulus of elasticity vs. fiber volume ratio.

It can be seen that as the fiber volume ratio increases, so does the modulus of elasticity. The rule of mixtures trend is linear whereas the analytical model starts with a smaller slope but increases more rapidly as the fiber volume ratio approaches one. Both calculations give the same value for fiber volume ratios for 0.0 and 1.0, with the largest discrepancy between the trends being 11%. The discrepancy between the two trends is a consequence of the analytical model accounting for the sinusoidal nature of the fibers

along with the rotation of the individual layers about the global coordinate system. Since the fibers have a higher modulus of elasticity than the matrix, the global modulus of elasticity will increase as the fiber volume ratio increases and the matrix volume ratio, in turn, deceases. Both calculations show at a 0.0 fiber volume ratio, the modulus of elasticity of the composite is equal to the modulus of elasticity of the matrix. This represents a composite where there are no fibers and the matrix makes up 100% of the composite. On the opposite side of the spectrum, the analytical model shows at a 1.0 fiber volume ratio, the modulus of elasticity of the composite is equal to the modulus of elasticity of the fibers. This represents a composite where there is no matrix and fibers consist of 100% of the composite. In conclusion, a manufacturing process that promotes higher fiber volume ratios is a key element for optimizing the stiffness of the composite.

6. Case Study

6.1 Description

The goal of a case study was to take an existing product that uses synthetic fibers and investigate replacing them with recycled jute fibers. Two products currently using composite materials as reinforcement are skis and snowboards. Traditionally, these products were made from one piece of wood (the type of wood varied depending on the region). Today, these products are made from a combination of layers that are put together to form the ski or snowboard. For snowboards, the major layers from bottom to top are as follows:

- P-Tex (Ultra-High-Molecular-Weight Polyethylene)
- Composite (Fiberglass or carbon composite)
- Wood Core (Varied by region)
- Composite (Fiberglass or carbon composite)

This study looked at replacing the fiberglass layers in a snowboard with jute composite as the reinforcing laminate. Each fiberglass layer in a snowboard is composed of one fiberglass lamina between 20 oz/yd^2 and 25 oz/yd^2 [25]. This is shown in Figure 58.

Figure 58: Fiberglass layer being placed on top of the wood core [26].

The fiberglass layers are made of different layups which depend on the type of snowboard and the manufacturer. The most common layups are biaxial (fibers running longitudinal and at 90°), tri-axial (fibers running longitudinal and at ±45°), and multi-axial (fibers running longitudinal, ±45°, and ±90°) [25]. Some snowboards also use a bias biaxial layup with 70-80% of the fibers running in the longitudinal direction and the remaining fibers running at 90° [25]. This indicates that the main concern is with the normal stresses running down the length of the snowboard. When the layers of the snowboard are being put into place, a wet-layup process is used for holding everything together. After each layer is in place, the board is put into a manufacturing press and heated until it is cured in its final state.

The main purpose of the composite laminate on either side of the core is to help increase the moment of inertia of the snowboard, in turn, reducing normal stresses caused by bending moments. A snowboard can be thought of as a 60 inch long beam with top and bottom composite laminates acting like the top and bottom flanges of an I-beam, which is typical of sandwich construction.

6.2 Static Loads and Boundary Conditions

The purpose of this section is to understand the types of extreme loading conditions that are encountered and design for the stresses seen from these cases. This section also provides a closed-form solution for the load cases used during testing. The main measurements of a snowboard are shown in Figure 59.

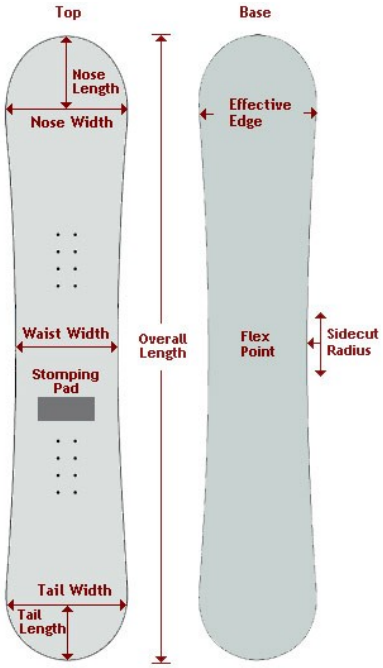

Figure 59: Main dimensions of a snowboard [27].

To obtain stresses, general values were assigned for the different dimensions (shown above) and also for the weight of the rider. The rider was assumed to have a weight of 250 pounds. For this analysis, a 60 inch snowboard was used because this length is common. An 11.5 inch and 12 inch waist width and nose width were used, respectively. Another dimension that must be given a value is the binding distance. This distance varies a bit to accommodate the style and individual of the person riding. For this thesis, the distance from the middle of one binding to the middle of the second binding was 20 inches. One of the main variables that can be changed is the thickness of the wood core. The wood core ranges anywhere between 0.245 to 0.300 inches in a fiberglass reinforced snowboard [28]. Finally, an average binding width of 6 inches was used. Figure 60 and Figure 61 summarize the dimensions listed above.

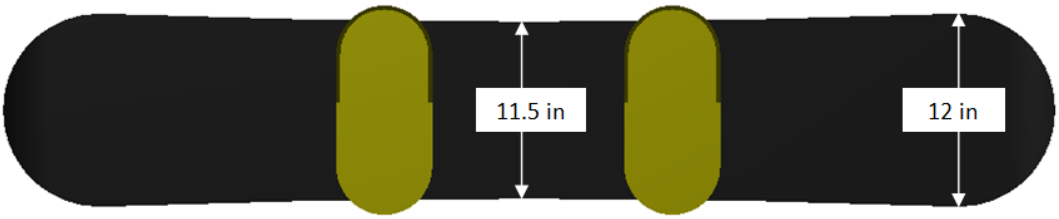

Figure 60: Top view of snowboard.

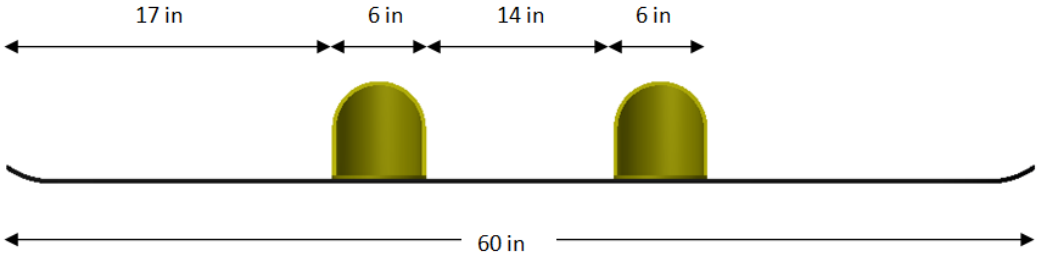

Figure 61: Side view of snowboard.

The most extreme bending cases occur when a snowboarder is riding in a terrain park. The terrain park has different types of jumps and rails that a snowboarder can ride on. Figure 62 shows one case where normal stresses are high due to bending.

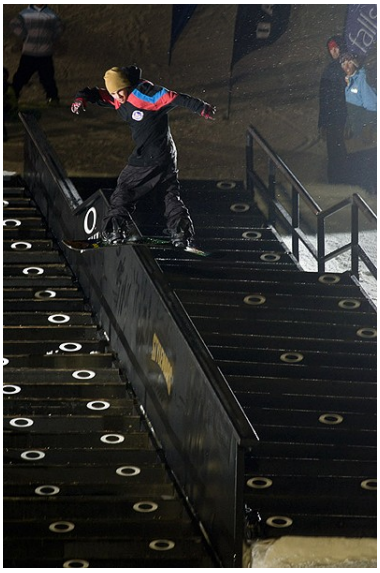

Figure 62: Three-point bending [29].

This type of loading can be broken down into a simple three-point bending problem. The weight of the person is what determines the shear forces and bending moments that occur throughout the length of the snowboard. Since the weight of the rider and general

dimensions were already determined, the three-point bending problem was broken down as shown in Figure 63. After determining the internal shear forces and moments, the simple beam-bending equation was applied to determine normal stresses. The general beam-bending equation is:

$$\sigma = \frac{-My}{I} \quad (10)$$

where σ is the normal stress, M is the bending moment, y is the distance from the neutral axis to the point of consideration, and I is the moment of inertia. Along with the three-point bending free body diagram, Figure 63 also shows the shear force and bending moment diagrams.

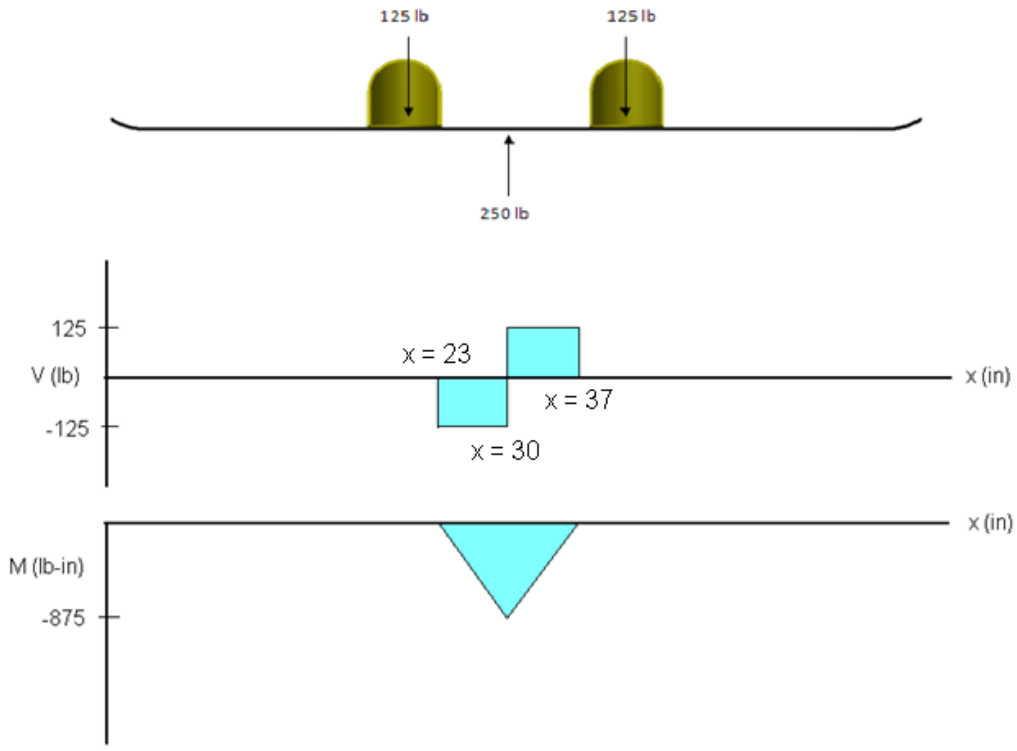

Figure 63: Three-point bending (FBD with shear and bending moment).

As shown above, the maximum bending moment for this load condition is -875 in-lb. The cross-section of the snowboard between the bindings can be thought of as a simple

rectangle with jute reinforcement sandwiching the wood core. A jute laminate thickness of 0.06 inches was used for these calculations because it was shown in 'Lamina/Laminate Testing' that Layup 5 has a thickness of 0.06 inches. The core thickness was varied from 0.250 inches to 0.385 inches. This variation will give a range of different normal stresses due to bending because the maximum y distance and the moment of inertia change as the core thickness changes. Since the cross-section under consideration is made from multiple materials, a transformed cross-section must be calculated before stresses can be determined. The new cross-section was assumed to be made entirely of the wood core. To obtain the correct dimensions for the transformed cross-section, a factor between the modulus of elasticity of the two materials is established. The modulus of elasticity of the jute composite is the value obtained from 'Lamina/Laminate Testing' for Layup 5 (371,610 psi) in the longitudinal direction. The wood is assumed to be ponderosa pine with a modulus of elasticity taken from literature (1,300,000 psi) [30]. Therefore, the factor used to reduce the width of the jute composite sections is the ratio of these two numbers (0.29). This gives a transformed width of 3.3 inches for the jute composite sections. After determining stresses in the cross-section using a transformed section, the stresses must be multiplied by the 0.29 factor to obtain stresses for the jute composite only. Doing this accounts for the fact that the jute composite is less stiff than the wood core and therefore will be subjected to less stress. Table 28 shows the core thickness and normal stresses due to bending for three-point bending for the transformed cross-section. Only the tensile stresses were considered because this is the type of experimental analysis that was done on the laminates. It is seen as the core thickness increases, the normal stresses on the top and bottom surface of the board decrease.

Table 28: Wood core thickness and normal stresses (three-point bending).

Core Thickness (in)	Normal Stress (psi)
0.250	1,883
0.265	1,697
0.280	1,537
0.295	1,397
0.310	1,275
0.325	1,168
0.340	1,074
0.355	990
0.370	916
0.385	850

Along with three-point bending, another case that results in high normal stresses occurs when the snowboarder rides, or lands, on the tip of the snowboard as shown in Figure 64. This loading can be broken down as a snowboard being subjected to a load applied at the tip of the snowboard at an angle. For the purposes of simplicity, the angle that was used is 45°. This is a pure static calculation and does not take dynamic impact into account. This type of loading is shown in Figure 65.

Figure 64: Riding/landing on the tip of a snowboard [31].

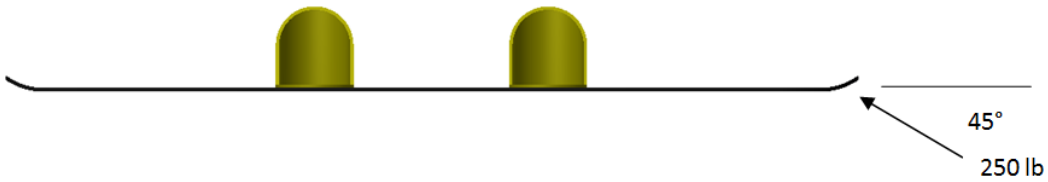

Figure 65: Snowboard tip riding/landing.

This type of problem can be broken down into a cantilever beam with an applied load at the free end. Since the applied load is at an angle, the board from the binding to the tip will see normal stresses due to compression and normal stresses due to bending. The normal stresses due to bending are given by beam bending described above, while the normal stresses due to compression are given below as:

$$\sigma = \frac{P}{A} \quad (11)$$

where σ is the normal stress, P is the normal load, and A is the cross-sectional area. The transformed section properties are only used to calculate stresses due to bending while stresses due to axial loads use the original cross-section. This is a combined loading problem with normal stresses occurring due to compression and bending. Along with the free body diagram, Figure 66 shows the shear force and bending moment diagrams for this situation.

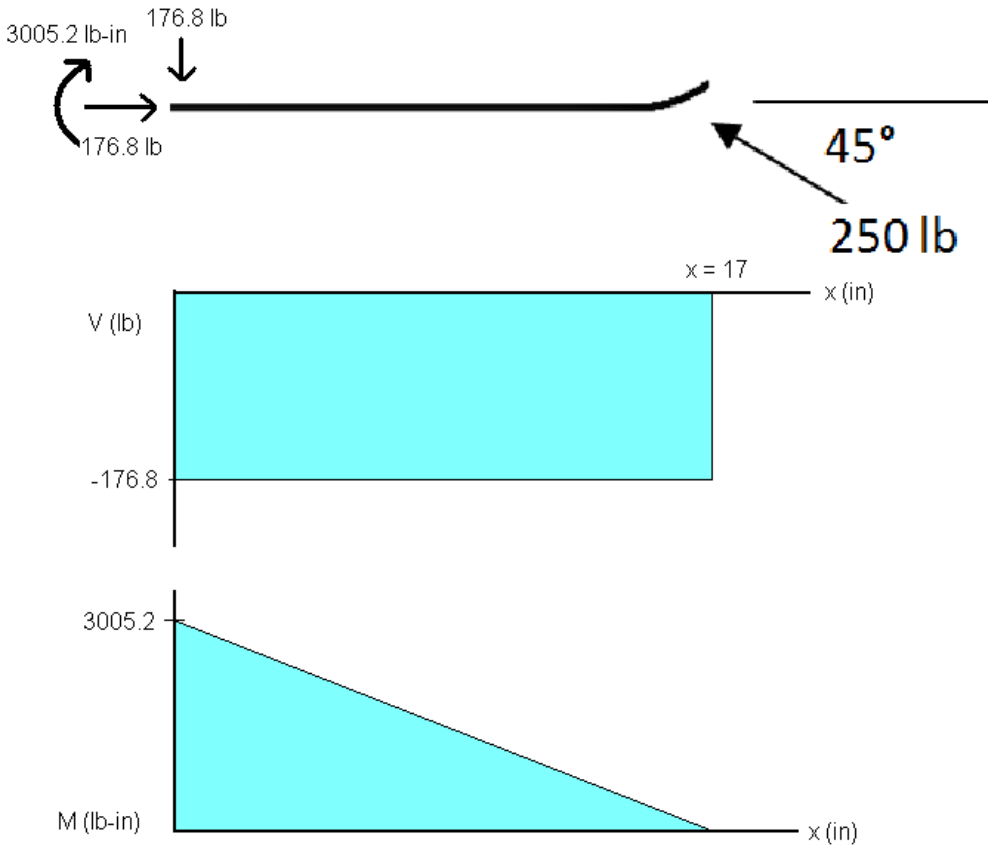

Figure 66: Combined loading (FBD with shear and bending moment).

As shown above, the maximum bending moment for this situation is 3,005.2 in-lb. Since the largest bending moment occurs where the binding is attached, the same cross-section used in three-point bending can also be applied here. Along with that, a composite thickness of 0.06 inches was used. The core thickness was varied as it was during three-point bending. Stresses due to bending dominate near the binding because this is where the largest bending moment occurs. Due to this, the normal tensile stresses are calculated in this area. The corresponding normal stresses at the bottom of the board are shown in Table 29.

Table 29: Wood core thickness and normal stresses (combined loading).

Core Thickness (in)	Normal Stress (psi)
0.250	6,427
0.265	5,789
0.280	5,239
0.295	4,761
0.310	4,344
0.325	3,978
0.340	3,655
0.355	3,369
0.370	3,115
0.385	2,888

The basis for this section is to find where the critical stresses are located and the type of loading that causes them. Therefore, if the board fails during testing, it will be easier to correlate the type of failure and the location of the failure with the type of loading. Based on the theory laid out, the board is most likely to fail during combined loading where the binding attaches to the snowboard. It is also prone to fail at the midpoint between the bindings. Even though stresses are based off idealizations, this closed-form solution shows good results and proves that it is possible to use jute fibers based on static tensile loads only. These numbers can be correlated to coupon testing and matched with the layup that gives the best results. The test coupon with the best results is Layup 5 and has ultimate stresses near the closed-form solution stresses calculated in this section.

6.3 Layup Design

Manufacturing of the snowboard occurred at K2 Sports (K2 Sports USA, Seattle, WA, USA). Their facilities include extensive manufacturing and in-house testing equipment providing a way to create a prototype snowboard using the same methods as production snowboards that are on the market. Snowboards are made with a wet-layup and a press for curing. In order to replace fiberglass layers with a jute composite, there

has to be a layup that is able to match the strength and stiffness of the fiberglass. There also has to be an acceptable resin system. Polyester and some phenolic resins are suitable for coupling with natural fibers because they are compatible with cellulose [11]. The jute fabric used to create a prototype snowboard were recycled jute fibers from local coffee shops.

The layup used to replace the fiberglass layer of a snowboard were two biaxial layers of the more dense jute fabric (Fabric B). Since the fibers that were used in the snowboard were sent via the mail, they were not soaked in any solutions for conditioning. From the 'Static Loads and Boundary Conditions' section, it was shown that closed-form solution stresses matched best with Layup 5 from 'Lamina/Laminate Testing'. Therefore, a snowboard made from a laminate similar to Layup 5 would have been ideal to create a snowboard. However, fabric was sent to K2 Sports early in the process before experimental testing and closed-form solutions were conducted. The jute fabric that was sent was chosen to match the mass per area of the fiberglass it was replacing therefore resulting in the same weight as a production snowboard. Since jute has a higher specific modulus than fiberglass, using the same weight will result in a snowboard that is more stiff than one made from fiberglass. Also, the specific strength of jute is lower than fiberglass so the laminate should have a lower ultimate strength. This situation becomes a case of balancing stiffness and strength. The manufactured snowboard is shown in Figure 67.

Figure 67: Snowboard made from recycled jute fibers.

6.4 Testing

Tests performed on the natural composite snowboard were similar to the closed-form analysis in the 'Static Loads and Boundary Conditions' section. However, the closed-form solutions derived above were static calculations while the testing performed at K2 Sports included dynamic behavior and impacts. The two major aspects of testing were to develop baselines for strength and fatigue. There are a number of different tests that can achieve this but the two that were used will help determine the durability of the snowboard. One test is designed to mimic riding on the tip of the snowboard (or landing on the tip) in exactly the same manner as applying a load to a cantilever beam in the analysis from the previous section. This test is performed up to 20 times to test for fatigue and durability. If there are no failures after 20 iterations, the test is stopped.

The second test is similar to the three-point bending analysis in the previous section as well. It is designed to test for impacts in a terrain park. The difference between the three-point bending analysis and the one performed on the snowboard is the placement of the impact. Instead of the impact happening in the middle of the two bindings, the test impacts the board directly under one of the bindings on the side wall (outside steel edge). This test is also performed multiple times (up to 4 times) to test for fatigue and durability. If there is no failure after 4 iterations, the test is stopped. After these preliminary tests are complete the snowboard can continue testing for bending (three-point bending), twisting, and further impact and fatigue testing. During the testing process, two snowboards were tested in parallel so a comparison could be made. The control board that was tested was a standard snowboard made with 22 oz/yd^2 fiberglass reinforcement.

6.5 Results

The test that simulated riding, or landing, on the tip of the snowboard was to be performed up to 20 times. The results for this test are as follows.

Table 30: Tip riding/landing results.

Tip Riding/Landing		
Snowboard	Test Iterations	Results
Jute Fiber	2	Fail
Fiberglass	20	Pass

The failure of the jute fiber snowboard was catastrophic and not typical of standard fiberglass snowboards. However, unlike the analysis in the 'Static Loads and Boundary Conditions' section, the board did not fail where the highest moment was taking place near the binding. Instead the board cracked at the tip. There could be a couple of explanations behind this. First, the 'Static Loads and Boundary Conditions' analysis doesn't take into account the impact that is applied by ramming a board into a surface.

Instead, the analysis assumed a static load and not an instantaneous load. Secondly, the 'Static Loads and Boundary Conditions' analysis does not account for the tip curling up. The snowboard is assumed to be a straight member. In reality, since the snowboard tip is curled up, there is a stress concentration around this curve. These two factors can explain why the snowboard failed near the tip and not by the binding. If the snowboard was loaded slowly at the tip, without a sudden impact, the 'Static Loads and Boundary Conditions' analysis would be more accurate and failure would possibly be seen where the bending moment is the highest. Figure 68 shows the failure of the snowboard due to tip riding/landing.

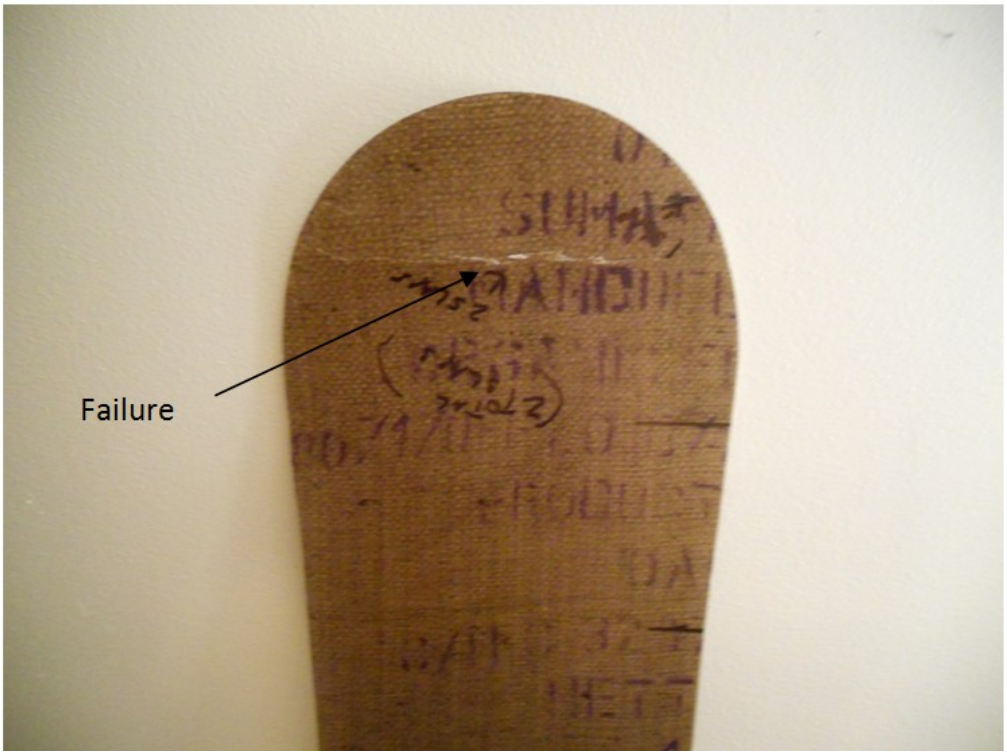

Figure 68: Tip riding/landing failure.

The test that simulated terrain park impacts was to be performed up to 4 times. The results for this test are as follows.

Table 31: Terrain park impact results.

Terrain Park Impact		
Snowboard	Test Iterations	Results
Jute Fiber	1	Fail
Fiberglass	5	Pass

The failure of the jute fiber snowboard was catastrophic and not typical of standard fiberglass snowboards. The snowboard failed directly where the impact took place after 1 test. The highest stresses would be concentrated around the location of impact. This failure can be seen in Figure 69.

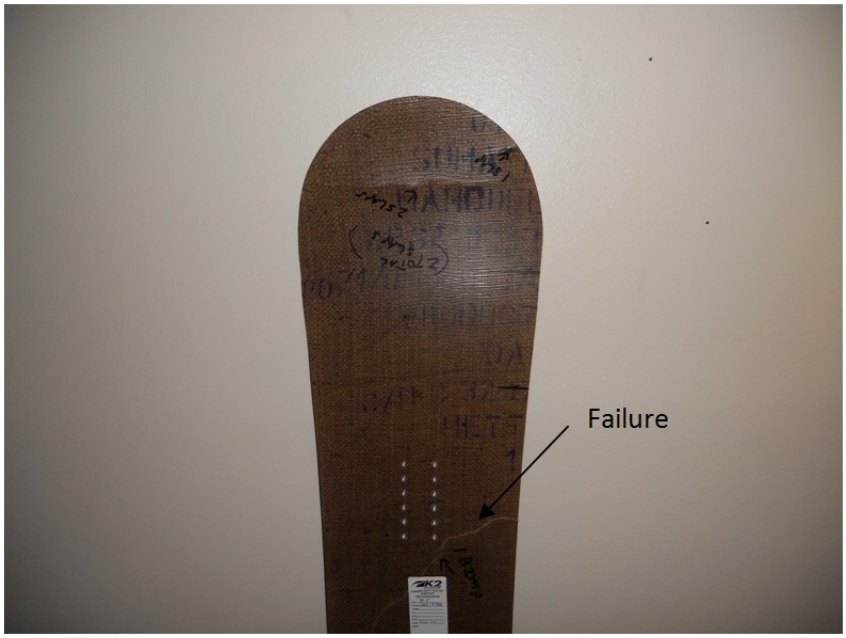

Figure 69: Terrain park impact failure.

In conclusion, coarse woven fabrics like jute fibers, show reduced global properties when compared to fiberglass and other manufactured fibers. One of the main reasons for the reduced properties is the "dryness" of the fibers. Since the fibers are coarse and dry, uneven distribution of resin takes place which results in pools or voids in the matrix. These imperfections correlate to a higher probability for crack propagation due to the micro cracks and voids in the area. Also, multiple layers of fabric, which is how the jute

fiber snowboard was constructed, tend to have lower fiber volume ratios than snowboards constructed with one layer of fabric. This lower fiber volume ratio causes the global properties to be lower and there is also greater potential for imperfections in the matrix. Since there is a higher probability of micro cracks and voids, failure of the board was likely due to the propagation of these imperfections.

These findings correlate well with the 'Finite Element Analysis' section. There are a couple of options to increase the strength of the snowboard. As shown in the 'Finite Element Analysis' section, pre-tensioning the fibers before curing can greatly increase the normal stress capacities. Also, preconditioning the fibers with alkali treatment can increase the properties as well by eliminating some imperfections. This process would also help eliminate imperfections due to the dryness of the fibers due to resin pooling. Soaking the fibers in a solution would wet the fibers and help put a more uniform coat of resin throughout the entire snowboard, thus minimizing resin pools. It would also cut down on the amount of resin that must be used because it is now only being used as a medium to transfer stresses to the fibers and not just being soaked up by the fibers.

It is plausible that different results would have been reached had a different laminate been used while also accounting for impact resistance. The laminate that best matches the closed-form solution is Layup 5. A combination of using Layup 5, preconditioning techniques, and an optimized manufacturing process, it is possible a snowboard can be created from jute fibers that pass the testing laid out in the previous sections.

7. Conclusions and Recommendations

7.1 Materials and Mechanical Characterization

The focus of this research was to characterize recycled jute fibers to determine the possibility of replacing synthetic fibers in products used today. Along with being available as a byproduct and readily accessible, jute has many other advantages as well. For this thesis, jute fibers were obtained as a byproduct from the coffee industry which means that classification between different jute fabrics is essential. Classification of the fabric was made possible by categorizing the different fibers using a weight measurement technique. This thesis categorized jute fabric into two groups: Fabric A and Fabric B. Fabric A had a mass per area of 7.3 oz/yd^2 while Fabric B had a mass per area of 13.8 oz/yd^2.

The natural fibers presented in this research were characterized through experimental testing, numerical simulations, and analytical modeling. Experimental testing provided a platform to characterize single jute fiber bundles and multiple jute fiber laminates. Fiber bundle testing was performed in accordance with ASTM D3822-07 [24] to obtain the modulus of elasticity for jute fiber bundles. The average value found through testing was 353,659 psi which was then used in finite element and analytical modeling. This value was consistent with other values in literature. Composite specimens with different layups were also tested. These different laminates were tested to obtain a replacement that could be used in the construction of a snowboard as a case study for this project. To replace fiberglass in a snowboard during the case study, the main aspects were to find a jute laminate with the same strength, stiffness, and weight characteristics. Jute has a higher specific modulus, therefore an equal stiffness should be maintained with less weight.

However, the specific strength of jute is less than fiberglass, therefore, it is hard to maintain the same strength and keep the same weight. From experimental analysis, it is apparent that a fabric must be used that lacks in available strength but may be more stiff than fiberglass. Matching mechanical properties with stresses obtained from the 'Static Loads and Boundary Conditions' section shows that it is theoretically possible to replace fiberglass with jute fabric in a snowboard based off static analysis only. Further testing on impact behavior is necessary if applications such as snowboards are to employ these materials.

7.2 Finite Element Models

Finite element modeling provided a method to show which characteristics of a composite are favorable and which are unfavorable. Four different finite element models were created to interrogate the effects of fiber undulation, fiber damage, and matrix porosity. Each of these characteristics had a noticeable influence when compared to the control geometry however, the effects due to fiber damage were the most significant.

The first finite element model that was compared to the control geometry was one in which the fiber had an amplitude half the size of the control geometry. The modified model with fiber undulation had negligible effects for the first principal stress throughout the fiber. However, the first principal stress decreased by 31.1% in some locations within the matrix. This was accompanied by an increase in shear stresses in the fiber and a decrease in the matrix. All of these results indicate that stresses are being transferred to the fibers more efficiently in the model with fibers that are more linear. It is beneficial to have fibers as linear as possible within a composite.

The second finite element model was one in which the fiber had damage located at the maximum amplitude. Fiber damage in this location will influence fiber stresses the most when compared to other locations. The model with fiber damage had an increase in the first principal stress of 56.1%. This was located around the area where damage occurred. There was also an increase in the first principal stress in the matrix by 14.7%. The fibers and matrix both had a decrease in shear stresses. These results indicate that stresses are not being transferred to the fibers as efficiently as the other models. Fiber damage has a negative impact on the composite and should be minimized.

The third finite element model was created to simulate voids in the matrix of the composite. This type of imperfection caused the stresses to increase in localized areas where voids were present at the fiber/matrix interface. At the specific locations being analyzed, stress differences were negligible. Voids in the matrix would have more influence on stresses if they were located at the maximum amplitude on the fiber wave. In the case of matrix porosity, voids are most sensitive around stress concentrations created by fiber undulation. It is important to eliminate voids as much as possible because this will reduce the chance of a void being located at a vulnerable area within the composite. Also, voids can coalesce and compromise the entire composite.

7.3 Summary of Significant Findings

Since the jute fabric used in the research was a byproduct, one of the most significant findings was the classification of the fabric based on its mass per area (oz/yd^2). The samples used throughout this work fell into two categories. Fabric A had an average mass per area of 7.3 oz/yd^2 while Fabric B had a mass per area of 13.8 oz/yd^2. Therefore, each sample can be placed into one of these categories based on its mass per area and it

can be assumed that the properties of the sample have the same behavior as the fabric in the same category. This is a significant finding when dealing with a fabric that is a byproduct and not one that is manufactured.

Another significant finding was determining the modulus of elasticity of single jute fiber bundles. Determining the modulus of elasticity was very important because this value was then used in the finite element analysis and analytical models. In this research, values were obtained from the exact fabric of interest (recycled jute fabric). Using ASTM D3822-07 [24], the modulus of elasticity for fiber bundles was determined to be 353,659 psi. The determination of the modulus of elasticity of jute fiber bundles was not only a significant finding in itself, but also in pursuing other analytical goals. From here, other significant findings were determined through finite element modeling. These findings are described in the previous section and provide evidence that fiber damage, matrix porosity, and fiber undulation can have different influences on a composite.

Analytical modeling was significant because it helped correlate the results from experimental testing and finite element analysis to a closed-form solution. It also presented different trends that mechanical properties have when different parameters (specifically aspect ratio and fiber volume ratio) are varied. As the aspect ratio of the fiber increases, the modulus of elasticity decreases initially at a steep rate but eventually converges onto a lower limit. This is significant because it shows how sensitive the modulus of elasticity is with a small change in aspect ratio and emphasizes the need to keep a tight control on this parameter during manufacturing. As the fiber volume ratio increases, the modulus of elasticity also increases. Changing this parameter also helped verify that the analytical model was calculating the mechanical properties correctly. The

analytical model has an 11% difference when compared to the rule of mixtures formulation for calculating stiffness.

The case study helped determine that it is possible to create a snowboard purely from a manufacturing standpoint. Problems that occurred during the manufacturing process can be circumvented with more preparatory work and research. During manufacturing it was noted that jute fibers were very dry and absorb resin more than synthetic fibers. This can be resolved by soaking the fibers in an alkaline solution which will also help strengthen the fibers by dissolving imperfections. Soaking the fibers helps cut down on the amount of resin that must be used and prevents dry pockets from forming. Other manufacturing problems such as fiber undulation can be resolved by pre-tensioning the fibers before they are cured. The specifics on how this could be done require more research and greater familiarity with the equipment being used.

In all, this research shows that it is plausible to use jute fabric for structural purposes and more specifically for reinforcement in snowboards. During the case study, the snowboard did not pass testing but manufacturing steps were not taken that could improve the mechanical properties of the composite. In general, jute fabric can be of significant value to an engineer in the proper situations where natural fibers can be applicable. Its high specific stiffness lets an engineer obtain the same stiffness as other materials with less weight which can be taken advantage of in certain situations. Along with this, jute fabric is very cheap (if not free as a byproduct) and can be categorized into different categories so an engineer knows the material that is being considered. This thesis focused on static behavior and does not get into the details of dynamic analysis. Therefore, implications of dynamic behavior must be considered before jute composites

can be considered applicable. However, all of these findings make jute a desirable fiber when introduced to the proper situation from a static perspective.

7.4 Suggestions for Future Research

The purpose of this research was to characterize jute fibers and different laminates created from jute fabrics. This research has successfully investigated the mechanical properties of recycled jute fabrics and applied these results to finite element and analytical analyses. Results from experimental testing, finite element analysis, and analytical modeling can be used to optimize the type of laminates and manufacturing practices to create a composite that will be able to withstand specified applications. Combined with snowboard theory, it was confirmed that substituting jute composite for fiberglass in a snowboard is theoretically possible. However, the case study provided results showing that the snowboard that was manufactured did not withstand testing. Future work should be focused on ways to reduce stresses in the fibers via better manufacturing methods or strengthening fibers through chemical processes. Other literature has specified different chemical solutions, such as ammonia hydroxide, that will eliminate some imperfections in the fiber in turn causing the tensile strength to increase. This increased tensile strength can be taken advantage of and help create a laminate that can possibly withstand the physical testing snowboards have to endure. Along with this, dynamic and impact modeling should be analyzed to better understand the forces snowboards face on a regular basis. This analysis would help determine if jute composites could withstand the forces they would encounter if they replaced fiberglass in a snowboard.

Future work can be focused on ways to eliminate typical imperfections that were modeled in the finite element analysis. Research can be done on different ways to pre-tension fibers in snowboards while they are being cured. This will help reduce fiber undulation and minimize stress concentrations created by imperfections. Soaking the fibers in a chemical solution will also help moisten the fibers which will minimize voids in the matrix and fiber damage. Other manufacturing methods such as vacuum resin infusion or resin transfer molding should be looked at to help minimize the amount of imperfections within the composite.

8. References

[1] Thomas, S., S.A. Paul, L.A. Pothan, and B. Deepa. "Natural Fibres: Structure, Properties and Applications." *Cellulose Fibers: Bio- and Nano-Polymer Composites*. (2011): 3-42. Print.

[2] "Jute." Encyclopedia Britannica. Encyclopedia Britannica Online. Encyclopedia Britannica Inc., 2012. Web. 10 Sep. 2012 <http://www.britannica.com/EBchecked/topic/308941/jute>.

[3] "Coffee Statistics Report." Coffee-Statistics. Coffee-Statistics, 2011. Web. 8 May 2011. <http://coffee-statistics.com/coffee_statistics_ebook.html>.

[4] Rowell, Roger. "Potentials for Jute Based Composites." Biological Systems Engineering Dept., University of Wisconsin, USA. (1997): 84-90. Print.

[5] Vilaseca, F., J.A. Mendez, A. Pelach, M. Llop, N. Canigueral, J. Girones, X. Turon, P. Mutje. "Composite materials derived from biodegradable starch polymer and jute strands." *Process Biochemistry*. 42.3 (2007): 329-34. Print.

[6] Davallo, M., H. Pasdar, and M. Mohseni. "Mechanical Properties of Unsaturated Polyester Resin." *International Journal of ChemTech Research*. 2.4 (2010): 2113-17. Print.

[7] Ku, H., H. Wang, N. Pattarachaiyakoop, and M. Trada. "A review on the tensile properties of natural fiber reinforced polymer composites." *Composites Part B: Engineering*. 42.4 (2011): 856-73. Print.

[8] Netravali, Anil N., and Shitij Chabba. "Composites get greener." *Materials Today*. 6.4 (2003): 22-29. Print.

[9] Ray, D., B.K. Sarkar, A.K. Rana, and N.R. Bose. "The mechanical properties of vinylester resin matrix composites reinforced with alkali-treated jute fibres." *Composites Part A: Applied Science and Manufacturing*. 32.1 (2001): 119-27. Print.

[10] Corrales, F., F. Vilaseca, M. Llop, J. Girones, J.A. Mendez, P. Mutje. "Chemical modification of jute fibers for the production of green-composites." *Journal of Hazardous Materials*. 144.3 (2007): 730-35. Print.

[11] Santulli, C., and W.J. Cantwell. "Impact Damage Characterisation on Jute Reinforced Composites." University of Liverpool Dept. of Engineering Materials Science. 1-4. Print.

[12] Roe, P.J., and M.P. Ansell. "Jute-reinforced polyester composites." *Journal of Materials Scienc*e. (1985): 4015-20. Print.

[13] Ray, D., B.K. Sarkar, and N.R. Bose. "Impact fatigue behaviour of vinylester resin matrix composites reinforced with alkali treated jute fibers." *Composites Part A: Applied Science and Manufacturing*. 33.2 (2002): 233-41. Print.

[14] Daniel, Isaac M., and Ori Ishai. *Engineering Mechanics of Composite Materials*. Second Edition. New York: Oxford University Press, Inc., 2006. Print.

[15] Pelegri, Assimina A., and Diwakar N. Kedlaya. "Design of composites using a generic unit cell model coupled with a hybrid genetic algorithm." *Composites Part A: Applied Science and Manufacturing*. 39.9 (2008): 1433-43. Print.

[16] Bonora, Nicola, and Andrew Ruggiero. "Micromechanical modeling of composites with mechanical interface – Part 1: Unit cell model development and manufacturing process effects." *Composites Science and Technology*. 66.2 (2006): 314:22. Print.

[17] Xia, Zihui, Chuwei Zhou, Qiaoling Yong, and Xinwei Wang. "On selection of repeated unit cell model and application of unified periodic boundary conditions in micro-mechanical analysis of composites." *International Journal of Solids and Structures*. 43.2 (2006): 266-78. Print.

[18] Sun, W., F. Lin, and X. Hu. "Computer-aided design and modeling of composite unit cells." *Composites Science and Technology*. 61.2 (2001): 289-99. Print.

[19] Potter, E., S.T. Pinho, P. Robinson, L. Iannucci, and A.J. McMillan. "Mesh generation and geometrical modeling of 3D woven composites with variable tow cross-sections." *Computational Materials Science*. 51.1 (2012): 103-11. Print.

[20] De Carvalho, N.V., S.T. Pinho, and P. Robinson. "Analytical modeling of the compressive and tensile response of woven composites." *Composite Structures*. 94.9 (2012): 2724-35. Print.

[21] Shokrieh, Mahmood M., and Mohammad S. Mazloomi. "An analytical method for calculating stiffness of two-dimensional tri-axial braided composites." *Composite Structures*. 92.12 (2010): 2901-05. Print.

[22] Quek, Shu Ching, Anthony M. Waas, Khaled W. Shahwan, and Venkatesh Agaram. "Analysis of 2D triaxial flat braided textile composites." *International Journal of Mechanical Sciences*. 45. 6-7 (2003): 1077-96. Print.

[23] Shokrieh, Mahmood M., and Mohammad S. Mazloomi. "An analytical method for calculating stiffness of two-dimensional tri-axial braided composites." *Composite Structures*. 92.12 (2010): 2901-05. Print.

[24] D3822-07, Standard Test Method for Tensile Properties of Single Textile Fibers. ASTM International.

[25] McGinty, Paul. "Natural Composite Snowboard." Message to Patrick. 3-3-11. E-mail.

[26] "Inside Mervin Manufacturing." Shayboarder.com. Shayboarder, 2011. Web. 6 March 2011. < http://www.shayboarder.com/2009/02/inside-mervin-manufacturing.html >.

[27] "A Detailed Look At Snowboards." *Selecting a Snowboard*. Web. 14 Apr 2011. <http://www.modernskate.com/modernskate/dept.asp?dept_id=702>.

[28] McGinty, Paul. "Natural Composite Snowboard." Message to Patrick. 4-12-11. E-mail.

[29] "Charles Reid." *STYLEWARS 2008 DAY 3 – CANADIAN CHARLES REID WINS THE 28 STAIR RAIL JAM presented by VOLVO*. Web. 14 Apr 2011. <http://www.boardtheworld.com/Home/Magazine/Features?&riID=2462>.

[30] Beer, Ferdinand P., E. Russell Johnston Jr., and John T. DeWolf. *Mechanics of Materials*. Third Edition. New York: McGraw-Hill, 2002. Print.

[31] "How to start doing snowboarding tricks." *How Easy Is It To Learn Snowboard Tricks?*. Web. 14 Apr 2011. <http://www.snowboardcabin.com/snowboards/how-easy-is-it-to-learn-snowboard-tricks/>.